INFORMATION TO USERS

This manuscript has been reproduced from the microfilm master. UMI films the text directly from the original or copy submitted. Thus, some thesis and dissertation copies are in typewriter face, while others may be from any type of computer printer.

The quality of this reproduction is dependent upon the quality of the copy submitted. Broken or indistinct print, colored or poor quality illustrations and photographs, print bleedthrough, substandard margins, and improper alignment can adversely affect reproduction.

In the unlikely event that the author did not send UMI a complete manuscript and there are missing pages, these will be noted. Also, if unauthorized copyright material had to be removed, a note will indicate the deletion.

Oversize materials (e.g., maps, drawings, charts) are reproduced by sectioning the original, beginning at the upper left-hand corner and continuing from left to right in equal sections with small overlaps. Each original is also photographed in one exposure and is included in reduced form at the back of the book.

Photographs included in the original manuscript have been reproduced xerographically in this copy. Higher quality 6" x 9" black and white photographic prints are available for any photographs or illustrations appearing in this copy for an additional charge. Contact UMI directly to order.

UMI

A Bell & Howell Information Company
300 North Zeeb Road, Ann Arbor MI 48106-1346 USA
313/761-4700 800/521-0600

Université d'Ottawa · University of Ottawa

Dedicated to my Mother and Father

Abstract

This thesis involves laser flash photolysis studies of the kinetic behaviour of photochemical reactions in heterogeneous media with the emphasis on the effects of magnetic fields on the reactions involving triplet radical pairs. Chapters 3 and 4 present results of the effects of magnetic fields on the behaviour of radical pairs in organized systems. The possibility that electromagnetic fields have deleterious health effects has received much attention in recent years. It has been well documented in the literature that magnetic fields can influence the behaviour of free radicals in heterogeneous media, and that an applied magnetic field increases the lifetime and concentration of some types of free radicals. The mechanism by which a magnetic field can influence triplet radical pairs is based on the fact that a magnetic field can slow down the rate of intersystem crossing of the triplet to the singlet radical pair where product formation can occur.

Free radicals are known to be involved in many biological processes and are thought to be a major initiator of some types of cancer. As a result, we have determined how free radical behaviour is modified in the presence of a 60 Hz oscillating magnetic field superimposed over a static magnetic field of comparable magnitude. We showed that the effect of an oscillating magnetic field on radical behaviour is identical to that exerted by a static magnetic field of the same strength provided the frequency is low in comparison with radical pair dynamics. This criterion is easily met by environmental fields. It has been suggested that oscillating magnetic fields play a particularly important role in fluctuating biological processes. We have used a test system involving radical pairs generated in micellar solutions by photolysis of benzophenone in the presence of 1,4-cyclohexadiene. Our results show

that radical pair reactions in micellar solutions exhibit the same behaviour under 60 Hz oscillating fields as under static field conditions at any point in time.

Given that a) radicals play an important role in metabolic processes, and b) that radical behaviour is strongly influenced by magnetic fields, it was clearly necessary to undertake experiments that better mimic *in vivo* systems. Laser flash photolysis of probe molecules, such as benzophenone and some of its derivatives, leads to a triplet spin-correlated radical pair due to the hydrogen abstraction of the triplet from Bovine and/or Human Serum Albumin. The analysis of the kinetics of the radical pair, where one of them is derived from the protein, in the presence and in the absence of a magnetic field, shows that the protein-probe radical pair is subject to a magnetic field effect. Thus, it can be concluded that proteins host radical reactions which are influenced by an external magnetic field. In the case of radicals bound to proteins, the concentration of the escaped free radicals are found to increase up to 20% in the presence of static fields up to 1400 Gauss. However, at half saturation a higher field is required for radical pairs in proteins than needed for those in micelles. The quenching experiments of different amino acids and peptides with a water soluble derivative of benzophenone suggests that lysine residues and amide links in a peptide bond act as possible hydrogen donor sites.

In Chapter 5, the photophysical properties of microheterogeneous systems have been characterized using the triplet state of an appropriate probe. A hydrophobic solute is incorporated into micelles having hydrophobic interiors of varying size. The solute, xanthone, whose triplet-triplet absorption maximum is known to shift with the solvent polarity is selected for this study. Xanthone is used as a sensor to obtain information on the mobilities of probe molecules between a

microphase, or host, and the main continuous medium in organized systems. We have monitored the time evolution of the xanthone spectrum in micelles of varying size using a combination of picosecond and nanosecond laser photolysis techniques and determined the rate constants of the probe exit from the micelles. Our results show that there are two processes occurring prior to the actual exit of the probe into the aqueous phase. The first process is occurring in around 100 ps. This process is attributed to the intersystem crossing of the singlet to the triplet state of xanthone in micelles. The singlet lifetime of xanthone in various micelles is found to be in the range of 50-150 ps. Thus, the fluorescence data correspond to the initial fast spectral change observed in the picosecond absorption experiments. This is followed by a second process occurring in the 1-50 ns range. This stage is attributed to the time it takes for the probe to migrate to the surface of the micelle. Even thought the exit into the aqueous phase occurs in the nanosecond to microsecond region, the observed spectral changes in these times are small. The slowest rate constant, which corresponds to the exit from the micelle and into the continuous medium, is determined by quenching the probe with water soluble quenchers.

Acknowledgements

I would like to take this opportunity to thank the people who have greatly helped me through some very difficult times in the past four years. The enormous love and support of all the members of my family have given me the strength I needed to pull through. My two very best friends, my husband and my sister, have given me the greatest support and love that made the successful and on-time completion of this thesis possible. My parents have sacrificed much for the completion of my PhD studies. I would like to express my deep appreciation to Tito Scaiano, my PhD supervisor, for always being there to help me. I have learned a great deal from him. I will never forget the support that he and his wife Elda have given me. I thank the Scaiano's for being there for me in both the good times and the bad.

I would like to thank all the members and visitors of the Scaiano group with whom I have had the opportunity to work. I would especially like to thank the people who helped me during the early days of my graduate work. Many thanks to my very good friend Fran Cozens who has helped me greatly with my work. Most importantly, Fran has helped me through very difficult times and I am very grateful. Andre Simard has been there for me from day one to help me with the laser systems and the computers.

I am very happy to have worked closely with Alain Berinstein and Ron Boch. Both Alain and Ron have always rushed to my rescue when I needed them, and I cannot thank them enough. I would like to thank John McClean from the Radiation Protection Bereau of Health Canada for many helpful discussions regarding our studies on magnetic field effects. I would like to express my heartfelt appreciation to my very good friends, Nanci De Lucas and Monica Barra, for their continuous love and support. I cherish the memories I have with them. I thank Lydia Martinez for sharing very useful information with me and Terry Connolly for helping me with my other projects. I thank Annette Fournier for her support and friendship. I treasure the many good times that I have shared with Jeff Banks, Dean Weldon, Sonia Corrent, and William Skene and my many other friends in the group.

I would also like to thank the Natural Sciences and Engineering Research Council and the University of Ottawa for financial support during my PhD studies.

Table of Contents

List of Figures

Chapter 1

Chapter 2

Chapter 3

Chapter 4

Chapter 5

List of Tables

Chapter 3

Chapter 5

List of Abbreviations

AC	alternating current
αT	α-terthienyl
B	magnetic field
BP	benzophenone
BSA	Bovine Serum Albumin
CTAC	cetyl trimethyl ammonium chloride
CIDEP	chemically induced dynamic electron polarization
CIDNP	chemically induced dynamic nuclear polarization
DC	direct current
DFBP	decafluorobenzophenone
DBK	dibenzylketone
DODCI	3,3-diethyloxodicarbocyanine iodide
DPMP	1,2-diphenyl-2-methyl-propan-1-one
DPP	2,4-diphenyl-3-pentanone
DNA	deoxyribonucleic acid
FS	field sensitivity
FWHM	full width at half maximum
H	Henry
HFC	hyperfine coupling
HFI	hyperfine interactions
HSA	Human Serum Albumin
ISC	intersystem crossing
J	exchange interaction
KDP	potassium dihydrogen phosphate
LFP	laser flash photolysis
LAT	light absorbing transients
MCP	microchannel plate
MFs	magnetic fields
MFEs	magnetic field effects
MDB	methyldeoxybenzoin
MV	methyl viologen
OD	optical density
OMA	optical multichannel analyzer
PFBP	pentafluorobenzophenone
PMT	photomutliplier tube
RP	radical pair
S	singlet state
SDS	sodium dodecyl sulfate
SDecS	sodium n-decyl sulfate
SHG	second harmonic generator
STDS	sodium tetradecyl sulfate
SOC	spin orbit coupling
T	triplet state
THG	third harmonic generator
YAG	yttrium:aluminum:garnet

1. Introduction

1.1. Background

Micelles belong to the group of molecular aggregates referred to as microheterogeneous systems. Upon dispersion of an appropriate concentration of surfactant and/or lipid molecules (with a long alkyl chain and a polar head group) in water, spherical micelles form. These organized structures have their hydrocarbon chains forming the inner hydrophobic core, while the polar head groups align themselves towards the water. Micelles have received much attention in many different scientific fields. It is well established that micelles catalyze a variety of thermal reactions.[1,2] One of the first studies reported the catalysis of the reaction of crystal violet with phenol blue.[3] Also, their use in the study of photochemical reactions has expanded research in this area. The use of micelles offers a number of advantages in the field of photochemistry.[4] Micelles are capable of solubilizing an organic molecule in aqueous solutions where it is otherwise nearly insoluble.

We have used this characteristic of micelles to selectively solubilize probe reactants inside a micellar cage. Other convenient characteristics of micelles for photochemical studies are that their solutions are clear and frequently exhibit no optical absorption at the monitoring wavelengths.[5]

Micelles are also considered to be the simplest organized structure.[5] As a result, they are utilized in many biological studies since they mimic some characteristics of biological structures. For example, they provide compartmentization as cell membranes do. As with proteins, their structure is influenced by hydrophobic interactions.[1] In general, the above systems are referred to as "organized systems", where there exists some degree of aggregation relative to the bulk.[5] As a result of this compartmentization, the kinetics of a chemical reaction can be very different from that in a homogeneous solvent. One difference is that an increased local concentration of the reactants can be obtained inside the micelle, which in turn can lead to an increase in the rate of a bimolecular reaction. In addition, the lifetime of the "cage" is longer than that in homogeneous solutions. One example is the effect of a micellar environment on the rate of the recombination of radicals through enhanced cage effects.[6,7] These effects will be discussed further on. Other applications of micelles include the enhancement of the rates of photodimerization and excimer formation.[5,8-10]

1.2. Micelles

Low concentrations of surfactant molecules such as fatty acids in aqueous solutions form monolayers on the water surface, with their hydrophilic head directed toward the water. At a threshold concentration, the monolayers begin to aggregate and form micelles. Above this specific concentration, often called the critical micelle concentration (CMC), micelles have nearly spherical structures. The relationship between the CMC and the micelle's concentration is given by Eq. 1.1,[4]

$$[M] = \frac{[\text{surfactant}] - \text{CMC}}{N} \qquad \textbf{Eq. 1.1}$$

where [M] is the micelle's concentration and N the aggregation number. The aggregation number is defined as the average number of surfactant molecules that make up the micelle.[4] It should be pointed out that the formation of micelles above the CMC from its monomers is a reversible process.[5] However, they can be considered to be static structures for the time scales seen in our studies (10^{-9}-10^{-6} s). It is reported that the rate of micellar breakup is in the range of ~10- 10^{3} s^{-1}.[11] In comparison, the entrance rates of neutral arenes are known to be almost diffusion controlled, while typical exit rates are of the order of 10^{4}-10^{6} s^{-1}.[12]

At and above the CMC, dramatic changes occur in such solution properties, such as viscosity, conductivity, and light absorption and/or scattering.[5] In fact, light scattering and fluorescence techniques are often used to measure the aggregation number of micelles, while conductimetry has revealed most of the available data for CMC's.[5] These measurements have also revealed that at much higher surfactant concentrations than the CMC, the shape of micelles changes from spherical (Figure 1.1) to rod-like (Figure 1.2) structures (taken from ref. [13]).

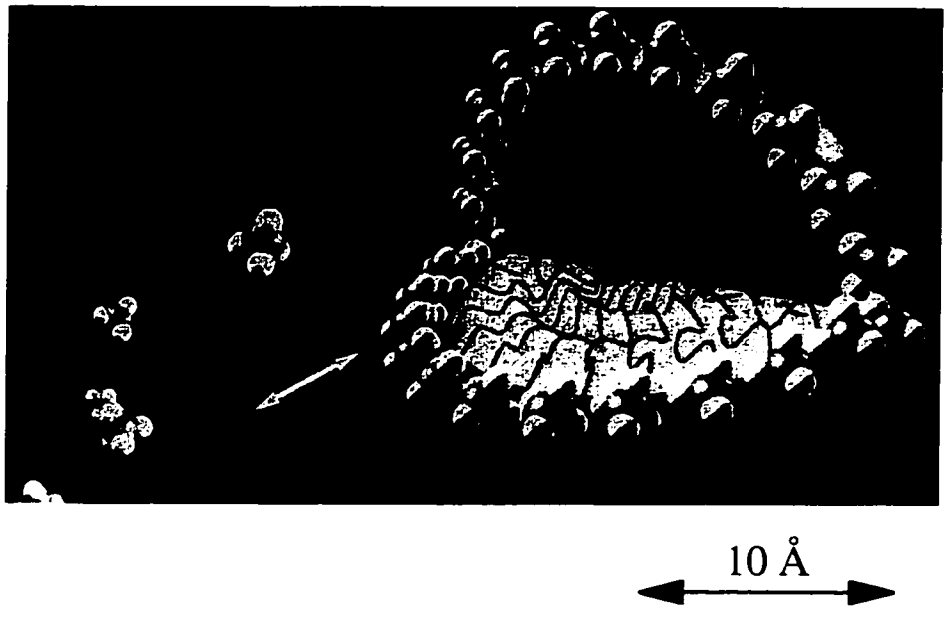

Figure 1.1. A representation of a spherical sodium dodecyl sulfate micelle.[13]

In general, a surfactant molecule consists of a hydrocarbon chain and a polar head group. The number of carbon atoms in the hydrocarbon chains ranges from 6 or 8 to 16 or more. The polar group may be

anionic, cationic, or nonionic.[5,8] The interior of the micelles used in our studies contains the hydrophobic chain part of the amphiphiles, while the polar head groups are located at the surface.

At concentrations near the CMC, the radius of the micelles used in this work is estimated to fall in the range of 15-30 Å.[5] However, both the size and the shape of micelles are known to depend on many factors, such as the size of the surfactant chain, temperature, solute concentration, ionic strength, and the electrical separation of head groups. In fact, it is found that the size of ionic micelles increases with the addition of electrolytes like NaCl. In contrast, temperature is found to mostly influence the size of the nonionic micelles.[14]

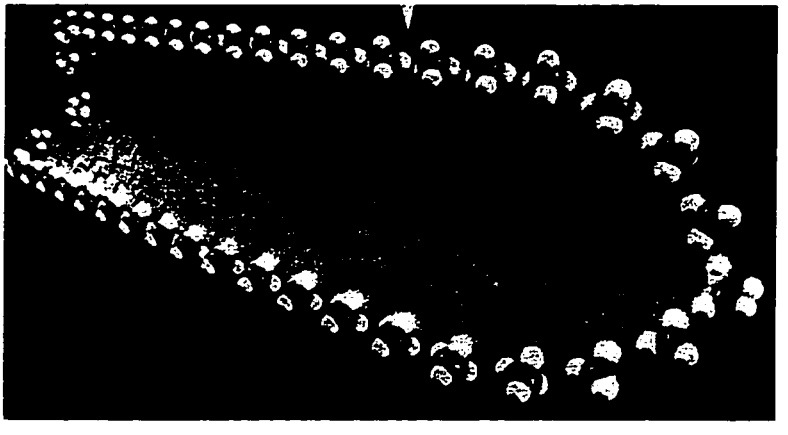

Figure 1.2. A representation of cylindrical sodium dodecyl sulfate micelle.[13]

We have used the anionic micelle, sodium dodecyl sulfate (SDS) with a CMC of 8.2 mM and aggregation number of 65,[11] as a host for confining a guest molecule in our studies of magnetic field effects on radical

dynamics. An average radius of 20-25 Å has been determined for SDS micelles by light scattering experiments.[15] Cetyl trimethyl ammonium chloride (CTAC) is an example of cationic micelles with a CMC of 1.3 mM and aggregation number of 113.[14]

1.3. Microemulsion systems

When surfactant molecules are mixed vigorously with emulsions of oil (O) and water (W), a turbid homogeneous solution is produced.[5] This milky solution is not useful in photochemical studies. However, this emulsion becomes transparent upon addition of a fourth component, the co-surfactant, such as a long-chain alcohol. The resulting clear solutions of aggregates with a radii of ~100 Å are called microemulsions.[5,8] A representative scheme of a microemulsion is shown below.

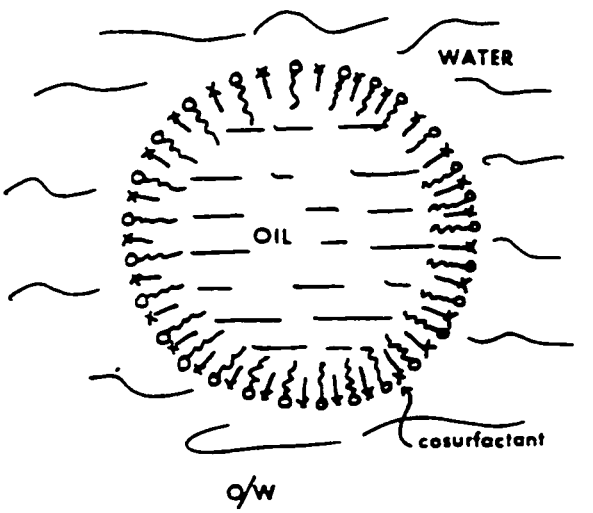

Figure 1.3. A simplified scheme of an oil-in -water microemulsion.[5]

In this scheme, the oil is the dispersed phase and water the continuous. It is hence labelled the O/W emulsion, so as to distinguish it from the water in oil type (W/O).[5]

Compared to micelles, microemulsions are far larger aggregates. In our studies, we use O/W emulsions which can solubilize hydrophobic molecules. As with the micelles, microemulsions are also known to catalyze several thermal reactions and facilitate photoinduced redox processes.[5,8] For example, the larger dimensions of a microemulsion allow for the adequate incorporation of chlorophyll in the surface region. Studies of the behaviour of chlorophyll with the added oxidants and reductants in microemulsions have been reported by Jones *et al.*[16] We have investigated the differences in the effects of magnetic fields on radical pair dynamics in microemulsions and micelles.

1.4. Proteins

Serum albumins have been studied and used as model proteins for measuring the binding of various drugs[17-20] and for conjugating with photosensitizers, such as α-terthienyl.[21] The molecular weight of both human- and bovine- serum albumin (HSA and BSA, respectively) is approximately 66,000 daltons.[22] Between pHs 5-8, the overall dimensions of HSA and BSA are estimated to be 38 X 150 X 30 Å[23,24]

and 40 X 140 X 30 Å,[22,24] respectively. Similar dimensions have been estimated by another group on the basis of only the primary sequence.[25] Both proteins comprise six homologous subdomains that compact to form a heart-shaped structure (see Figure 1.4, taken from the ref. [24]).

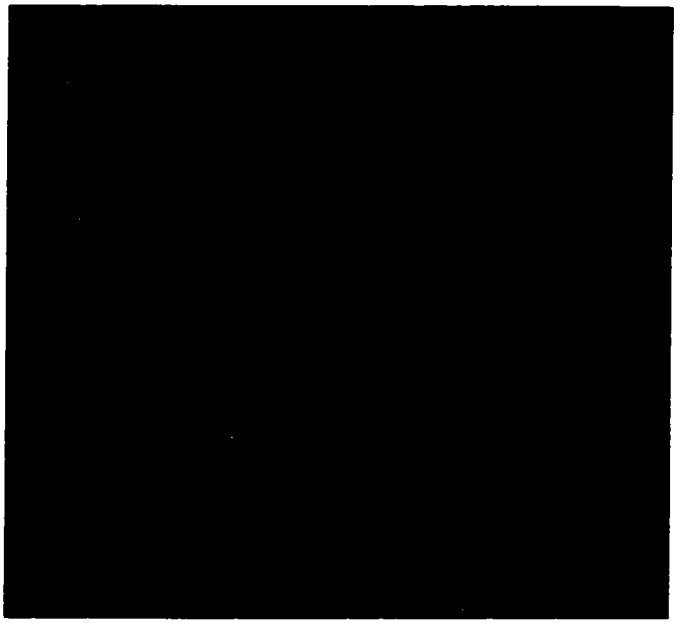

Figure 1.4. The three-dimensional structure of Human Serum Albumin.[24]

The presence of glutamic acid, aspartic acid, and lysine residues result in more than 200 positive and negative charges in both proteins, with a net overall charge of -18 at pH 7.[26] Bovine serum albumin is known to contain 19 tyrosine groups and 2 tryptophan groups, while HSA has 18 tyrosines and one tryptophan.[27] The UV absorption spectra of both proteins show a strong absorption at 280 nm due to the presence of the tryptophan groups.[28] When the proteins are excited at ~280 nm, they exhibit an emission maximum at around 340 nm, attributed to the

fluorescence of tryptophan. This fluorescence is quenched when various drugs and ligands are bound to the albumin.[29]

It is suggested that the albumins are folded in such a way that a hydrophobic interior is generated.[25] Thus, like micelles, they are able to solubilize hydrophobic molecules. We have used these proteins as a model system for biological systems in tests designed to measure the effect of magnetic fields on the behaviour of radical pairs generated by photolysis of an appropriate probe molecule in proteins.

1.5. Radical pair processes in "cages" and "super cages"

In a homogeneous liquid, solvent molecules serve as a "cage" for the reactive radical pairs (RPs). Organic compounds can be photo-dissociated to produce a geminate (born-together) radical pair (RP). Scheme 1.1 illustrates the Norrish Type I cleavage of a carbonyl compound.

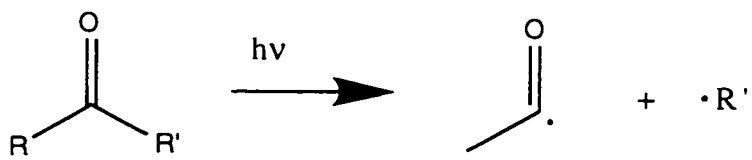

Scheme 1.1

The radical pairs generated in the above example can recombine to regenerate the precursor molecule in the ground state or disproportionate to yield other in-cage products.[7] The presence of a solvent cage, compared to the gas phase processes, leads to an increase

in the fraction of RPs that undergo recombination by retarding their separation.[30] Recombination and/or disproportionation of geminate RPs are often called cage reactions.[7] It is useful to also define a "cage effect" which can be determined by comparing the number of radical recombinations to the number of radical escapes from the cage.[31] There are, however, three types of RPs that can result from the above reaction in liquids. A primary geminate RP is the result of photodissociation of the precursor before either of the radicals has escaped the cage (i.e., $R^{\bullet}\ R'^{\bullet}$). A secondary geminate RP is formed from a re-encounter of solvent separated geminate pairs (i.e., $R^{\bullet} \mid R'^{\bullet}$). Lastly, a RP can be formed from the re-encounter of radicals that have already undergone random separation (i.e., a non-geminate pair).[7,32,33]

The lifetime of the solvent cage containing the primary RP is considered to be very short in liquids (10^{-9} - 10^{-11} s). The formation of a cage by secondary geminate pairs is found to occur on the time scale of ~10^{-8} s, while that by random radicals occurs in times >10^{-6} s.[32,34-37] These time scales are especially important when the dynamics of electron spin evolution of the RP are taken into consideration. A micellar aggregate is often referred to as a "supercage" host.[31] It has dimensions of tens of Angstroms which thus allow for multiple re-encounters of the geminate pair. It is found that the extent of cage reactions is greater for photolysis of an organic molecule in highly

viscous micelles than it is for that in a viscous solvent, due to a slow rate of radical separation.[40] Cage lifetimes are longer in micelles (~10^{-6} s) than in ordinary liquid solvents (~ 10^{-9} - 10^{-11} s).[31] The in-cage reactions in micelles are thus considered to be reversible, since the micellar boundary prevents radicals from diffusing too far apart. On the other hand, the escape processes in ionic micelles can be irreversible in the sense that the radicals escaping the micelle are being scavenged by an added radical scavenger that is only soluble in the aqueous phase.[7] The probability of recombination of RPs within a primary solvent cage is often reported as the cage effect. In fact, this method is a common one for evaluating the cage effect for RPs in a solvent cage. Thus, it is the competition between the reversible and the irreversible processes of radicals that determine the values of cage effects (*vide infra*).[7]

The dynamics of a reaction involving RPs is influenced by magnetic fields (MFs) due to the existence of radical spins, a property of the angular momentum of a particle. The spin state of a RP produced from a photochemical reaction is the same as that of the parent molecule.[7] This is known as Wigner's spin conservation rule.[38] A RP can either be a singlet (i.e., with antiparallel spins) and/or a triplet (i.e., with parallel spins) being generated from an excited singlet and/or triplet precursor, respectively. These types of RPs are called correlated pairs being produced by a precursor with a certain spin state.[7] Uncorrelated

RPs are formed by re-encounter of random RPs, each radical being in a doublet spin state.[7] Note that the formation of products from random encounters of the radicals is different from geminate encounters. Due to the need for the conservation of the overall spin angular momentum, it is concluded that the recombination of a reactive singlet RP is spin allowed and hence fast. However, triplet RPs are considered inert or unreactive, since the orientation of their electron spins forbids the two radicals to recombine.[7,30,39]

In the singlet spin correlated pair, the electron spins cancel each other leading to an overall spin angular momentum of zero. However, in the triplet spin correlated pair, the electron spins add up to give a spin angular momentum of one.[7] Thus, there are three different ways that the electron spin can orient itself in the presence of an MF. The projection of these spin orientations in space and that of the singlet state can be seen in Figure 1.5.[7]

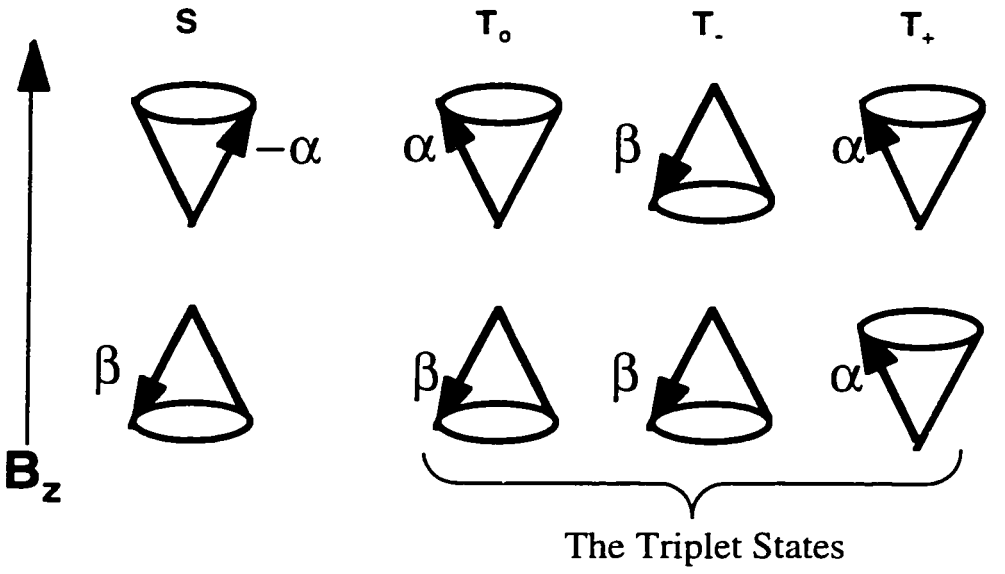

Figure 1.5. Vector model of the singlet and the triplet states of a radical pair.[7]

B_z is the MF axis determined by the strongest magnetic interactions experienced by the spins. The spin vectors precessing in the direction of B_z are α spins and those precessing opposite to B_z are β spins. Thus, $(\alpha\alpha)$, $(\beta\beta)$, and $(\alpha\beta)$ correspond to T_+, T_-, and T_0 components, respectively. The singlet state of the RP is designated by $(-\alpha\beta)$.[7] Note that the spin vectors of T_0 precess in phase while those of S are out of phase by 180^0. Thus, the $S \rightarrow T_0$ transition is induced by a mechanism that can rephase the spin vectors. However, a rephasing of the spin vectors cannot lead to transitions between T_+ and T_- to S. For such transitions to be possible, one of the spin vectors must flip with respect to the axis.[7] The vector representations of "spin rephasing" and "spin flip" are shown in Figure 1.10 and Figure 1.11, respectively, and will be explained later on.

The probability of triplet geminate recombination in a solvent such as benzene is found to be negligible.[31] The experimental values of the cage effects for 2,4-diphenyl-3-pentanone (DPP) and methyl-deoxybenzoin (MDB) are found to be close to zero in either benzene or acetonitrile.[41] The photolysis of DPP in alkyl sulfate micelles, however, leads to cage effects between 10% - 60%, depending on the size of the micelles.[42]

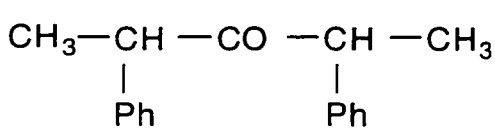

DPP

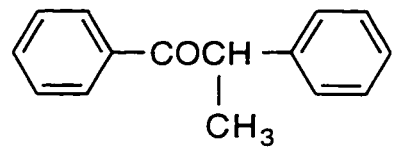

MDB

The values of the cage effect for benzyl RPs generated from the photolysis followed by decarbonylation of dibenzylketone (DBK) (see Scheme 1.2) and 4-methyl-DBK in CTAC micelles are found to be 31% and 52%, respectively.[31]

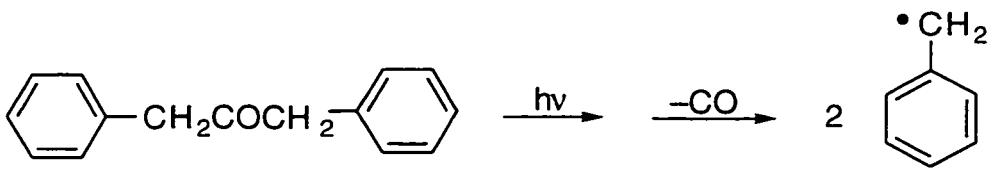

DBK

Scheme 1.2

The values of the cage effect for DBK (reported as the fraction of geminate benzyl RPs that recombine within the micelle) are determined by the scavenging method. Since some of the radicals

undergo escape, the exiting radicals can be scavenged by a radical quencher. As the CTAC micelles are cationic, a positively charged scavenger such as Cu^{2+} is used to trap the radicals that escape the micelle. Since the surface of CTAC micelles are also positively charged, due to the Coulombic repulsive forces the positively charged trapping agent remains in the aqueous phase only.[31] Therefore, those radicals that are outside the micelle can only be quenched. In these studies, it is also found that at sufficiently high concentrations of scavenger, the escape eventually becomes irreversible, as all the radicals escaping the micelle are being quenched.[31]

The photolysis of 1,2-diphenyl-2-methyl-propan-1-one (DPMP) has a value of ~4% for its cage effect in organic solvents such as benzene, acetonitrile, and dichloromethane, as compared to 30% for the same in CTAC micelles.[6] The values of the cage effects are also found to vary under the influence of an MF. It is found that an external MF of 200 gauss reduces the cage effect for DPMP from 30% to 20%.[6] This decrease has been attributed to the decoupling of the T_+ and T_- sublevels of the triplet RP from the singlet RP. This is why a MF can greatly affect the reactivity of reactions involving RPs through the control of ISC rates. At this point, a brief discussion of the origins of magnetic field effects (MFEs) and the different mechanisms of ISC of RPs must be undertaken.

1.6. Magnetic field effects on the behaviour of triplet radical pairs

Triplet RPs are commonly generated in either of two ways. In the first, triplet geminate RP produced by rapid α-cleavage of the triplet ketone (see Scheme 1.1) undergoes one of the following processes: it can either intersystem cross to the singlet state which is then followed by RP recombination and/or disproportionation or separate from its geminate partner and subsequently participate in free radical reactions with other molecules.[7] However, in the case of the Norrish Type I photoreaction of DBK shown in Scheme 1.2 the loss of CO is solvent-dependent with rate constants ranging from 5 X 10^6 to 1 X 10^7 s^{-1}.[43,44] Therefore, the nature of the RPs at a given time following pulsed excitation depends on the rate of CO loss.

In the second, an aromatic ketone such as benzophenone can be photochemically excited into a singlet state, typically 76 kcal mol^{-1} above the ground singlet state. The singlet state of benzophenone, with a lifetime of about 10^{-11} s, efficiently undergoes intersystem crossing (ISC) to produce the triplet state which lies 69 kcal mol^{-1} above the ground state.[45] For benzophenone both the singlet and the triplet states are (n,π^*) states. One unpaired electron is in the non-bonding orbital of the oxygen atom. The other unpaired electron is in the antibonding π^* orbital, which is delocalized over the carbonyl group.[45] Aromatic ketones with low lying (n,π^*) states are known to be very reactive

towards hydrogen abstraction reactions and usually exhibit radical-like behaviour.[45] Hence, benzophenone is easily photoreduced in the presence of a hydrogen-donating molecule to produce a triplet RP as an intermediate.[39] The photochemistry of benzophenone in the absence[46-49] and presence[50-52] of a hydrogen donor in micelles has been studied extensively.

The triplet RP produced in the photoreaction of benzophenone with an added hydrogen donor leads to ground state products (see Scheme 1.3).[53] The main products of this reaction in both homogeneous solutions[45,54] and in micelles[50,51] are often called pinacols in the literature. However, small traces (1-2%) of a para-coupling (or ortho-coupling) product is also produced. This product shows a strong absorption at 320 nm and consequently is called a "light absorbing transient" (LAT) (see Scheme 1.3).[45,50,51] A commonly used hydrogen donor is 1,4-cyclohexadiene.[51,56] In fact, triplet benzophenone undergoes hydrogen abstraction reaction with 1,4-cyclohexadiene with 94% efficiency and a rate constant of 2.7 X 10^8 M^{-1} s^{-1} at 26 ^{0}C in benzene.[56]

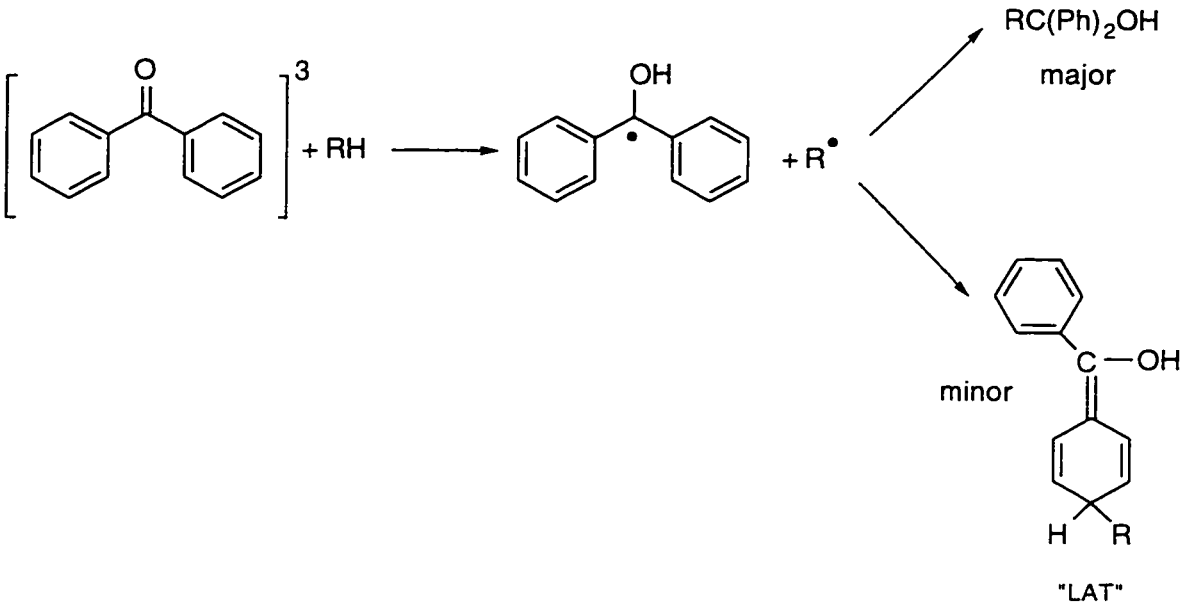

Scheme 1.3. The photoreduction of triplet benzophenone by a hydrogen donor.[55]

Photolyzing benzophenone in the presence of [SDS] = 0.22 M and [1,4-cyclohexadiene] ≥ 0.024 M leads to a triplet lifetime of ~20 ns; in the absence of the hydrogen donor the lifetime is ~320 ns.[51] Triplet benzophenone leads to the formation of a correlated triplet RP consisting of a ketyl and a cyclohexadienyl radical, R˙ (see Scheme 1.3).

A typical transient absorption of the ketyl radical is shown in Figure 1.6. The decay of the ketyl radical corresponds to two processes. The first part is a fast decay due to geminate recombination processes, while the second part is a slow component of the decay due to the escape processes. This escape process leads to the loss of the geminate character and possibly to radical-molecule reactions.

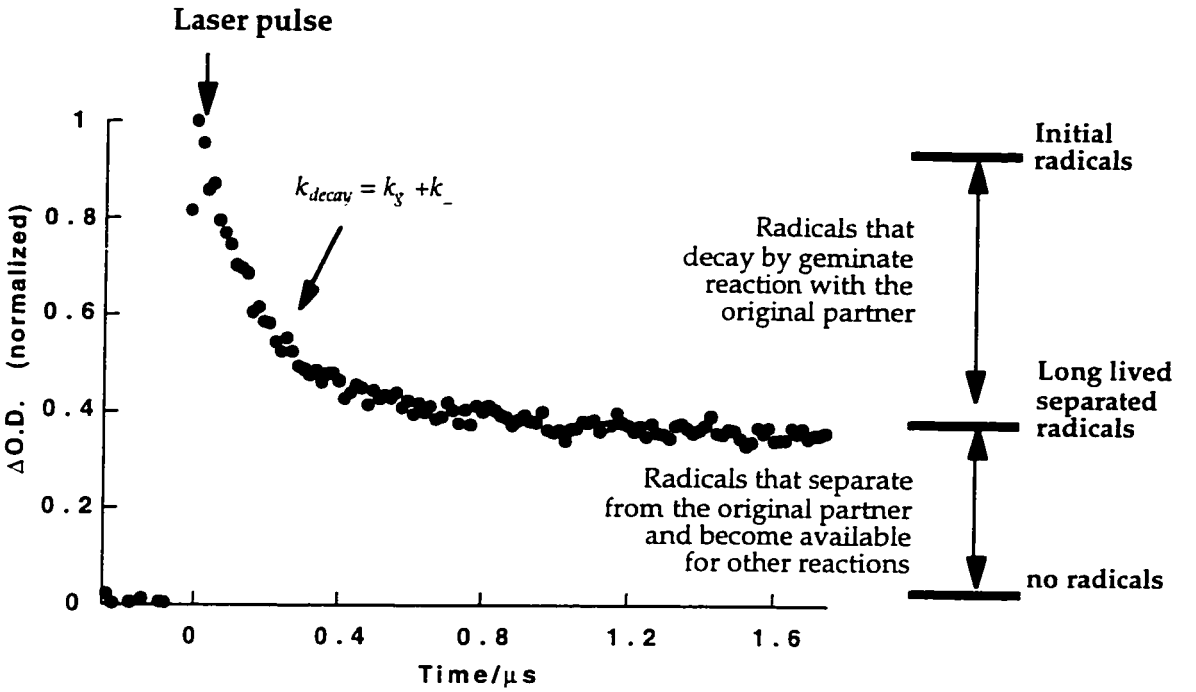

Figure 1.6. A typical transient absorption decay observed upon 308 nm laser excitation of benzophenone in the presence of 0.032 M 1,4-cyclohexadiene in 0.2 M SDS monitored at 545 nm.

Thus, going from homogeneous systems, i.e., solvents, to heterogeneous systems, i.e., micelles, the geminate character of triplet RPs is maintained for a longer period of time, up to 10^{-6} s.[7] The consequence of a longer cage lifetime is a balanced competition between the escape processes and the ISC of the triplet RP into the singlet state.[7]

Application of an external MF lowers the rate of geminate recombination by decoupling the S state of the RP from the $T_{\pm}$ sublevels. As a result, as the MF strength increases, the fraction of radicals that escape from the micelle also increases.

1.7. The radical pair mechanism

Reports and experiments related to studies of MFEs on the kinetics of chemical reactions date back to the late 1920s.[57] However, the major understanding of the influence of MFs on reaction kinetics began with the introduction of nuclear and electronic spin polarization phenomena in 1967.[58,59] The chemically induced nuclear polarization (CIDNP) and chemically induced electron polarization (CIDEP) are two useful methods for characterizing the mechanisms of reactions involving RPs. The radical pair mechanism, which originated from the above phenomena, is the key to our understanding of the MFEs on chemical yields and rates of reactions involving RPs. However, it should be emphasized that these phenomena apply to two radical centers interacting in a cage, constituting a RP, and not to a single free radical.[60] In the radical pair mechanism, the triplet-singlet ISC of a RP is affected by a MF, which causes the nuclear spin levels of the RP to become polarized. This polarization, in turn, leads to the removal of the degeneracy between the S and T states. Note also that the magnetic interaction can be due to the hyperfine interactions between the electron and nuclear spins, which in turn leads to the observation of polarization at zero MF.[61] The polarization effect was first observed in the NMR lines of reactions of RPs exhibiting both enhanced absorption and emission characteristics.[58,59,62] This mechanism, which applies to RPs as opposed to free radicals, works well at MFs $\leq$ 23 kgauss.[63]

As stated earlier, the probability of recombination of a RP depends on the spin multiplicity of the RP. It is the spin-dependency of a RP recombination that can give rise to the observation of MFEs in radical reactions. The effect is maximized when the geminate radicals are in a confined region, so that the probability of their recombination with each other is much higher than with other radicals. Another contributing factor is that the two partners of the RP should be able to diffuse apart within the confinements of the cage, without losing their geminate character. During this period of time, the nuclear spin may then operate on the radical spin, resulting in a competitive process between the processes of radical recombination and radical escape.[7,30] These competitive processes can be seen in the reaction mechanism of Scheme 1.4.

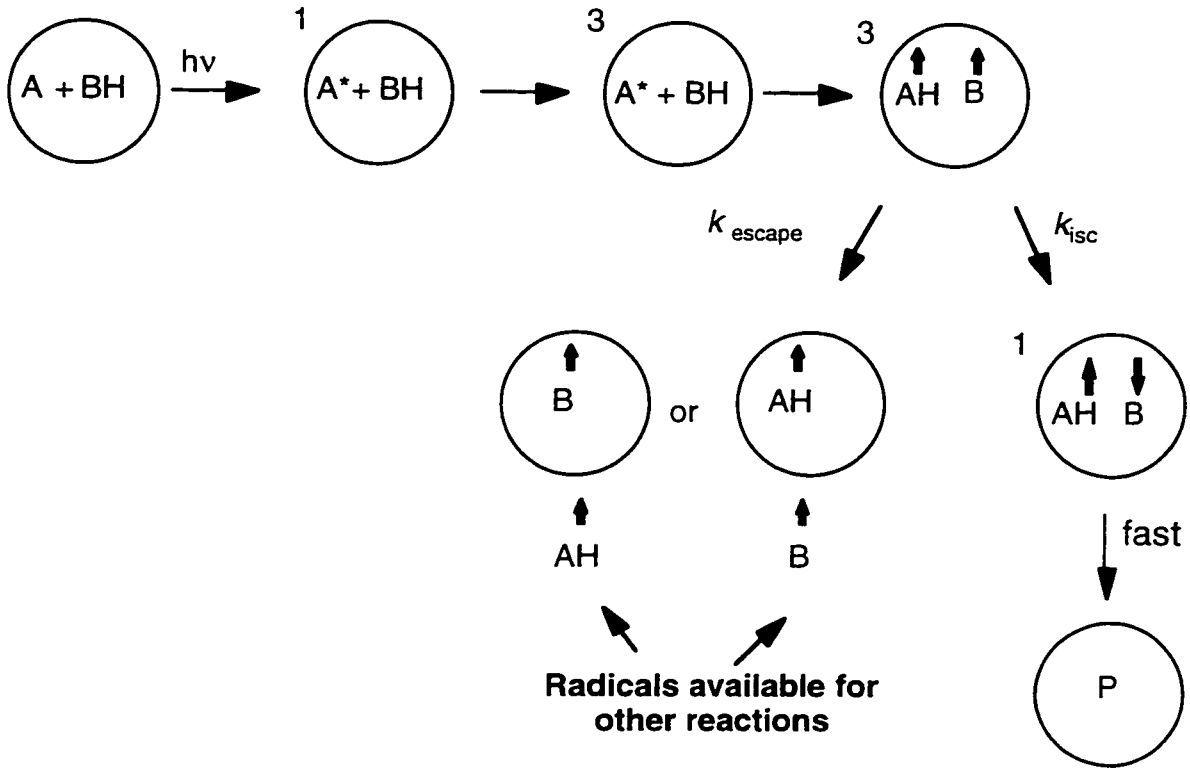

Scheme 1.4. Primary reaction steps following photoreduction of a ketone (A) in the presence of a hydrogen donor (BH) in a micelle.

Two unpaired electron spins in a cage coexist long enough, up to 10^{-6} s, to undergo spin evolution. This change in the spin character with time is due to mainly three mechanisms, which arise from the interaction of the radical spin with a MF (either external or internal).[30] These mechanisms are collectively called ISC mechanisms in a RP. Upon application of an external MF, the operation of the nuclear spin on the radical spins leading to ISC between triplet and singlet states of RPs can be influenced greatly.[7]

The term magnetic effect, in general, refers to the effects produced on the rates of radical reactions by either an external MF or an internal MF

induced by a nuclear spin (hyperfine coupling, HFC).[30] A magnetic field influences S↔T transitions in both geminate and random RPs.[7]

The internal magnetic forces can be separated into two categories. The first is the interaction of the MF associated with the spin angular momentum and the MF associated with the orbital motion of the same electron in the electrostatic field of a nucleus. This interaction or force is called the spin-orbit coupling (SOC), and it contributes to the total electronic angular momentum. In the absence of an external applied field, the second arises when the electrons on two different radicals experience local fields arising from nearby magnetic nuclei. This coupling is the origin of the hyperfine interactions (HFI) which can lead to the flipping of an electron spin.[7,30,64] Each of these internal magnetic forces can lead to ISC between the singlet and the triplet states. They will be discussed separately in the following section.

1.8. The intersystem crossing mechanisms of radical pairs

Before discussing the different ISC mechanisms, a very important interaction, which leads to the splitting of the triplet energy levels and thus influences spin dynamics, must be first introduced. It is an interaction between the two radical centers called the exchange interaction, J. Although non-magnetic, it influences the rates of spin evolution in an indirect way. In other words, the energy gap between S

and T is given by 2J as seen in the energy diagram of the lone singlet and the three triplet levels in the presence of a MF (see Figure 1.7).[7,60]

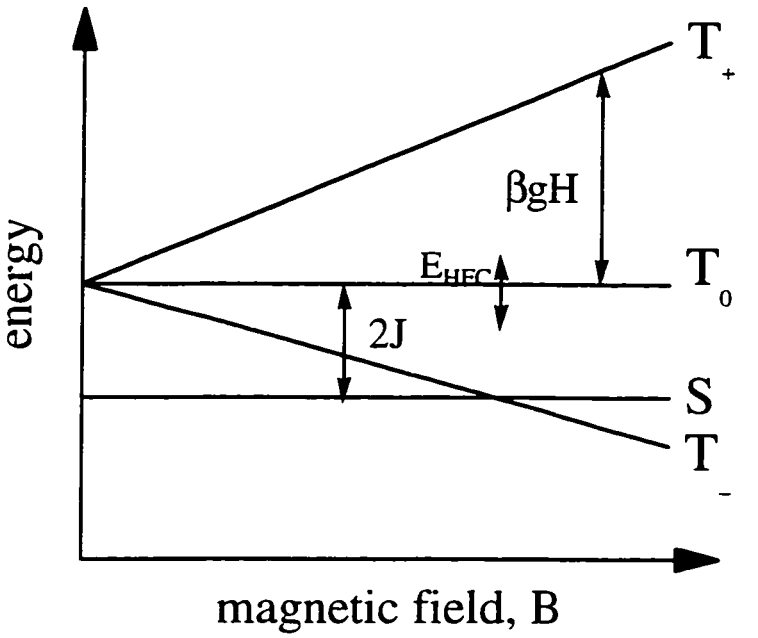

Figure 1.7. The energy diagram of the electronic spin states of a radical pair in a magnetic field.[60]

In the absence of a force stronger than J (i.e., 2J> E_{HFI}), the initial multiplicity is retained as a result of the tendency of the exchange interaction to energetically split the triplet sublevels from the S state. This columbic interaction can thus inhibit ISC from the S state to T levels. It should be noted that the value of J is distance-dependent and decreases very rapidly as the pair separates (see Figure 1.8).[7] Therefore, an MF, producing very small energy differences (e.g., 100 gauss $\approx 10^{-5}$ kcal mol^{-1}), can compete with exchange interactions only when the RP

is well separated. This separation distance of the RP is estimated to be around 8-10 Å.[7]

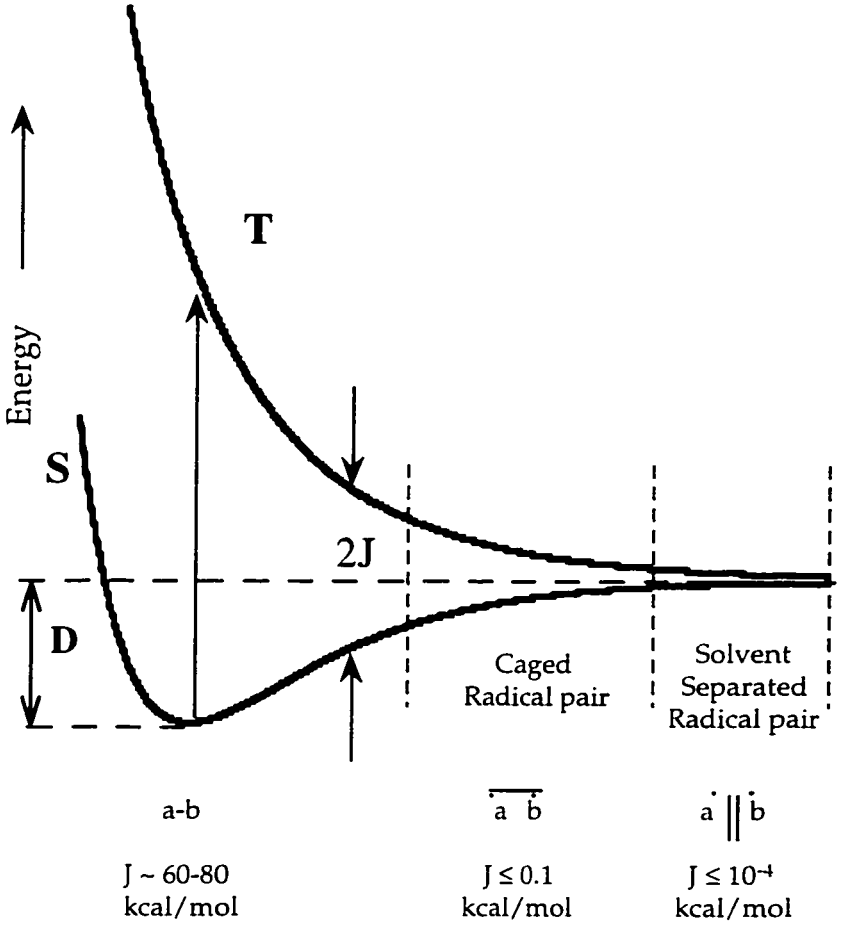

Figure 1.8. A representative scheme of the exchange interaction (J) of an electron pair localized in a bond between a and b.[7]

The first mechanism of RP ISC in the absence of an external MF is due to SOC, which is the interaction between the spin angular momentum and the orbital angular momentum. It is the MF associated with each of these angular momenta that gives rise to SOC.[7] This type of interaction is known to be important in two situations. One is when the electron density or atomic number associated with the atom is high.

In other words, the presence of heavy atoms (such as sulfur) enhances SOC, which in turn accelerates ISC between the singlet and the triplet.[65] This results in the quenching of MFEs usually observed in heterogeneous media.[65] Spin orbit coupling is also significant when a strong interaction between the two radical centers exist either through space or through bonds. Thus, SOC becomes the dominant mechanism when the orbitals of the two centers overlap appreciably. This situation usually happens when the two radical centers are in the same molecule (such as in short chain biradicals). There also exists a strong exchange interaction between them at the same time due to significant overlap. Therefore, the large J value tends to inhibit ISC by breaking the degeneracy of the S-T levels.[7,30] It should be also noted that the distance-dependent exchange interactions are found to be very small in micelles of size $\geq C_{12}$.[42] In a recent study using time-resolved electron paramagnetic resonance spectroscopy, Forbes reported the value of the exchange interaction to be ~1 gauss for the photoexcitation of benzophenone-d_{10} in SDS micelles.[66] In general, ISC due to SOC is not as important in the case of carbon centered RPs, as it is for short chain biradicals.[7]

The second mechanism also involves the internal magnetic forces. In the absence of an MF, the triplet sublevels are nearly degenerate. It is the HFI that promotes ISC from the S state to T sublevels or vice versa (see Figure 1.9).[30] The hyperfine interaction occurs between the

magnetic moment of an unpaired electron and the magnetic moment of a nearby nucleus. This interaction, which leads to the precession of angular momentum under a torque, can change the orientation of the electron spins between parallel and anti-parallel alignments.

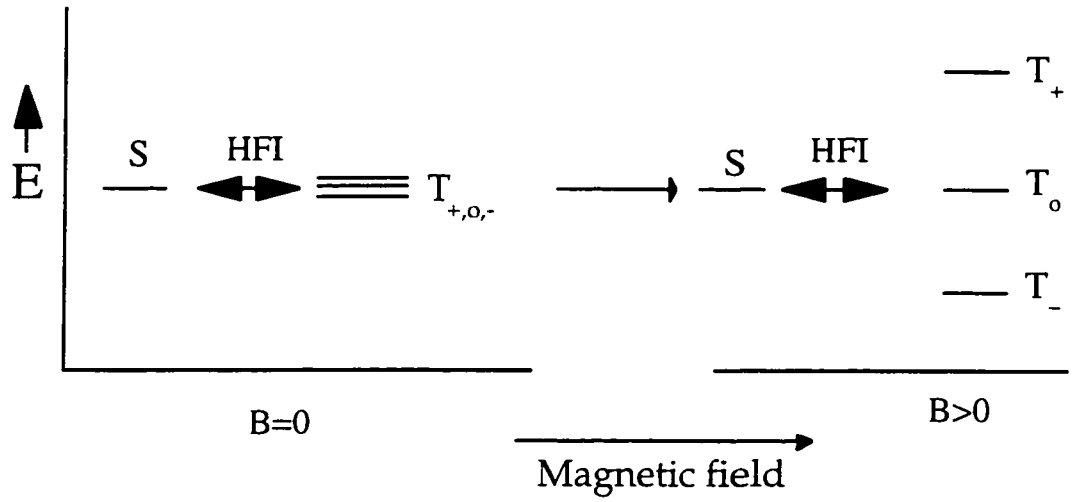

Figure 1.9. The energy diagram representation of the hyperfine interaction in the absence and presence of a magnetic field.[30]

As the MF strength increases and exceeds the ΔE_{HFI} (see Figure 1.7 and Figure 1.9), S can mix only with the T_0 sublevel through the HFI. This transition is called the "spin rephasing" transition.[64] A vector representation of this transition can be seen in Figure 1.10.

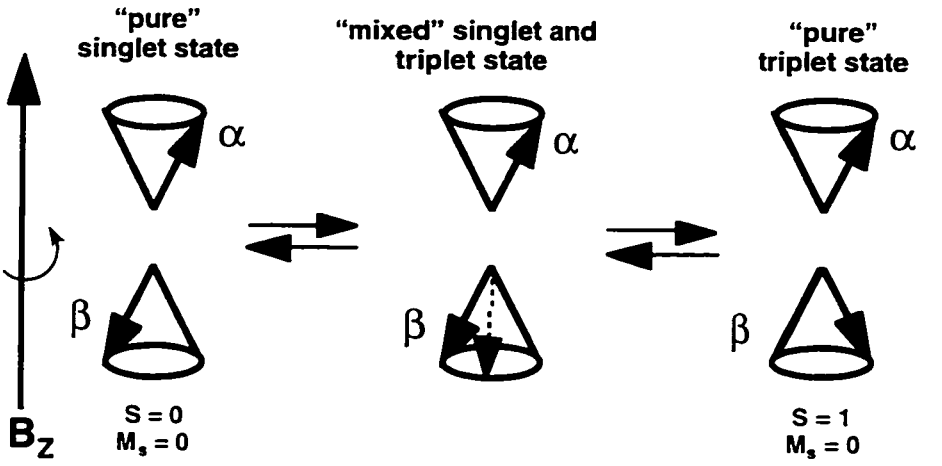

Figure 1.10. The vector representation of the "spin rephasing" mechanism.[64]

A MF generated by a nucleus results in a torque causing the β spin to undergo "spin rephasing" converting a pure triplet to a pure singlet.[64]

The last mechanism of spin evolution is due to the interactions with external MFs through the Zeeman effect. The energy splitting due to the Zeeman effect is given by the following equation.[64]

$$\Delta E = \beta g \bar{B} \qquad \text{Eq. 1.2}$$

Where $\bar{B}$ is the MF strength, β the Bohr magneton (9.274×10^{-24} J T^{-1}) and g a spectroscopic splitting factor with a value of roughly 2.00 for the free electron and for most organic radicals.[30]

As the strength of an applied MF increases, the Zeeman splitting of the triplet sublevels becomes larger than the ΔE_{HFI}, and they cease to be degenerate with the S state. This means that the $T_{\pm}$ sublevels do not

participate in ISC. However, if $2J > E_{HFI}$, no singlet and triplet interconversion can occur (see Figure 1.7). Thus, at MFs > 0 there is a competition between the internal MFs and the applied MFs for the control of the orientation of the electron spin vectors. The vector representation of this transition, called "spin-flip", is shown below.[64]

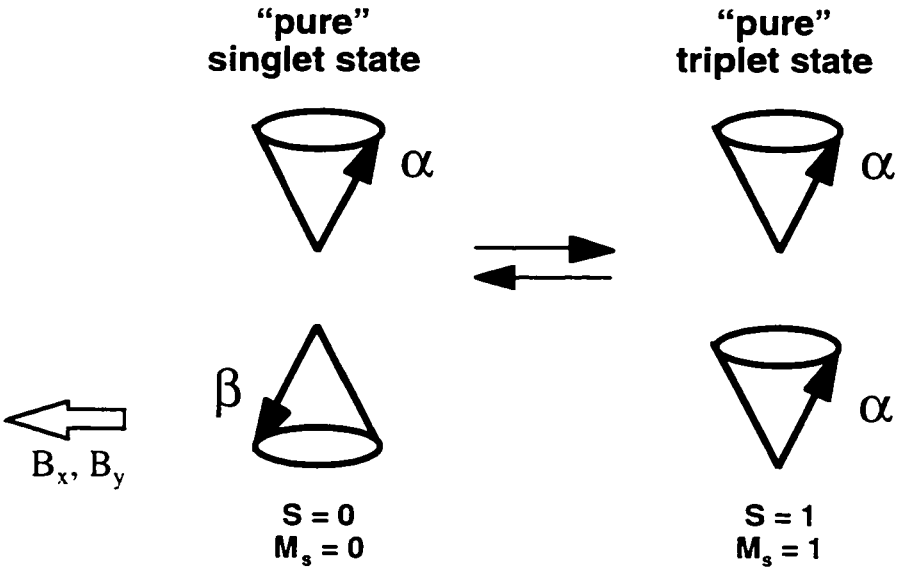

Figure 1.11. The vector representation of "spin-flip"mechanism.[64]

In this case, T_+ (or T_-) can be interconverted into S by a force from a torque coming from MFs in the xy plane. The change in the electron spin is usually accompanied by a change in nuclear spin, so that the total spin angular momentum of electrons and nuclei remains conserved. Consequently, the interconversion is an allowed process.[64]

The three ISC mechanisms summarized above are considered to be mostly important for reactions involving spin correlated RPs. The MF

strength also plays a major role in the determination of the appropriate ISC mechanism. It should be emphasized that extremely high field strengths (i.e., > 20 kgauss) are not necessary to produce large magnetic effects in RP reaction rates. The Zeeman effect is the most important ISC mechanism for field strengths of 100-1000 gauss. The HFC is responsible for ISC in the RPs at low field strengths (10-100 gauss)[30] and in the absence of an MF. In the case of RPs confined in micelles with cross-section dimensions of ≥20 Å (e.g., SDS and CTAC micelles), the exchange interactions can be considered very small and the S and T_0 are (nearly) degenerate.[67]

Thus, both the local fields associated with the nuclei and an external MF can affect the ISC rate of a spin correlated RP. When the RPs are confined in a supercage, they have a long residence lifetime due to their lower mobility within the micelles's highly viscous interior. Also, depending on the nature of the radicals, the need to exit into the aqueous phase and to separate from their partner is high for the more hydrophilic radicals. Consequently, a fast geminate recombination process is in competition with a slower decay due to the reactions of the escaped radicals. A MF influences these two processes by affecting the rate of ISC.

1.9. Magnetic field effects on the behaviour of singlet radical pairs and on those generated by random encounters

The examples discussed so far involve triplet RPs. As shown in Figure 1.8, the potential energy surface of the triplet state is dissociative. Hence triplet RPs are unreactive. Also, as they separate, the exchange interaction becomes weaker and the two S and T surfaces thus become closer.[7] Triplet RPs confined in supercages can separate within the boundaries of the cage and retain their geminate character for a long time (~10^{-6} s) before escaping the cage. (see Scheme 1.4). During this time, the triplet RP would have enough time to undergo many re-encounters and spin evolution. A MF decreases the rate of geminate recombination and increases the fraction of radicals that escape the cage irreversibly. In conclusion, the nature of the radicals, the size, and the viscosity of the micelles, which provides the extent of the RP diffusion, along with the time scales of the ISC mechanisms are the main factors determining the rate-determing step of the reaction.[7]

The situation is clearly different when the RP is formed in the singlet state. Unlike the triplet RPs,[39,55,68-71] few studies of the MFEs on the reactions of singlet RPs[72-74] have been carried out in heterogeneous systems. The in-cage radical recombination of singlet RPs occurs on the nanosecond time scale. Thus, the role of a MF on the control of rates of recombination and escape is not as significant as it is on triplet RPs. That is, the rate-determining step is mainly the geminate reaction. In

order to observe a MFE on the behaviour of the singlet RP, the rate of the geminate recombination should be comparable with that of the spin evolution. These requirements are met when nitroxide radicals react with stable carbon-centered radicals.[75] In particular, the reaction of 2,2,6,6-tetramethylpiperidine N-oxide radical (TEMPO) with resonance stabilized radicals (such as the benzyl radical) is found to occur with rate constants lower than the diffusion limit. For example, the singlet RP can be formed instantaneously upon excitation by a nanosecond laser pulse (Scheme 1.5). However, the recombination reaction (Scheme 1.6) occurs with a rate constant ~9 X 10^7 $M^{-1}s^{-1}$ in acetonitrile.[76,77]

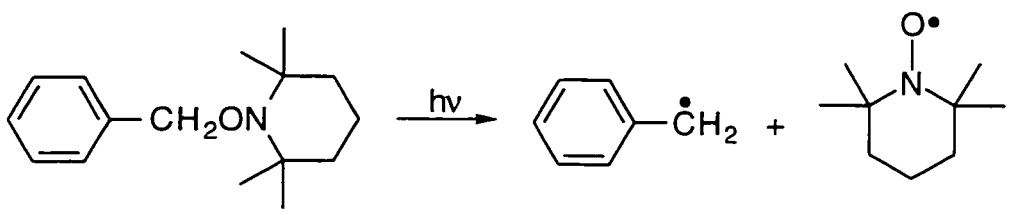

Scheme 1.5

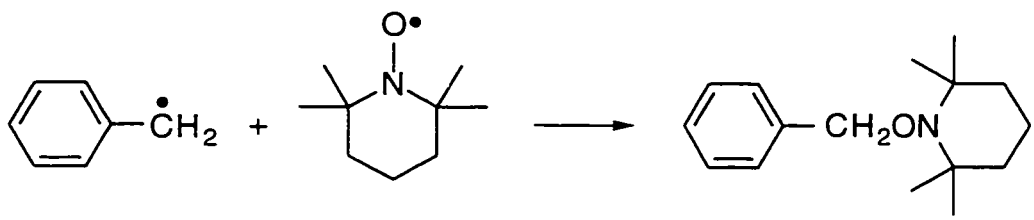

Scheme 1.6

The lifetime of the RP in the SDS micelles is even longer (250 ns).[75] As discussed earlier, the longer residence time of the RPs in supercages is a requirement for radical recombination and radical escape processes to compete and for MFEs to be appreciable. The observed decay of this RP

(Scheme 1.6) in SDS micelles exhibits two decay components also seen with triplet RPs. The decay consists of a fast initial process, the geminate recombination of the primary singlet RPs, followed by a slower process, the recombination of random RPs after the geminate pair has separated.[75]

In the presence of an MF with a strength of 1300 gauss, the RP decays with a rate constant of 5.1 X 10^6 s^{-1}, as compared to 3.9 X 10^6 s^{-1} in the absence of a field.[75] One can explain this effect using arguments similar to those presented for triplet RPs. The reactive singlet RP can intersystem cross to the triplet, since they are degenerate in the absence of an applied MF. In the presence of MFs, the Zeeman splitting between the T sublevels increases, thus leading to $S \rightarrow T_0$ conversion only.[75] Consequently, the observed decay of the RP in the presence of an MF is accelerated due to the fewer number of RPs interconverting into an unreactive T state.

In addition to the singlet and triplet RPs, MFs are found to influence the kinetics of RPs generated by random encounters.[78] In this study, the Norrish Type I reaction of DBK, shown in Scheme 1.2, was examined. The MFEs on RPs formed by random encounters are particularly relevant in biological systems,[78,79] since it is anticipated that most RPs in biology are a result of random radical-radical encounters rather than geminate pairs. Spin statistics predicts that the

random radical-radical encounters lead to the triplet spin state 75% of the time, while the remaining 25% lead to the singlet spin state.[78] In this case, the effect of a MF is found to have a strong influence on the dynamics of the recombination reaction of the singlet RPs. That is, the triplet pairs cannot react with each other to yield ground state products, unless they undergo spin evolution.

By analyzing the kinetic behaviour of the self-reaction of benzyl radicals both in the absence and presence of an external MF, the same conclusions can be made for the random encounters as for the geminate RPs. That is, there exists a competition between the two processes of geminate recombination and escape that control the extent of the observed effects. The decay of the benzyl-benzyl RP via random encounters follows second-order kinetics. This decay occurs on long time scales (i.e., 50-100 μs), when geminate recombination is already over and does not contribute to the overall decay.[78] On the other hand, the rate depends on the rates of escape processes which also occur on long time scales, as discussed earlier in the case of geminate RPs undergoing escape from micelles. A MF strength of 200 gauss is found to cause a 44% reduction in the rate of the self-reaction of benzyl radicals in SDS micelles.[78]

In an earlier study of the same system carried out in 1982,[80] no significant MFE was observed on this decay. However, the new results,

obtained with improved laser techniques and interpreted with a better understanding of the radical processes that occur in heterogeneous systems, are the first to show the effects of MFs on the decay of the random radical encounters.[78]

The above studies indicate that the occurrence of MFEs in organized systems are not limited to the presence of triplet RPs. Reactions involving singlet RPs and random radical encounters may also be influenced by an MF. In particular, random reactions affected by an MF may be significant in biological systems where radical reactions are mostly due to random encounters. The concentration of free radicals can be controlled by radical-radical reactions that eventually regulate the radical-molecule reactions. The occurrence of radical-molecule reactions (compared with radical-radical) in biological systems can further cause damage to different cellular components. However, more studies of radical-mediated biological processes under the influence of an MF are needed in the future.

1.10. References

(1) Muller, N. In *Reaction Kinetics in Micelles*; E. Cordes, Ed.; Plenum Press: New York, 1973.

(2) Fendler, J. H.; Fendler, E. J. *Catalysis in Micellar and Macromolecular Systems*; Acedemic Press: New York, 1975.

(3) Duynstee, E. F. J.; Grunwald, E. J. *J. Am. Chem. Soc.* **1959**, *81*, 4540.

(4) Bohne, C.; Redmond, R. W.; Scaiano, J. C. In *Photochemistry in Organized and Constrained Media*; V. Ramamurthy, Ed.; VCH Publishers: New York, 1991; pp 79.

(5) Thomas, J. K. *Chem. Rev.* **1980**, *80*, 283.

(6) Turro, N. J.; Mattay, J. *Tetrahedron Lett.* **1980**, *21*, 1799.

(7) Turro, N. J. *Pure Appl. Chem.* **1981**, *53*, 259.

(8) Kalyanasundaram, K. *Photochemistry in Microheterogeneous Systems*; Academic Press: New York, 1987.

(9) Förster, T. In *The Exciplex*; M. Gordon and W. R. Ware, Eds.; Academic Press: New York, 1975; pp 1.

(10) Turro, N. J.; Cox, G. S.; Paczkowski, M. A. *Top. Curr. Chem.* **1985**, *129*, 57.

(11) Aniansson, E. A.; Wall, S. N.; Almgren, M.; Hoffmann, H.; Kielmann, I.; Ulbricht, W.; Zana, R.; Lang, J.; Tondre, C. *J. Phys. Chem.* **1976**, *80*, 905.

(12) Almgren, M.; Grieser, F.; Thomas, J. K. *J. Am. Chem. Soc.* **1979**, *101*, 279.

(13) Huo, Q.; Margolese, D. I.; Ciesla, U.; Demuth, D. G.; Feng, P.; Gier, T. E.; Sieger, P.; Firouzi, A.; Chmelka, B. F.; Schüth, F.; Stucky, G. D. *Chem. Mater.* **1994**, *6*, 1176.

(14) Leigh, W. J.; Johnston, L. J. In *Handbook of Organic Photochemistry*; J. C. Scaiano, Ed.; CRC Press: Boca Raton, Florida, 1989; Vol. II; pp 401.

(15) Missel, P. J.; Mazer, N. A.; Benedek, G. B.; Carey, M. C. *J. Phys. Chem.* **1983**, *87*, 1264.

(16) Jones, C. E.; Mackny, R. A. *J. Phys. Chem.* **1978**, *82*, 63.

(17) Jusko, W. J.; M., G. *Pharmacokin Drug Metabol. Rev.* **1976**, *5*, 43.

(18) Gibaldi, M. *Am. J. Med.* **1977**, *62*, 471.

(19) Anton, A. H.; Solomon, H. M. *Ann. N.Y. Acad. Sci.* **1973**, 226.

(20) Vallner, J. J. *J. Pharm. Sci.* **1977**, *66*, 447.

(21) Boch, R.; Mohtat, N.; Lear, Y.; Arnason, J. T.; Durst, T.; Scaiano, J. C. *Photochem. Photobiol.* **1996**, *64*, 92.

(22) Squire, B. G.; Moser, P.; O'konski, C. T. *Biochemistry* **1968**, *7*, 4261.

(23) Hughes, W. L. In *The Proteins*; H. Neurath and R. Bailey, Eds.; Academic Press: New York, 1954; pp 633.

(24) Min He, X.; Carter, D. C. *Nature* **1992**, *358*, 209.

(25) Brown, J. R. In *Albumin Structure, Function, and Uses*; V. M. Rosenoer, M. Oratz and M. A. Rothschild, Eds.; Pergamon: Oxford, 1977; pp 27.

(26) Peters, T. In *The Plasma Proteins: Structure, Function, and Genetic Control*; 2nd ed.; F. W. Putnam, Ed.; Academic Press: New York, 1975; pp 133.

(27) Herskovits, T. T. *J. Biol. Chem.* **1962**, *237*, 2481.

(28) Steinhardt, J.; Krijin, J.; Leidy, J. G. *Biochemistry* **1971**, *10*, 4005.

(29) Chignell, C. F. In *Drug Fate and Metabolism. Methods and Techniques*; E. R. Garrett and J. L. Hirtz, Eds.; Marcel Dekker: New York, 1976; pp 187.

(30) Molin, Y. *Spin Polarization and Magnetic Effects in Radical Reactions*; Elsevier: New York, 1984.

(31) Turro, N. J.; Weed, G. C. *J. Am. Chem. Soc.* **1983**, *105*, 1861.

(32) Noyes, R. M. *J. Am. Chem. Soc.* **1955**, *77*, 2042.

(33) Noyes, R. M. *J. Am. Chem. Soc.* **1956**, *78*, 5486.

(34) Koenig, T.; Fischer, H. *Free Radicals*; Wiley: New York, 1973; Vol. V. 1.

(35) Kaptein, R. *Adv. Free-Radical Chem.* **1975**, *5*, 381.

(36) Frank, J.; Rabinowich, E. *Trans. Faraday Soc.* **1934**, *30*, 120.

(37) Rabinowich, E.; Wood, W. C. *Trans. Faraday Soc.* **1936**, *32*, 1381.

(38) Buchachenko, A. L. *Russ. J. Phys. Chem.* **1977**, *51*, 1445.

(39) Scaiano, J. C. *Trans. Roy. Soc. Canada* **1983**, *21*, 133.

(40) Turro, N. J.; Mattay, J. *J. Am. Chem. Soc.* **1981**, *103*, 4200.

(41) Baretz, B. H.; Turro, N. J. *J. Am. Chem. Soc.* **1983**, *105*, 1309.

(42) Tarasov, V. F.; Ghatlia, N. D.; Buchachenko, A. L.; Turro, N. J. *J. Am. Chem. Soc.* **1992**, *114*, 9517.

(43) Lunazzi, L.; Ingold, K. U.; Scaiano, J. C. *J.Phys.Chem.* **1983**, *87*, 529.

(44) Turro, N. J.; Gould, I. R.; Baretz, B. H. *J. Phys. Chem.* **1983**, *87*, 531.

(45) Scaiano, J. C. *J. Photochem.* **1973/74**, *2*, 81.

(46) Sakaguchi, Y.; Nagakura, S.; Hayashi, H. *Chem. Phys. Lett.* **1980**, *72*, 420.

(47) Sakaguchi, Y.; Nagakura, S.; Minoh, A.; Hayashi, H. *Chem. Phys. Lett.* **1981**, *82*, 213.

(48) Hayashi, H.; Sakaguchi, Y.; Nagakura, S. *Chem. Lett.* **1980**, 1149.

(49) Lougnot, D.; Jacques, P.; Fouassier, J. P. *J. Photochem.* **1981**, *17*, 75.

(50) Scaiano, J. C.; Abuin, E. B. *Chem. Phys. Lett.* **1981**, *81*, 209.

(51) Scaiano, J. C.; Abuin, E. A.; Stewart, L. C. *J. Am. Chem. Soc.* **1982**, *104*, 5673.

(52) Scaiano, J. C.; Lougnot, D. J. *J. Am. Chem. Soc.* **1984**, *88*, 3379.

(53) Turro, N. J.; Kraeutler, B. *Acc. Chem. Res.* **1980**, *13*, 369.

(54) Chilton, J.; Giering, L.; Steel, C. *J. Am. Chem. Soc.* **1976**, *98*, 1865.

(55) Scaiano, J. C.; Abuin, E. B.; Stewart, L. C. *J. Am. Chem. Soc.* **1982**, *104*, 5673.

(56) Encinas, M. V.; Scaiano, J. C. *J. Am. Chem. Soc.* **1981**, *103*, 6393.

(57) Bhatagnar, S. S.; Mathur, R. N.; Kapur, R. N. *Phils. Mag.* **1929**, *8*, 457.

(58) Kaptein, R. *Chem. Commun.* **1971**, 732.

(59) Kaptein, R.; Fráter-Schröder, M.; Oosterhoff, L. J. *Chem. Phys. Lett.* **1971**, *12*, 16.

(60) Steiner, U. E.; Ulrich, T. *Chem. Rev.* **1989**, *89*, 51.

(61) Ward, H. R.; Lawler, R. G.; Loken, H. Y.; Cooper, R. A. *J. Am. Chem. Soc.* **1969**, *91*, 6251.

(62) Kaptein, R. *J. Am. Chem. Soc.* **1972**, *94*, 6251.

(63) Kaptein, R.; Hollander, J. A. d. *J. Am. Chem. Soc.* **1972**, *94*, 6269.

(64) Turro, N. J. *Proc. Natl. Acad. Sci. USA* **1983**, *80*, 609.

(65) Autrey, T.; Devadoss, C.; Sauerwein, B.; Franz, J. A.; Schuster, G. B. *J. Phys. Chem.* **1995**, *99*, 869.

(66) Forbes, M. D. E. *The Spectrum* **1995**, *8 (Summer issue)*, 1.

(67) Closs, G. L. In *Chemically Induced Magnetic Polarization;* A. R. Lepley and G. L. Closs, Eds.; John Wiley & Sons: 1973; pp 95.

(68) Bittl, R.; Schulten, K.; Turro, N. J. *J. Chem. Phys.* **1990**, *93*, 8260.

(69) Evans, C. H.; Scaiano, J. C.; Ingold, K. U. *J. Am. Chem. Soc.* **1992**, *114*, 140.

(70) Gould, I. R.; Zimmt, M. B.; Turro, N. J.; Baretz, B. H.; Lehr, G. F. *J. Am. Chem. Soc.* **1985**, *107*, 4607.

(71) Taraban, M. B.; Leshina, T. V.; Salikov, K. M.; Sagdeev, R. Z.; Molin, Y. N.; Margoiskaya, O. I.; Vyazankin, N. S. *J. Organomet. Chem.* **1983**, *256*, 31.

(72) Baumann, D.; Ulrich, T.; Steiner, U. E. *Chem. Phys. Lett.* **1987**, *137*, 113.

(73) Shokhirev, N. V.; Korolenko, E. C.; Taraban, M. B.; Leshina, T. V. *Chem. Phys.* **1991**, *154*, 237.

(74) Weller, A.; Staerk, H.; Treichel, R. *Faraday Discuss. Chem. Soc.* **1984**, *78*, 271.

(75) Korolenko, E. C.; Cozens, F. L.; Scaiano, J. C. *J. Phys. Chem.* **1995**, *99*, 14123.

(76) Beckwith, A. L. J.; Bowry, V. W.; Ingold, K. U. *J. Am. Chem. Soc.* **1992**, *114*, 4983.

(77) Bowry, V. W.; Ingold, K. U. *J. Am. Chem. Soc.* **1992**, *114*, 4992.

(78) Cozens, F. L.; Scaiano, J. C. *J. Am. Chem. Soc.* **1993**, *115*, 5204.

(79) Scaiano, J. C.; Cozens, F. L.; McLean, J. *Photochem. Photobiol.* **1994**, *59*, 585.

(80) Turro, N. J. *Tetrahedron* **1982**, *38*, 809.

2. Laser Techniques and Experimental Setup

2.1. Instrumentation

The laser facilities of the University of Ottawa are specifically designed for the studies of short-lived intermediates. This lab is equipped with two nanosecond flash photolysis systems which can use any one of the following lasers: EX 530 Lumonics excimer (308 nm, XeCl), EX 510 Lumonics excimer (248 nm, XeF), a Molectron UV-24 nitrogen (337 nm), and two Surelite Nd:YAG lasers with adjustable wavelengths of 266, 355, and 532 nm. The pulse duration of these lasers are < 10 ns.

This lab is also set up for flash photolysis on picosecond time scales. The laser is an active/passive mode-locked Continuum PY-61 Nd:YAG delivering a pulse length of ~35 ps with powers of 3-5 mJ / pulse at 1064 nm. The detection system for absorption consists of a pump and probe setup and an optical multichannel analyzer (OMA, from Princeton

Instruments) which provides the transient absorption spectra. This system is also set up for time-resolved emission spectroscopy using a CCD streak camera from Hamamatsu.

A brief description of the nanosecond laser flash photolysis (LFP) setup used for the studies of radical reactions in the presence of an MF will be presented next, followed by a more complete description of the picosecond facilities as they have yet to be described to any great extent by others. A very detailed description of the nanosecond LFP has been explained in earlier reports[1,2] and recently in the thesis[3] of A. Berinstein.

2.1.1. Nanosecond laser flash photolysis

The word laser is an acronym for "light amplification by stimulated emission of radiation." Lasers operate by using a general principle that was originally implemented for microwave frequencies, where it was called "microwave amplification by stimulated emission of radiation", or maser action. Lasers generate or amplify coherent radiation at a broad range of frequencies, such as infrared (IR), visible, and ultraviolet (UV). In addition, lasers emit or amplify radiation with remarkable properties of directionality, spectral purity, and intensity.

Electronically excited states are commonly produced by absorption of a photon of visible or UV light. Thus, the laser provides the excitation

source. Short-lived intermediates or transient species involved in a photophysical or photochemical process can be detected using the technique of LFP. The time resolution of this technique depends on the duration of the pulse. Information concerning the elementary steps of a chemical reaction on the time scale of their occurrence have relied heavily on time-resolved laser spectroscopic methods of detection. The use of pulsed lasers for studying fast reactions enables the investigator to measure the rate of the reaction accurately, since the half-life of the reaction is usually longer than the duration of the pulse. A condition that greatly facilitates the study of any fast reaction is that the generation of a particular intermediate species should be initiated in a time shorter than the decay processes. Moreover, in order to obtain any mechanistic information, changes in the physical parameters must be associated with these decay processes.

The monitoring beam is provided by a 150 W Xenon lamp. This beam is required to be first concentrated and then passed through the small pin hole (1-2 mm) on the sample cell holder. After passing through the sample, the beam is focused onto the slit of a monochromator which selects the monitoring wavelength. The photons are then detected and converted into an electrical signal by a photomultiplier tube (PMT). This voltage signal is then captured by a Tetronix 2440 digital oscilloscope which is interfaced to a Power Macintosh computer with

the LabVIEW software program. A diagram of a typical nanosecond LFP setup equipped with a magnet can be seen in Figure 2.1.

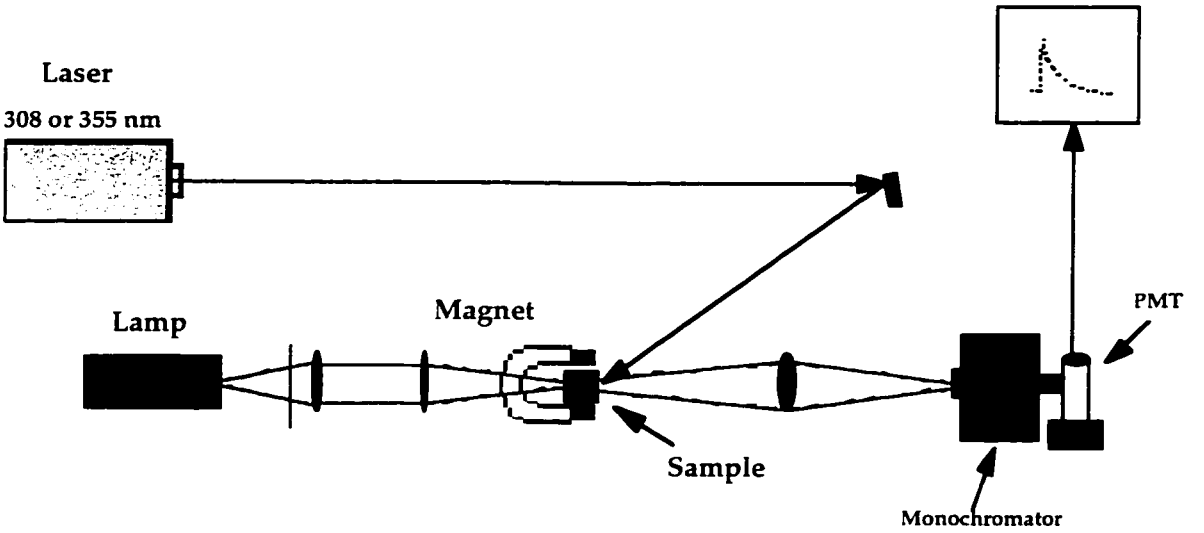

Figure 2.1. Schematic diagram of a 308 nm or a 355 nm nanosecond laser system equipped with a magnet.

The various components of the LFP system are coordinated by a line synchronizer through a series of transistor-transistor link pulses. These pulses originate at the same point on a 60 Hz AC sine wave leading to the proper time sequence of events in an LFP experiment (see Scheme 2.1).

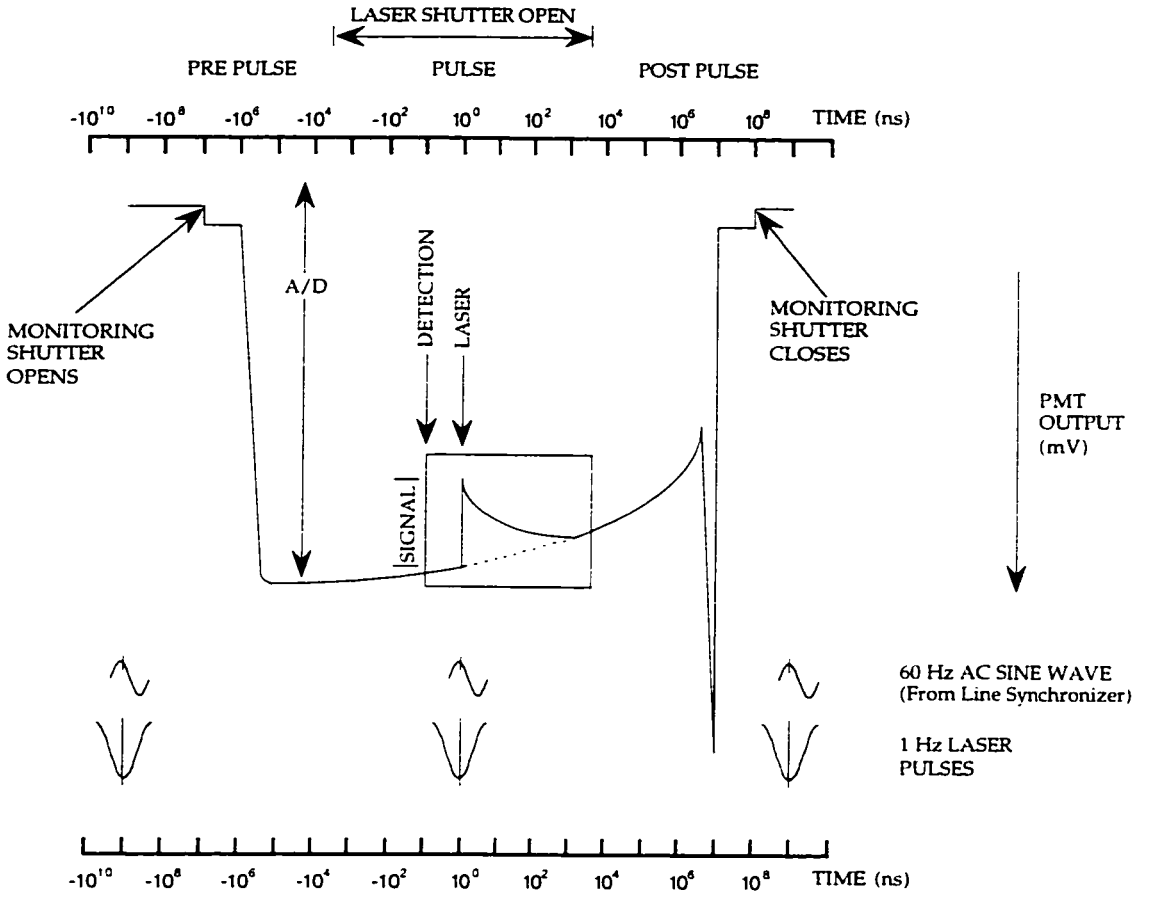

Scheme 2.1. Plot of PMT output versus time for a period from one second before to one second after a laser pulse.[3]

The intensity of the monitoring beam (I_0) representing the baseline and the electrical signal from the PMT (shown above in the small box) can be converted to a change in the optical density (ΔO.D.) of the sample by the following equation.[4]

$$\Delta O.D. = -\log\left(1 - \frac{Signal}{I_0}\right) \qquad \text{Eq. 2.1}$$

The strong intensity of the laser pulse is capable of generating a relatively high concetration of transients (up to 50 μM). The optimum

concentration of the precursor of interest must be such that its ground state absorption at the excitation wavelength is around 0.3 or that it falls in the range between 0.2-0.4. At optical densities greater than 0.4, unwanted shock waves or a concentration gradient of transient species might occur.

The nanosecond LFP is capable of detecting those phenomena that occur on time scales between 20 ns to <100 μs. The excitation beam can be directed to the sample at either 90^0 or at smaller degrees (~15^0 - 20^0), also referred to as "front-face", with respect to the monitoring beam. For the 90^0 setup, the ground state absorption of sample should not exceed 0.3, thus minimizing its complete absorption of excitation light before an overlap with the monitoring beam has occurred. The advantage of having a smaller angle is that it allows for a higher signal-to-noise ratio. This is convenient when the laser beam is not very intense. Thus, the optical absorption of the chromophore can be greater than 0.3 at the laser wavelength when the alignment is "front-face".[4] Note that with this arrangement the laser light is always overlapping with the monitoring beam.

For LFP experiments involving use of the magnet, the 90^0 alignment of the excitation beam with the sample is impossible since the magnet, surrounding the area of the sample holder, would block the beam.

Therefore, the beam has to be directed at the sample in the "front-face" alignment (see Figure 2.1).

2.1.2.The DC field setup

For DC fields, a homemade magnet powered by a Xantrex XKW 3000 watts DC power supply or a Hewlett-Packard 6282A power supply can be used. The former power supply, with an output of 150 Volts/20 Amps, is capable of producing DC field strengths of up to 10 kgauss, while the latter provides a maximum DC field of up to 1.5 kgauss. The power supplies also have an internal GPIB interface for easy computer control. For zero-field experiments, the magnet can be moved away from the region of the sample holder (see Figure 2.1). The field strength was independently calibrated with a gaussmeter by both A. Thansandote of the Radiation Protection Bureau of Health Canada and by A. Simard in our laboratory.

2.1.3. The AC field and the AC+DC field setup

Figure 2.2 shows the time dependence of an alternating MF. The horizontal axis indicates the time (60 Hz = 16.67 milliseconds), while the vertical axis represents the strength of the current. In our experiments, a maximum AC MF strength of 350 gauss is employed. An alternating current of the type shown below follows a sine wave. In these experiments, the decay of the ketyl radical is monitored at

different points of a 60 Hz oscillating MF. It should also be noted that the process being monitored, on each point throughout the cycle, occurs in much faster times (~10^{-9} - 10^{-6} s) than the time duration of the 60 Hz cycle (~10^{-2} s).

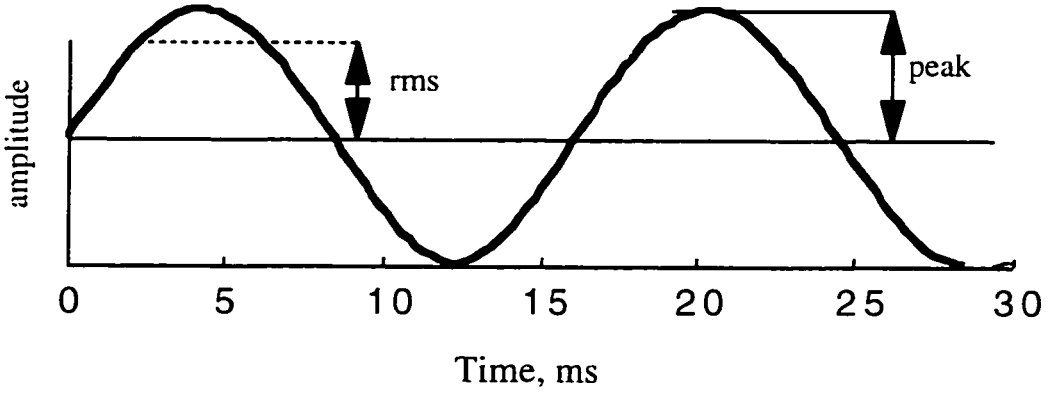

Figure 2.2. Time dependence of a 60 Hz oscillating wave.

In order to obtain each AC decay trace, the time at which the laser fires is synchronized with the beginning of a 16.67 ms cycle of a 60 Hz oscillating MF. The time at which the firing of the laser occurs, at zero oscillating field, is defined as the zero time (t_d = 0). Using a Stanford delay unit (model 535), the firing of the laser is then set for different delay times, relative to the zero time, along the 60 Hz cycle.

To produce AC fields, a capacitor, with a suitable resonance at 60 Hz, is added to the magnet in series. The reason for the addition of the circuit to the magnet is to minimize its reactance. The current is determined by the circuit resistance. The voltage drop accross the coil and the

capacitor is equal because they are 180^0 out of phase and thus cancel each other.

The 60 Hz cycle can be generated by a synthesizer and amplified to drive the magnet. A simple diagram of the circuit and the magnet, with its internal resistance, is shown below.

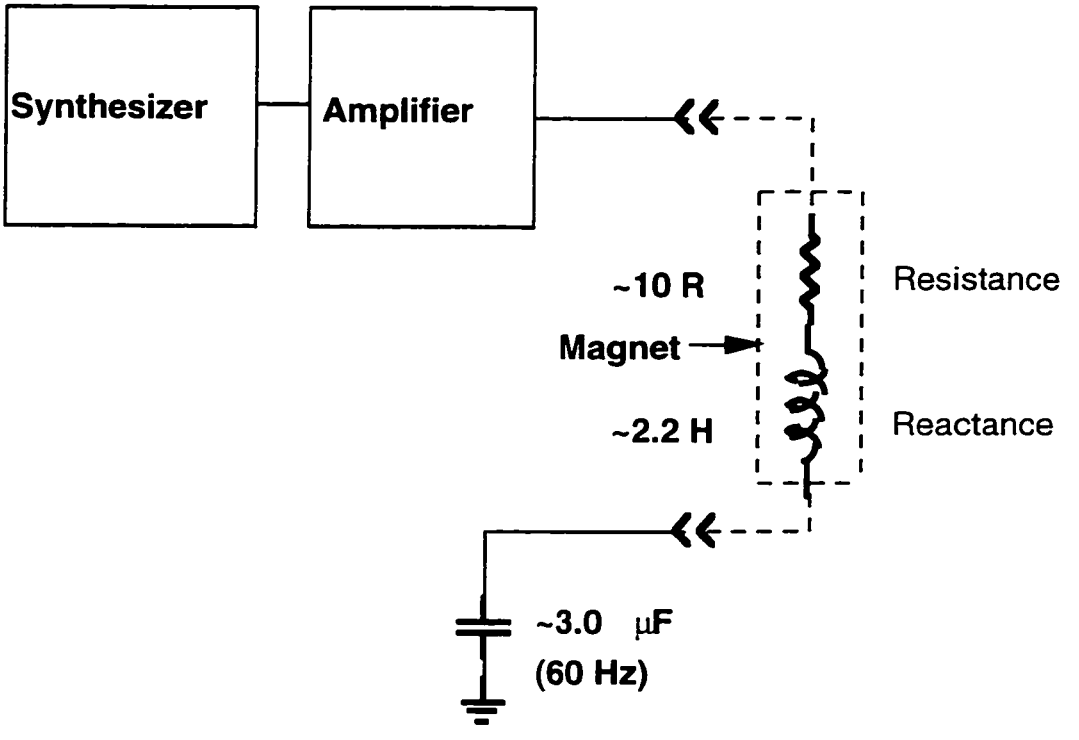

Figure 2.3. Schematic diagram of the AC field circuit and the magnet with its internal resistance shown.

To add the DC offset to the AC signal, a floating power supply and an inductor are added to the magnet in parallel. The inductor is selected so that its reactance at 60 Hz is large enough (>10 H) compared to that of the magnet. The following diagram shows this setup. Note that the inductor is shown with its internal resistance.

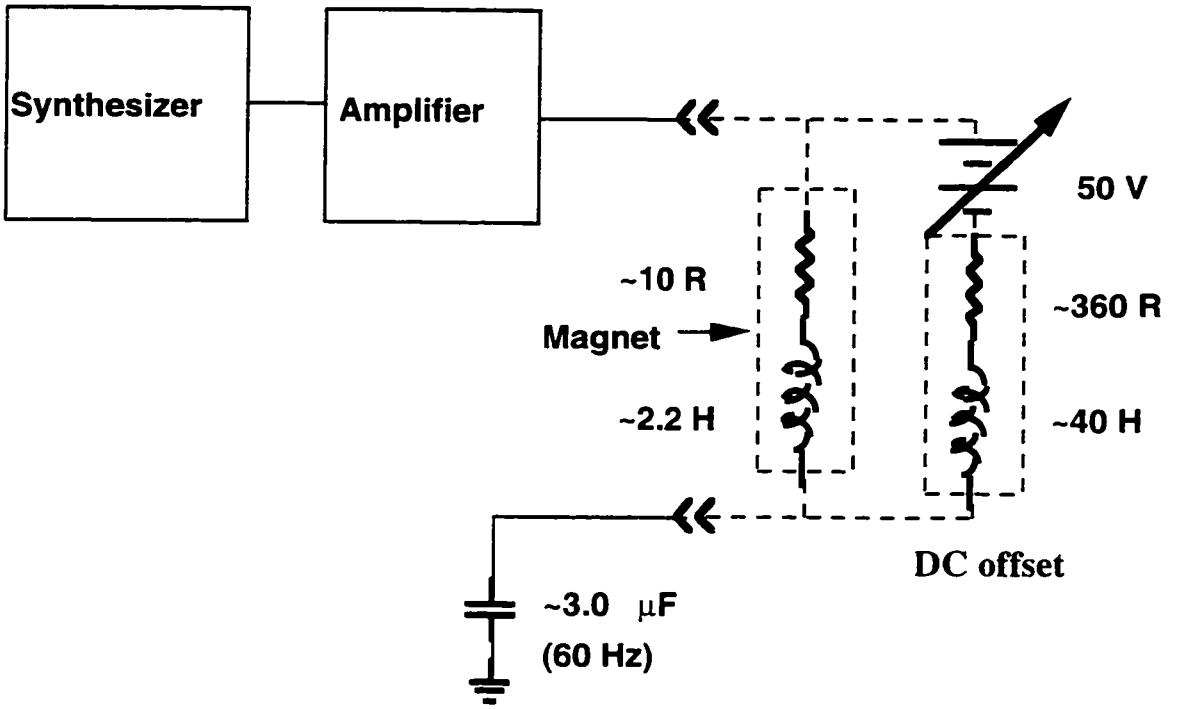

Figure 2.4. Schematic diagram of the AC field circuit with the added DC offset. The magnet and the inductor are shown with their internal resistance.

2.1.4. Picosecond laser flash photolysis

Picosecond spectroscopy is a powerful technique which uses mode-locked lasers for studying fast reactions. Picosecond LFP techniques allow for the direct observation of chemical processes that are as short as 10^{-12} s. On this time scale, sufficient time resolution exists for studying complex mechanisms of important chemical and biological reactions in far greater detail than was previously possible. In addition to the identification of the transient species, their formation and decay kinetics can be measured at specific wavelengths in order to describe chemical change by means of picosecond emission and absorption.[5]

The frequency spectrum of a laser is governed by the emission profile of the lasing medium and by the characteristics of any wavelength selective elements in the laser cavity. However, only discrete frequencies (ω_n), longitudinal modes, are allowed to oscillate in the laser cavity.[6] The frequency separation of these modes is given by the following equation

$$\omega_{n+1} - \omega_n = \frac{\pi c}{L} = \omega = 2\pi\nu \qquad \text{Eq. 2.2}$$

where L is the length of the optical path between the mirrors and c is the speed of light. Thus, those longitudinal modes with sufficient gain to lie above the lasing threshold constitute the emission spectrum of the laser. The relative phases (Φ_n) of the modes should be locked in order to prevent random variation in the intensity of the laser resulting from random interference between modes. This fixation of the modes, called mode locking, leads to the production of an optical electric field with a period[7]

$$T = \frac{2L}{c} \qquad \text{Eq. 2.3}$$

where T is the cavity round-trip time of the train of pulses (see Figure 2.5, taken from ref. [7]).

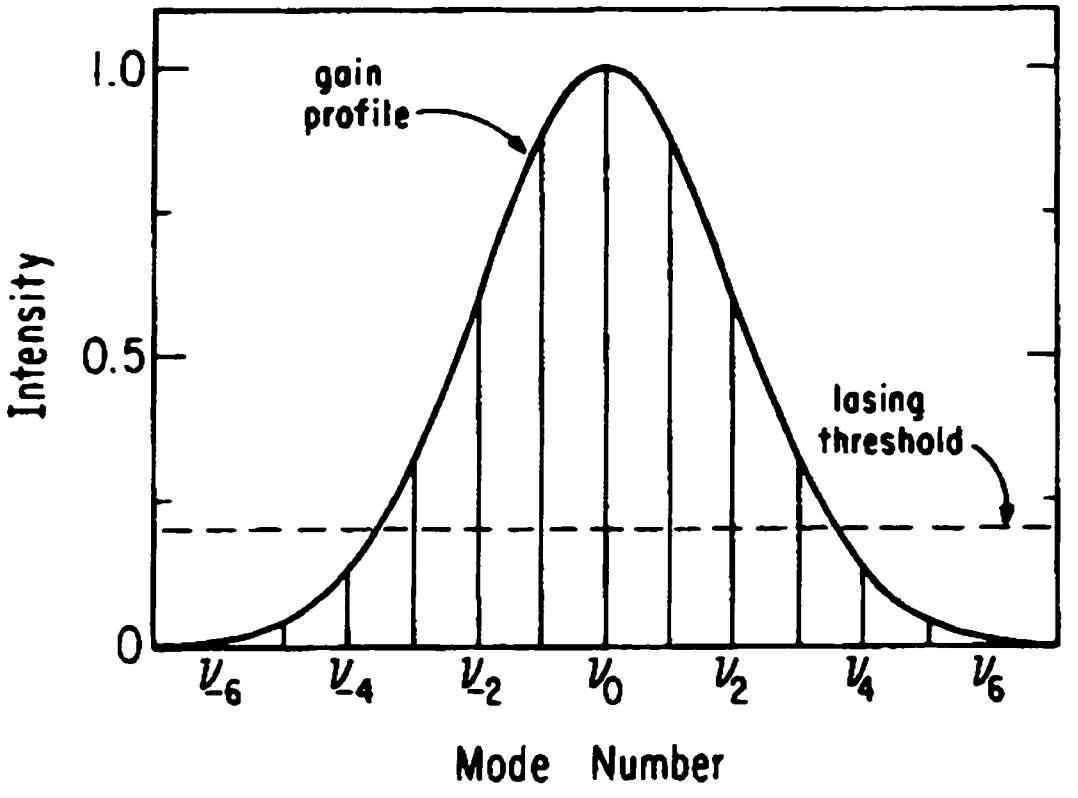

Figure 2.5. Longitudinal modes in a laser cavity. The line marked "lasing threshold" indicates the intensity where gain and loss are equal.[7]

The pulse width is given by the following equation[7]

$$\tau = \frac{T}{N} \qquad \text{Eq. 2.4}$$

$$N \approx \frac{\Delta\omega}{\omega} \qquad \text{Eq. 2.5}$$

where N is the number of oscillating modes and $\Delta\omega$ is the width of the laser spectrum. From the above equations, τ can be obtained by the following expression:[7]

$$\tau \approx \frac{2\pi}{\Delta\omega} = \frac{1}{\Delta\nu} \qquad \text{Eq. 2.6}$$

From Figure 2.6 (taken from ref. [7]), it can be seen that as the number of locked modes increases, τ decreases, as does the intensity between the pulses.[6]

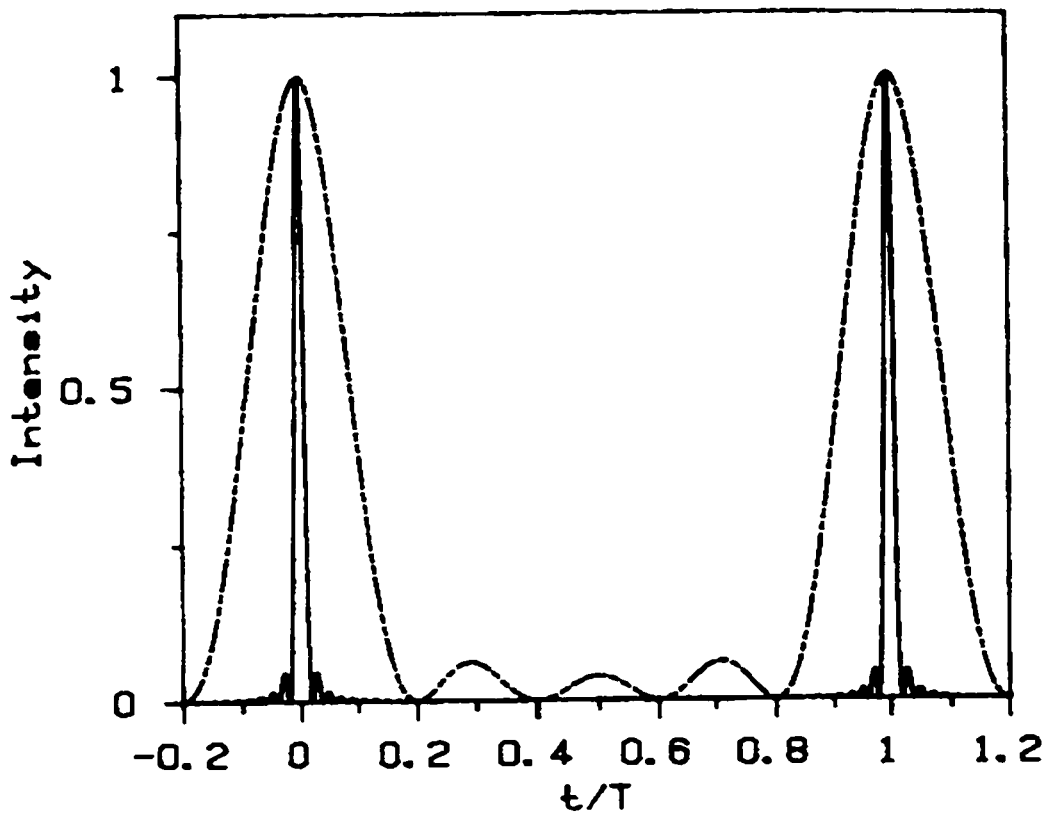

Figure 2.6. A plot of intensity of pulses for the locking of N=5 (dashed lines) and N=50 (solid line) equal amplitude modes each separated by an angular frequency $2\pi/T$.[7]

Two types of lasers that can produce light pulses of picosecond duration for the study of chemical, physical, and biological processes are (1) solid-state mode-locked oscillators, such as Nd^{3+}:YAG (yttrium-aluminium-garnet) or Nd^{3+}:glass and (2) those based on synchronously pumped dye lasers. The two general mode-locking methods are called "passive" and

"active". The passively mode-locked lasers utilize a solution of a "saturable absorber" (e.g., 3,3-diethyloxodicarbocyanine iodide, DODCI) located in the laser cavity. Passive mode locking can be done in both Nd:glass and dye lasers.[5] In the former, a rapid recovery time in the saturable absorber is needed for the formation of ultrashort pulses, since the lifetime of the excited-state of the laser medium is long. Whereas, in the latter, pulses with duration much shorter than the saturable absorber recovery time are produced, since the dye has a short (~1 ns) excited state lifetime. Also, since the transmission of the laser wavelength of the saturable absorber increases nonlinearly with increasing light intensity, the loss is lower as well. The laser can thus be operated in a pulsed mode producing a series of intense pulses.

Active mode locking is carried out using the method of synchronous pumping in which the gain is modulated at the round trip frequency and mode locking results. A train of pulses with interpulse spacing determined by the inverse modulation frequency $(2\omega_m)^{-1}$ arises from the periodic loss created when a stable radio frequency source is applied through a transducer to the prism and an acoustic standing wave is set up in the prism. Generally, pulses produced by synchronously pumped dye lasers are of duration >10 ps. A passively mode-locked Nd:YAG oscillator produces a train of pulses at 1064 nm with a full width at half maximum (FWHM) of 35 ps. A single pulse is passed through a

potassium dihydrogen phosphate (KDP) crystal to generate 532 nm light. The 355 nm or 266 nm excitation pulses (~2-4 mJ/pulse) can be generated by passing 532 nm and 1064 nm radiation through a third or fourth harmonic generating crystal, respectively.

The pump-probe technique is considered to be a simple method for picosecond studies using two pulses: the initiating picosecond pulse (the pump) is delayed in time from the second pulse (the probe). The latter determines the response of the system, as a function of delay time after excitation. In this time-resolved technique, the time resolution of the detector is unimportant and the experimental time resolution is limited by the pump- and probe-pulse durations.[8] The two common techniques based on the pump-probe concept are (1) broad spectral coverage for the probe beam and (2) single-wavelength methods.[9]

The continuum picosecond pulse is generated by focusing the probe pulse into a cell containing liquids, such as D_2O, H_2O, and phosphoric acid (5% by weight).[10] White-light continuum generation by self phase modulation is a remarkable application of nonlinear frequency mixing. An intense optical pulse sees an intensity-dependent refractive index when travelling through a medium. The nonlinear refractive index changes continuously as the pulse rises to a maximum intensity and then decreases in intensity on the trailing edge. The intensity dependence modulates the instantaneous phase of the pulse and thus

the frequency distribution is altered. The picosecond continuum is synchronous with the exciting pulse and so can be used in time-resolved transient absorption measurements. Redder and bluer frequencies are generated, with the redder components arising from the rising edge of the pump pulse and the bluer components arising from the trailing edge.[5] Thus, when the 1064 nm light is focused into a 1:1 mixture of H_2O:D_2O solution of the continuum cell, white light ranging from 400-800 nm is produced.[9]

The recovery of the sample can be observed by monitoring the absorption of the continuum as a function of time and wavelength. Spectral resolution is provided by a spectrometer and an OMA, whereas time-resolved data is obtained by varying the path length of the continuum beam, i.e., the delay time between the pump and probe pulses.[10] By measuring transmitted light intensities of both the sample cell (S) and a reference cell (R) as a function of wavelength when the sample is not subjected to an excitation laser pulse and when it is excited by a laser pulse, a difference absorption spectra can be recorded.[10] An average of 200 transient acquisitions at 10 Hz can be collected for the reference, fluorescence, and background corrections, in order to obtain an adequate signal-to-noise ratio.

Our system is currently set up for broad spectral coverage of the probe beam. As mentioned earlier, to construct a transient decay or growth

trace, the absorption spectrum of the transient is recorded at many different delay times after excitation. The time delay is adjusted by using the computer controlled delay rail stage which changes the pathlength of the 1064 nm light in relation to the excitation pulse (see Figure 2.7). The absorption intensity of the transient (ΔO.D.) at different delay times can be plotted as a function of time at a specific wavelength to produce information on the kinetics of the transient of interest.

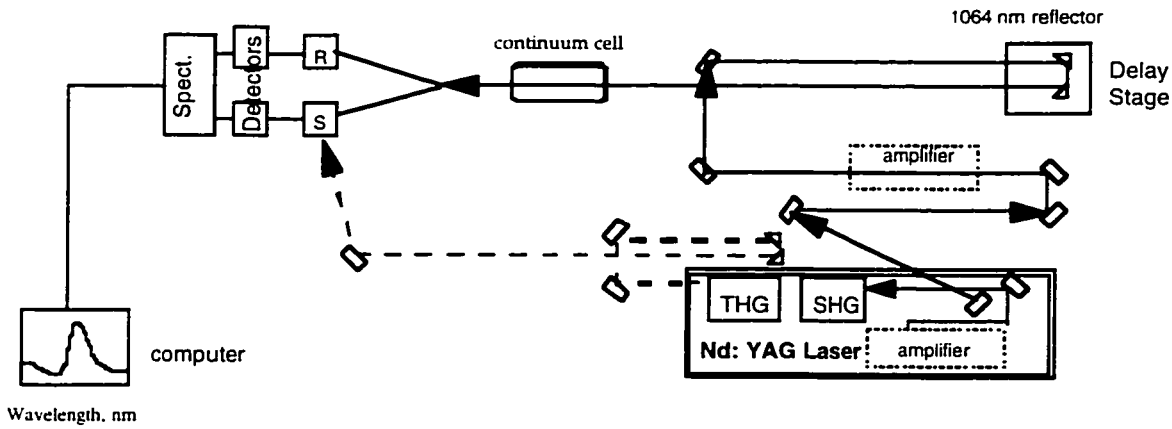

Figure 2.7. Schematic diagram of the picosecond laser system operated in the absorption mode. SHG and THG stand for second- and third- harmonic generating crystals, respectively.

In the single-wavelength method, the return of the molecules to the ground state can be followed by the change in transmission of a weak probe pulse through the sample as a function of time delay after the arrival of the strong pump pulse.[11] Here, the pump and probe pulses originate from the same laser and may have the same wavelength.

The modification of our setup for performing the experiments in the single-wavelength method can easily be done. This work is in progress.

The pump-probe technique has the advantage of detecting all kinds of transient species, such as excited states, ionic species, and neutral radicals. It is also possible to gain some quantitative information on the concentration of the reaction intermediate if its extinction coefficient is known. However, obtaining detailed information on the dynamic behaviour can be difficult, since the usual dynamic range of the measurements with low repetition rate of the laser source is ~$10^{2.5}$ Moreover, high concentrations of transient species are needed for absorption spectroscopy, as compared to fluorescence time-resolved techniques, thus necessitating high excitation intensities of the laser system. On the other hand, high intensity pulses may initiate multiphoton processes and/or total sample destruction. Careful use of picosecond-femtosecond laser flash photolysis is therefore required, especially for the contribution from nonlinear processes, since the peak intensity of the laser pulse increases as the pulse duration decreases. One drawback of dye and/or Nd:YAG lasers is their limited range of wavelengths; yet, by using thin crystals, such as lithium niobate and KDP for nonlinear frequency mixing and harmonic generation, ultraviolet and visible regions of the spectrum can be covered as well.[7]

2.1.5. Picosecond time-resolved emission spectroscopy

A brief description of the operation of a streak camera system for time-dependent measurements in emission mode is given below. A streak camera system for time-dependent measurements in emission studies has been used extensively where the sample emission is resolved by the detection apparatus.

Using the streak camera, it is possible to measure either a single picosecond pulse or a continuous image of a train of picosecond pulses. The light emitted by the sample is focused into the slit of the streak camera which is coupled to a computer. The image of the slit is then produced on the photocathode by a light pulse. The leaving photoelectrons are then accelerated toward the photographic film or a phosphor screen. By applying a voltage ramp across the deflection plates, the leading photoelectrons strike the film or the screen at a different position than the trailing photoelectrons.[12,13] The photo-electrons are thus swept linearly in time across the microchannel plate (MCP) in which each photoelectron can be amplified by a factor of $\geq 10^3$. After the exiting photoelectrons strike the phosphor screen, they create a light image, which gives the shape and duration of the pulse. It is now common to use a video system such as a CCD camera rather than a photographic film to record and digitize the streak image.

The electrode arrangement in a streak image tube can be seen in Figure 2.8 (taken from ref. [12]). Also, assorted interference filters are usually used to select the desired wavelengths to be measured instead of a grating monochromator, since a grating dispersion is shown to broaden picosecond pulses and limit the temporal resolution of the streak camera.

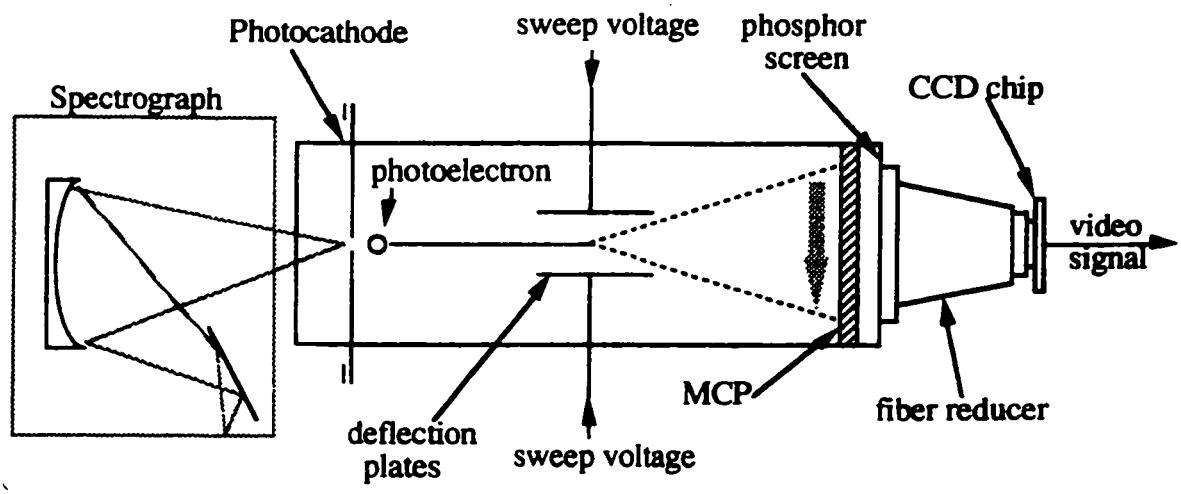

Figure 2.8. The various components in an electronic streak camera.[12]

Our streak camera system is equipped with the following parts: a Hamamatsu streak scope C4334, a spectrometer C5094, a pulse delay generator DG535, and an optical delay unit A2513. The Nd:YAG laser oscillator output pulse, amplified by a factor of 10, is transmitted through a beam splitter (BS) before it is amplified again via a second 6 mm diameter external amplifier (see Figure 2.9). The diameter of the rod influences the beam quality and its energy. Part of this 1064 n m

pulse (<1%) is first transmitted to a PIN diode head (Hamamatsu C1083) to trigger the streak camera. A single pass amplification is proved to be sufficient for most time-resolved emission measurements made with the streak camera system. The amplified 1064 nm pulse is reflected by two mirrors into the optical delay unit (the White cell) which allows for delays from 13-93 nanoseconds. The output beam is then propagated through a second harmonic-generating crystal (see Figure 2.9). Additional frequency changes may be achieved by using a third harmonic at 355 nm or a fourth harmonic at 266 nm. The fluorescence lifetimes can be calculated using the U4790 software (Hamamatsu).

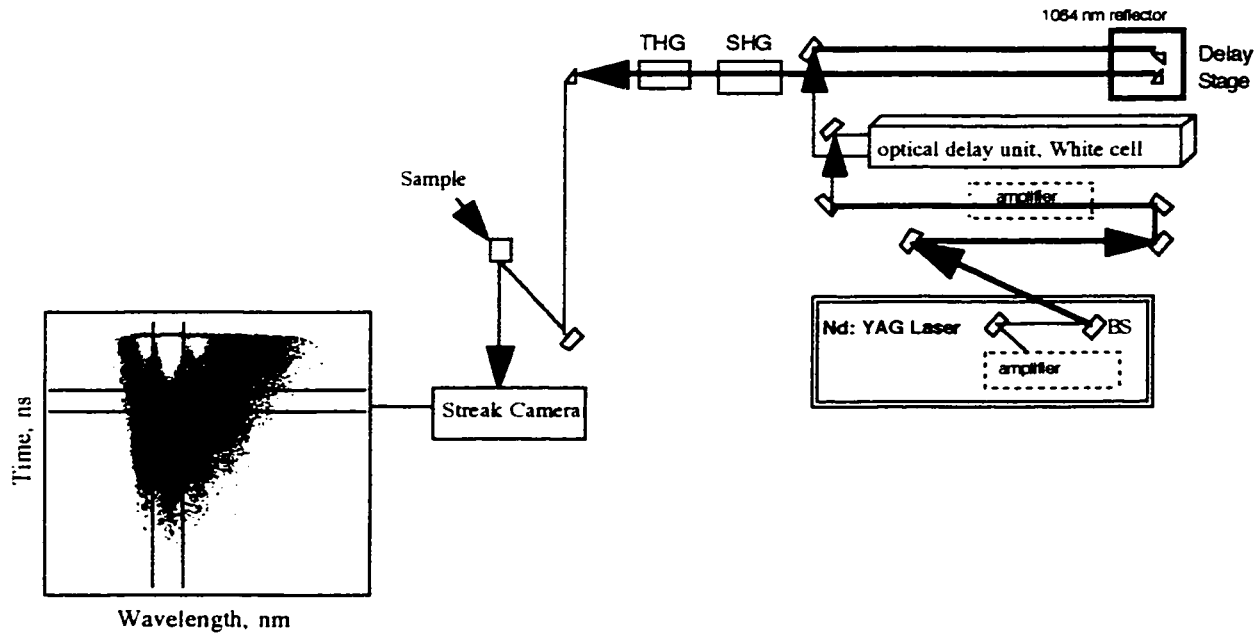

Figure 2.9. Schematic diagram of the picosecond laser system, equipped with a streak camera unit, operated in the emission mode.

The horizontal lines of the image correspond to the wavelength, while the vertical positions provide the time at which a photoelectron is emitted from the photocathode. The brightness of the spots is an indication of the intensity of the image; the brighter the spots, the more intense is the signal.

In our system, the frame-grabber is thus used to capture the signal from the CCD camera and then to transfer it to the computer. With cameras having a jitter, a reference pulse in advance of the excitation pulse is used to shift signals before computer averaging. This delay is necessary to allow time for the streak camera to react to the trigger pulse. About 200 shots can be averaged in a typical experiment. One important feature of the streak camera is its capability to produce a three-dimensional image which provides spectral information as well. It is also worth mentioning that no monitoring beam is used in this technique.

2.2. References

(1) Scaiano, J. C. *J. Am. Chem. Soc.* **1980**, *102*, 7747.

(2) Scaiano, J. C.; Tanner, M.; Weir, D. *J. Am. Chem. Soc.* **1985**, *107*, 4396.

(3) Berinstein, A. Ph.D. Thesis, University of Ottawa, 1997.

(4) Scaiano, J. C. In *Degradation and Stabilization of Polymers*; H. H. G. Jellinek, Ed.; Elsevier: Amsterdam, 1989; Vol. 2; pp 1.

(5) West, M. A. *Techniques of Chemistry: Investigation of Rates and Mechanisms of Reactions;* Forth ed.; Wiley-Interscience Publication: New York, 1986; Vol. VI.

(6) Atkins, P. W. *Physical Chemistry;* Fifth ed.; W. H. Freeman and Company: New York, 1994, pp 1031.

(7) Fleming, G. R. *Chemical Applications of Ultrafast Spectroscopy;* Oxford University Press: New York, 1986.

(8) Hubig, S. M.; Rodgers, M. A. J. In *Handbook of Organic Photochemistry*; J. C. Scaiano, Ed.; CRC Press: Boca Raton, Florida, 1989; Vol. I; pp 315.

(9) Schmidt, J. A.; Hilinski, E. F. *Rev. Sci. Instrum.* **1989**, *60*, 2902.

(10) Hilinski, E. F.; Rentzepis, P. M. *Anal. Chem.* **1983**, *55*, 1121 A.

(11) Hochstrasser, R. M.; Lutz, H.; Scott, G. W. *Chem. Phys. Lett.* **1974**, *24*, 162.

(12) Watanabe, M.; Koishi, M.; Roehrenbeck, P. W. In *The International Society for Optical Engineering*; SPIE: Los Angeles, California, 1993; pp 155.

(13) Holden, D. A. In *Handbook of Organic Photochemistry*; J. C. Scaiano, Ed.; CRC Press: Boca Raton, Florida, 1989; Vol. I; pp 261.

3. Oscillating Magnetic Field Effects on the Behaviour of Free Radicals in Heterogeneous Media

3.1. Introduction

Extensive studies of magnetic field effects on the reactions of radical pairs have been carried out by different groups over the last decade.[1-6] Much of this work has dealt with the effect of static magnetic fields which alter both the concentration and the lifetime of the radicals. There has also been some reports showing the effect of time-varying fields[7] on the yields of short-lived radicals formed through bond-breaking processes and radical-associated photochemical reactions. The radicals which are produced in pairs have the same spin multiplicity as their molecular precursor. When the precursor is an excited triplet state, the resulting pair of radicals conserve their electron spin resulting in a triplet radical pair (RP). Because the electron spins are parallel, the radicals can not recombine without change in the spin

configuration and must diffuse away from the site of formation. However, inert products have been observed as a result of radicals later recombining when they have the right relative spin to yield singlet products.

A magnetic field effect alters the spin dynamics involved through the Zeeman interaction on the energy levels of the radical pairs. This causes a slowdown in the intersystem crossing between the singlet and triplet states. An increase in the fraction of radical pairs that separate is thus observed, which may in turn enhance the probability of possible radical-molecule reactions. However, these effects are favorable in organized media such as micelles, lipids, and the intracellular environment. In these compartmentalized structures, the radicals tend to keep together longer, thus favoring the competition between spin evolution and radical pair separation.

The possibility that electromagnetic fields cause adverse health effects has received much attention in recent years.[8-11] The well-documented ability of static magnetic fields to alter free radicals has been implicated as a possible mechanism to explain the effects of magnetic fields on biological systems.[1,12,13] Recently it has been suggested that oscillating magnetic fields play a particularly important role in influencing biological processes.[14] In today's environment, we are constantly exposed to 60 Hz fields emanating from most appliances, power

transmission lines, and computers. However, there is a lack of experimental evidence and clear mechanisms addressing the problem at a molecular level and testing these predictions. As a result, this study is undertaken to determine how free radical behaviour is modified in the presence of 60 Hz oscillating magnetic fields as compared to static magnetic fields. Since the public is concerned with potential health risks from the effects of environmental fields, we attempt to approach the problem by first examining the influence of 60 Hz fields both in isolation and when they overlap with direct current (DC) field. The case of combined alternating current (AC) and DC fields is easily conceivable and of great interest because of the presence of the Earth's magnetic field (MF).

The goal of this project is to provide a possible explanation for magnetic field effects (MFEs) of this type as a function of the absolute and relative values of the oscillating and static field components in a model system. This study aims at establishing a solid foundation to guide the experimentalist in the design of meaningful experiments to test the possible role of MF perturbations in the radical chemistry of biological systems. The model system we have employed in our studies are radical pairs (RPs) generated in sodium dodecyl sulfate (SDS) micelles by photolysis of benzophenone in the presence of 1,4-cyclohexadiene. The two radicals produced this way are ketyl-cyclohexadienyl radical pairs (see Eq. 3.1).

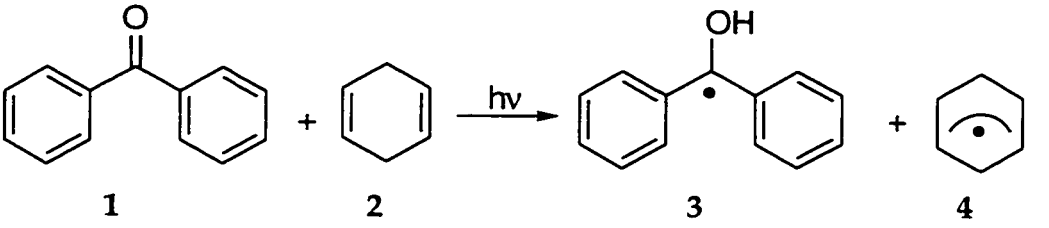

1 2 3 4 Eq. 3.1

A detailed study of the benzophenone system and its photochemistry has previously been performed in this laboratory.[2,15] The choice of our test system to form the RP is not surprising given the fact that benzophenone has been a very popular photophore in the photoaffinity labeling of proteins,[16] enzymes,[17,18] and nucleosides.[19] The ability of benzophenone and benzophenone-like probes to abstract a hydrogen atom (upon irradiation) from an available site make them good candidates for applications in photoaffinity labeling. The triplet state of molecules of these type can easily abstract a hydrogen from, for example, amino acid derivatives and result in relatively long-lived triplet radical pairs which can yield a labelled biomaterial.

Ketoprofen, a nonsteroidal anti-inflammatory drug, also contains a benzophenone group. This drug has been used by researchers because of its photoinducible properties *in vivo* . Artuso *et al.* have shown that when ketoprofen is irradiated at 285-315 nm in the presence of DNA, it efficiently leads to the breakage of double stranded DNA to single strands.[20] Therefore, our choice of benzophenone as a probe to study MFEs in organized structures is not unfounded.

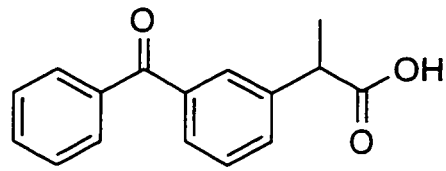

ketoprofen

As mentioned in Chapter 1, micelles with a hydrophobic interior can solubilize a hydrophobic molecule such as the reactants used in this study. The triplet-derived geminate RP born after the laser pulse in the microenvironment of the micelles can maintain its geminate character for a longer period of time than it would in homogeneous solution, where separation of radicals is the major process with only a minor geminate reaction between the radical partners.[3,21] Thus, RP reactions in micelles can be affected by magnetic fields. Our studies of the above benzophenone system in organized structures under the influence of both static and oscillating magnetic fields are presented below.

3.2. Experimental

Benzophenone (Aldrich) was recrystalized from ethanol twice. 1,4-Cyclohexadiene (Aldrich) was distilled prior to use. Sodium dodecyl sulfate (Fluka, microselect) was used as received. Water was purified through a Millipore MilliQ system. The solvents from BDH (Omnisolv) were used as received.

3.2.1. Sample preparation

Microemulsions are prepared by sonicating a mixture of 9 grams of the surfactant SDS with 20 ml of cyclohexanol and 10 ml of 1,4-cyclohexadiene in 100 ml of distilled water. The solutions of 1 m M benzophenone and 0.032 M 1,4-cyclohexadiene in 0.15-0.2 M SDS micelles and in microemulsions were contained in quartz cells made of 7 mm x 7 mm square tubing and deaerated by bubbling with a fine stream of oxygen-free nitrogen (high purity grade, 99.998). The optical density of the samples at the laser wavelength did not exceed 0.3. Since the samples were static, they were shaken after each measurement to avoid depletion. A Lumonics EX-530 providing 308 nm pulses (~6 ns, ≤60 mJ/pulse) was used for sample excitation (see section 2.1.1). The magnet, with both an AC and a DC power supply, were used to study these samples under the influence of a MF (see sections 2.1.2 and 2.1.3).

3.3. Effects due to DC fields

Even though the DC MFEs on radical chemistry are well documented in the literature,[3,22,23] a brief study of static MFE on our model system was first carried out. The results of this study will be used to explain the analysis of the AC and AC + DC MFEs presented in the next few sections. The fate of our triplet RP, generated "instantaneously" after laser pulse excitation inside the supercage environment of the

micelles, can best be seen in Scheme 3.1. In a micellar medium, the lifetime of geminate pairs is sufficiently long to allow for a balanced competition between the recombination of the RP and separation of the RP which then frees the radicals to react with other nearby molecules.[21]

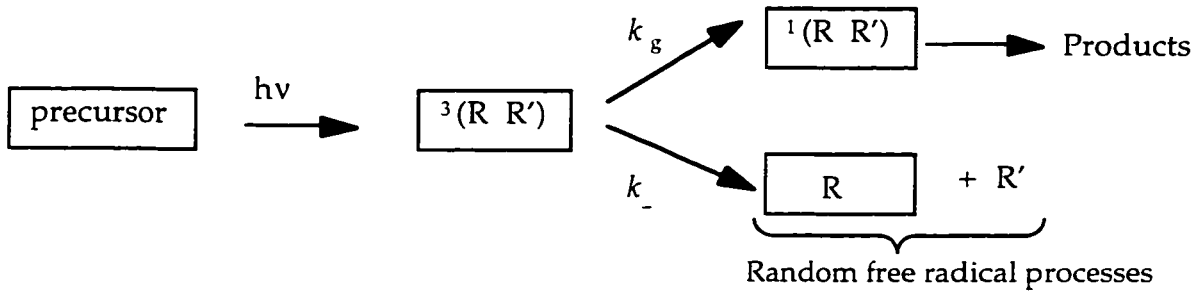

Scheme 3.1. Schematic representation of the processes available to a triplet radical pair confined within heterogeneous media. The boxes represent confinement.

The decay rate constant (k_{decay}) of ketyl radical monitored at 545 nm, shown in Figure 3.1, is a combination of geminate decay (k_g) and micellar exit (k_-) processes.[2]

$$k_{decay} = k_g + k_- \qquad \text{Eq. 3.2}$$

In the absence of an applied MF, the fast and the slow components of the decay trace are well separated and can be fit to a biexponential function. Note that the former behaves mono-exponentially, while the latter follows second-order kinetics.

The fraction of escaped radicals can then be determined by the following equation

$$\text{fraction escape} = \frac{b}{a} = \frac{k_-}{k_g + k_-} = \frac{k_-}{k_{decay}} \qquad \text{Eq. 3.3}$$

where the maximum ΔO.D. (a) gives the amount of total radical formation at the time of laser excitation and residual ΔO.D. (b) is due to the slow component of the decay (see Figure 3.1).

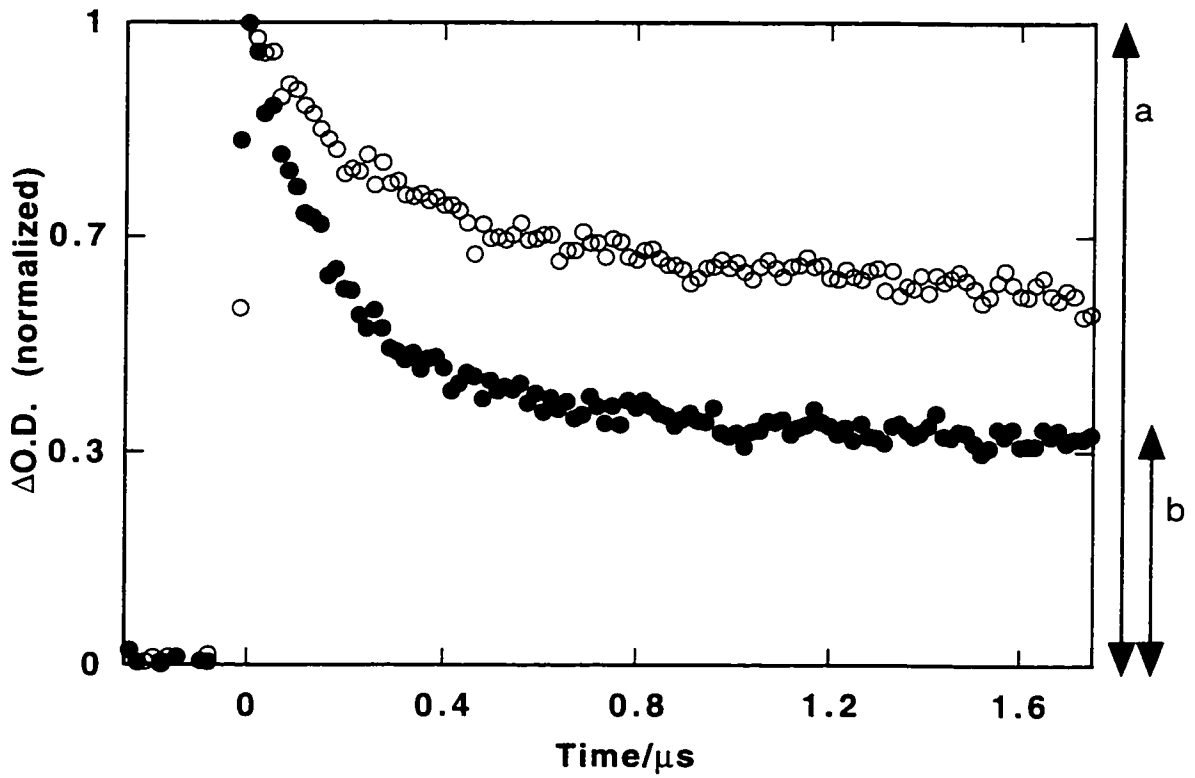

Figure 3.1. Effect of a static magnetic field on the evolution of benzophenone ketyl-cyclohexadienyl radical pairs in the absence of a field (●) and at 1000 gauss (o) in SDS micelles.

With the aid of Eqs. 3.2 and 3.3 and knowing k_{decay} from the fit of decay in Figure 3.1, we obtain values of 2.0 X 10^6 s^{-1} and 2.9 X 10^6 s^{-1} for k_- and k_g in the absence of a MF, respectively. Figure 3.1 also shows the decay of the ketyl radical, $Ph_2\dot{C}OH$, in the presence of a 1000 gauss DC field. The DC field increases the fraction of radicals that escape by decreasing the rate of spin evolution. It is also believed that the smaller radical, the cyclohexadienyl radical, is likely to be the one exiting the micelle, due to its larger mobility. The observed decay rate of the ketyl radical at 545 nm has been measured at various field strengths up to 1400 gauss.

Equations 3.2 and 3.3 are then used to determine the fraction of escaped radicals. This change in the fraction of escaped free radicals as a function of applied magnetic field is shown in Figure 3.2a. There are a number of aspects of this plot worth discussing. It is apparent from the figure that at fields over 1000 gauss, the MFE attains a plateau. This behaviour illustrates that the Zeeman splitting of the T_+ and T_- triplet sublevels at fields greater than 1000 gauss becomes decoupled with S, while the $T_0 \rightarrow$ S transition is largely independent of the applied fields. Thus as the MF strength is increased, intersystem crossing from T_+ and T_- to S slows down and eventually is completely shut down. At this point, the residual ΔO.D. is a contribution of T_+ and T_- sublevels which have no effect on the fast decay component. The reason being that the

long-lived absorption is due to the escape processes which effectively destroy the geminate RP.

This mechanism is proposed in terms of the RP having initially degenerate singlet and triplet levels. In this case, the exchange interaction, J, (see Figure 1.8) between the unpaired electrons is neglected as the interaction between the radicals in the pair becomes weak due to the large spatial separation allowed by the micellar cage. Even though the energy gap between T_+ and T_- is smaller than the thermal energy, kT, this thermodynamic consideration does not play a role on the degree of Zeeman splitting which decouples T_+ and T_- from S.

Similar experiments were performed for BP in SDS micelles with salt concentrations (NaCl) varying from 0.1 M- 0.34 M. Figure 3.3 illustrates representative MF-dependence plot of fraction escape for 0.29 M and 0.34 M NaCl with 0.15 M SDS micelles. It is known that addition of an electrolyte such as NaCl increases the aggregation number or the size of micelles.[24] Using a luminscent probe, the aggregation number for SDS micelles with 0.29 M and 0.34 M NaCl is calculated to be 95 and 110, respectively, where that of SDS in the absence of the added salt is ~65.[24]

The experimental data points of Figure 3.2 and Figure 3.3, subject to 5% error, can be fitted using the following exponential growth expression, Eq. 3.4,

$$\text{escape} = E_o + (E_\infty - E_o)(1 - \exp(-\beta B)) \qquad \text{Eq. 3.4}$$

where E_O is the fraction of escape in the absence of a field, E_∞ the fraction of escape in the plateau region at high field, and B the magnetic field. A convenient feature of this type of plot is that it provides the field required to achieve 1/2 of the maximum change in the fraction that escape, $B_{1/2}$. It is related to the parameter β of Eq. 3.4 by the following equation.

$$B_{1/2} = \frac{\ln 2}{\beta} = \frac{0.69}{\beta} \qquad \text{Eq. 3.5}$$

The fit in Figure 3.2a gives a $B_{1/2}$ value of 230 gauss for SDS micelles. Figure 3.2b is a representative plot of the MFE on the radical behaviour in a microemulsion environment. Comparing Figure 3.2a with Figure 3.2b, it is evident that the MFE on the escaped radicals is rather extensive in these larger aggregates of SDS-1,4-cyclohexadiene. This behaviour is consistent with the observed lower $B_{1/2}$ value of 170 gauss, as predicted when the size of the "cage" increases. Although lower values of $B_{1/2}$, 8 gauss, have been reported previously in the case of radical-ion pairs,[25] differentiating such low fields from the static

residual fields that are present around us can be difficult. A similar trend in the values of $B_{1/2}$ is observed with the SDS-NaCl systems. They are calculated to be 205 gauss and 185 gauss for SDS micelles in the presence of 0.29 M and 0.34 M NaCl, respectively (see Figure 3.3).

We further observe from the curve in Figure 3.2a that the escape fraction increases from ~38% in the absence of a field, E_0, to a maximum value of ~65% at E_∞. This is a 71% increase in the percentage of escaping radicals which may then react with nearby molecules.

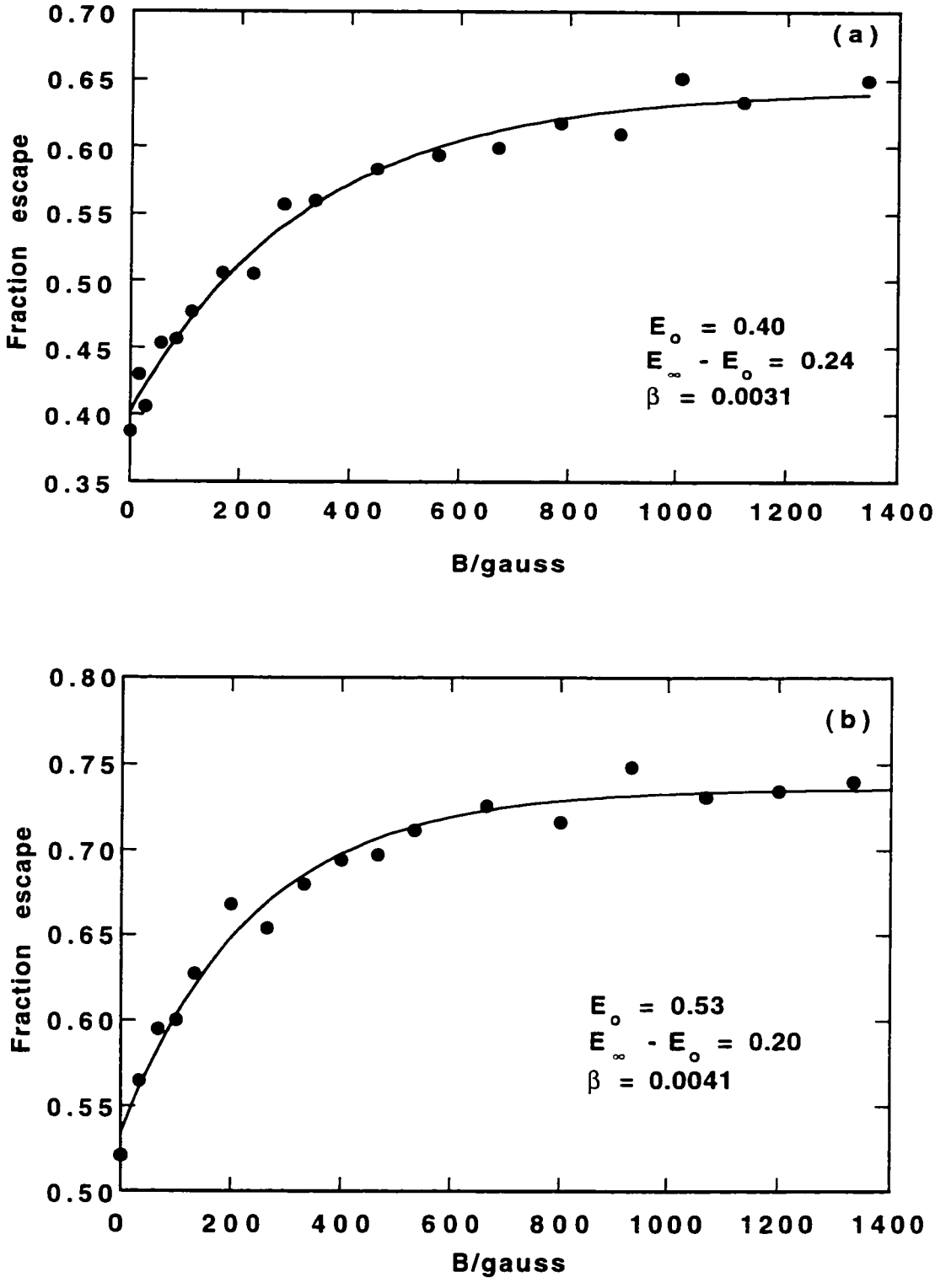

Figure 3.2. Effect of static magnetic fields on the efficiency of radical escape as a function of applied field strength in 0.15 M SDS (a) and in SDS-1,4-cyclohexadiene microemulsions (b).

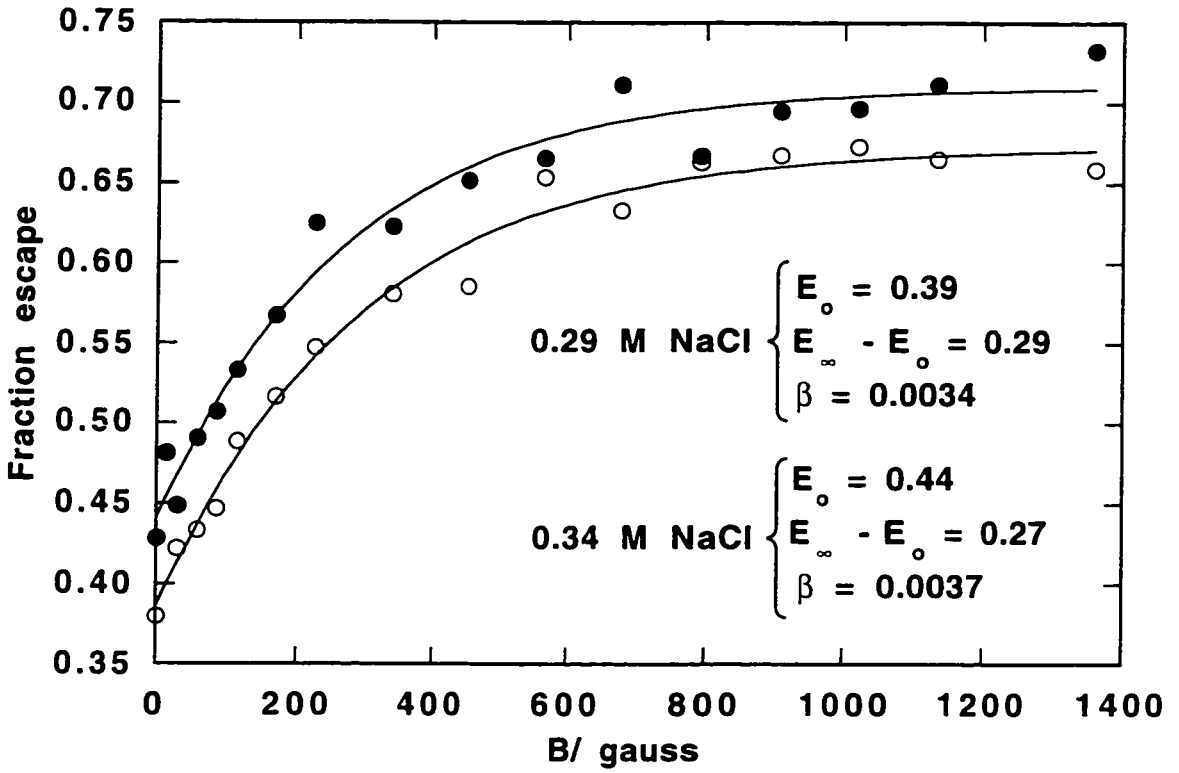

Figure 3.3. Effect of static magnetic fields on the efficiency of radical escape as a function of applied field strength in 0.15 M SDS in the presence of 0.29 M NaCl (●) and 0.34 M NaCl (o).

In light of the biological concerns, it might be useful to introduce a measure of the *field sensitivity* (FS) that relates the percentage change in escaping radicals per unit field increase.

$$FS = 100\frac{d\left(\frac{E-E_\infty}{E_\infty}\right)}{d(B)} \qquad \text{Eq. 3.6}$$

With equation 3.6 and the data from Figure 3.2, values of 0.20% gauss^{-1} and 0.16% gauss^{-1} are obtained for the FS at the origin, FS_o, in the SDS micelles and microemulsions, respectively. The more hydrophobic the

radicals are, the lower the values of exit at zero field (E_0) are, thus leading to higher FS values according to Eq. 3.6.

The interpretations discussed so far are in terms of degenerate S-T levels as depicted in Figure 3.4. This is usually the case when the strength of an applied field is much bigger than the difference between the T_0 and S states. In the above case, the two radical centers are separated by a physical boundary defined by the dimension of the organized assembly being used. The core diameter of these systems being >10-12 Å justifies neglecting the exchange interaction between the two radical centers.[26] However, when the two centers are in the same molecule, such as biradicals,[27,28] the exchange interaction must be included.

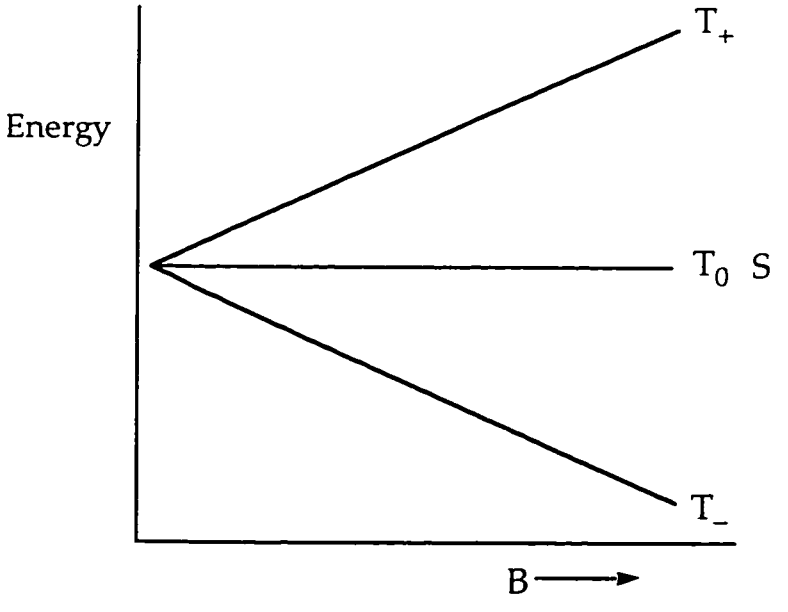

Figure 3.4. Energy splitting diagram for the effect of a magnetic field on the S-T energy for degenerate singlet and triplet levels.

Figure 3.5 illustrates the splitting of the triplet sublevels with respect to the S state for nondegenerate S-T levels. In this case, low fields enhance the probability of triplet to singlet conversion, depending on how closely the energies match near field B_x. In nondegenerate S-T levels, the energy splitting within the triplet sublevels are such that the T_- sublevel crosses the S level at fields near B_x.[27] The consequence of this crossing is an acceleration in the degree of spin evolution. The S state can also lie above T_0 and the crossing with S occurs with the T_+ sublevel. However, this ultimately produces the same effect in the rate of intersystem crossing, k_g.

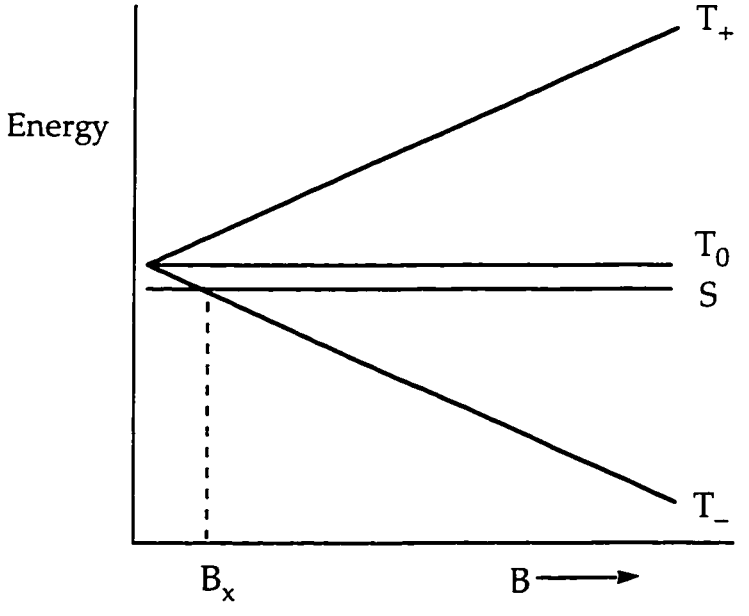

Figure 3.5. Energy splitting diagram for the effect of a magnetic field on the S-T energy for nondegenerate singlet and triplet levels.

As stated before, the splitting of S-T levels becomes important when the two radicals are close enough, J>0, that they undergo significant

spin interaction with each other. This happens when the separation between the radical spins is <10 Å. This also applies to biradicals and/or conjugated systems when the two electron centers can "communicate".[26-29] The case of nondegenerate S-T energy levels also becomes important when low fields are involved, e.g., environmental fields ranging from 0.5-10 gauss. One example is the geomagnetic field, ~0.5 gauss, where the field strength may be in the vicinity of the crossing point. The dynamics of radical exit as a function of the magnetic field strength for the nondegenerate case can be followed in Figure 3.6.[27]

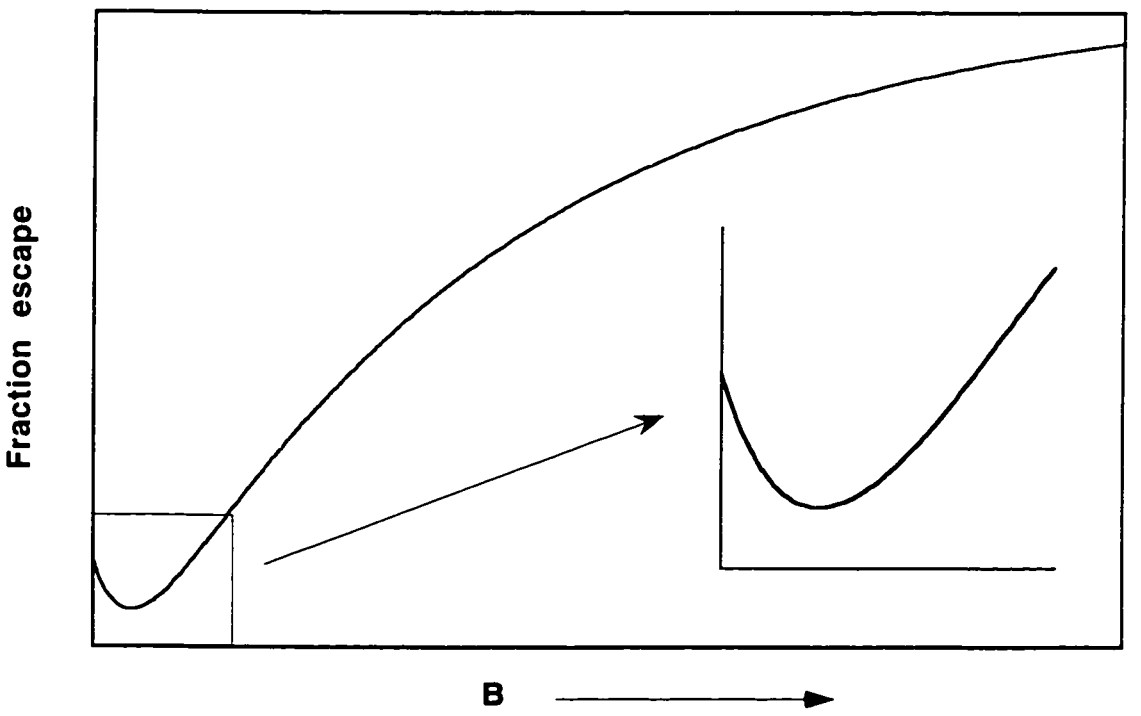

Figure 3.6. Qualitative dependence of the fraction escape with increasing static magnetic field under conditions where singlet and triplet levels are nondegenerate.

The above curve depicting dependence of the fraction escape of radicals on the MF follows a different shape from that of Figure 3.2. Qualitatively, this curve features a narrow window where the efficiency of ISC is increased by application of an MF.[30] This effect is opposite to what is observed with moderate-to-high fields.

Narrow ranges of B, provided by small fields, would thus lead to windows of field effects depending on the B_x of the specific system. Since the value of B_x can vary depending on the magnitude of the interaction between the two unpaired spins, different biological systems would exhibit windows specific to their properties at various fields. The following sections attempt to explain these effects by evaluating the effect of these low fields (<10 gauss) on the behaviour of radical pairs in micelles. An analysis of the effect of oscillating MFEs on radical behaviour will also be presented. However, it is worth noting that the qualitative analysis of such windows in terms of DC fields is simpler than those of oscillating fields where there exists a sinusoidal field dependency.

3.4. Effects due to pure AC fields

In North America the environmentally relevant MFs are usually produced by a 60 Hz alternating current. It is often thought that 60 Hz fields from power lines and appliances are more likely to have biological health effects than the steady (DC) fields. The reasoning given for the above suggestion is that the current induced in the human body depends on the time rate of change of the MF.[14] However, no concrete evidence for this belief has been provided to date.

The extremely high reactivity of free radicals has long been known. Their involvement has been proposed to enhance the probability of reactions with DNA and other biomaterials, which ultimately can lead to an increase in the levels of "radical" initiated carcinogen.[21] The ability of MFs to increase the lifetime of free radicals and their concentration is the reason behind this enhancement. Although the incidence of various diseases has been monitored in communities living close to power lines,[11] a definite relationship between these illnesses and the MF has not been accepted as the only contributing factor. Studies of this type are criticized for their failure to account for all possibilities of a health issue. Design of more reproducible, and meaningful, experiments is needed to assist in understanding MFs at a molecular level. After all, it has long been firmly established that MFs

affect chemistry at this level.[2,13,31-33] The important question is whether we can apply this knowledge within a biological context. Grissom *et al.* have looked at MFEs on enzymatic systems.[34,35] Our work demonstrates the effect of 60 Hz fields on free radical processes.

The model system chosen is the same as that used in the previous section, except that the RPs are generated by LFP in the presence of an AC field alone. Here the AC field strength is much higher than the difference between the splitting of S-T levels, so that approximations of a degenerate S-T level is applicable. Equation 3.4 is used to predict the field dependence of fraction escape. As before, the non-degenerate case presented in Figure 3.5 and Figure 3.6 may also be analyzed using a more elaborate mathematical formula. A 60 Hz cycle is complete in 16.67 ms; on the other hand, the RP recombination, even in organized systems, occurs on a nanosecond/microsecond time scale. Thus the frequency of oscillating MF is much lower than the free radical encounters. In fact, any oscillating frequency < 100 kHz can be considered slow compared with the typical lifetimes of a RP evolution, ~1 μs. It should be emphasized that for our purposes, we are concerned with the duration of radical-radical encounters, and not the lifetime of the radicals. Also, our experiments involve the effect of AC MF on neutral RPs. Other reports have dealt with the effect of fields produced by different frequencies on radical ion behaviour.[7,36,37]

A representative plot of a 60 Hz time-varying MF is shown in Figure 3.7 along with that of a field with an absolute value. The important point here is not the sign of the field. Rather, it is that the absolute magnitude of the field is oscillating at 120 Hz. Thus the effect of a 60 Hz field on the behaviour of RPs in solution or any fluid system results in radical concentrations oscillating at 120 Hz. The amplitude of oscillating fields, usually expressed in terms of its root mean square (rms) value, is related to the peak value by the following (see Figure 3.7 and Figure 3.8).

$$B_{rms} = B_{pk}/\sqrt{2} \qquad \text{Eq. 3.7}$$

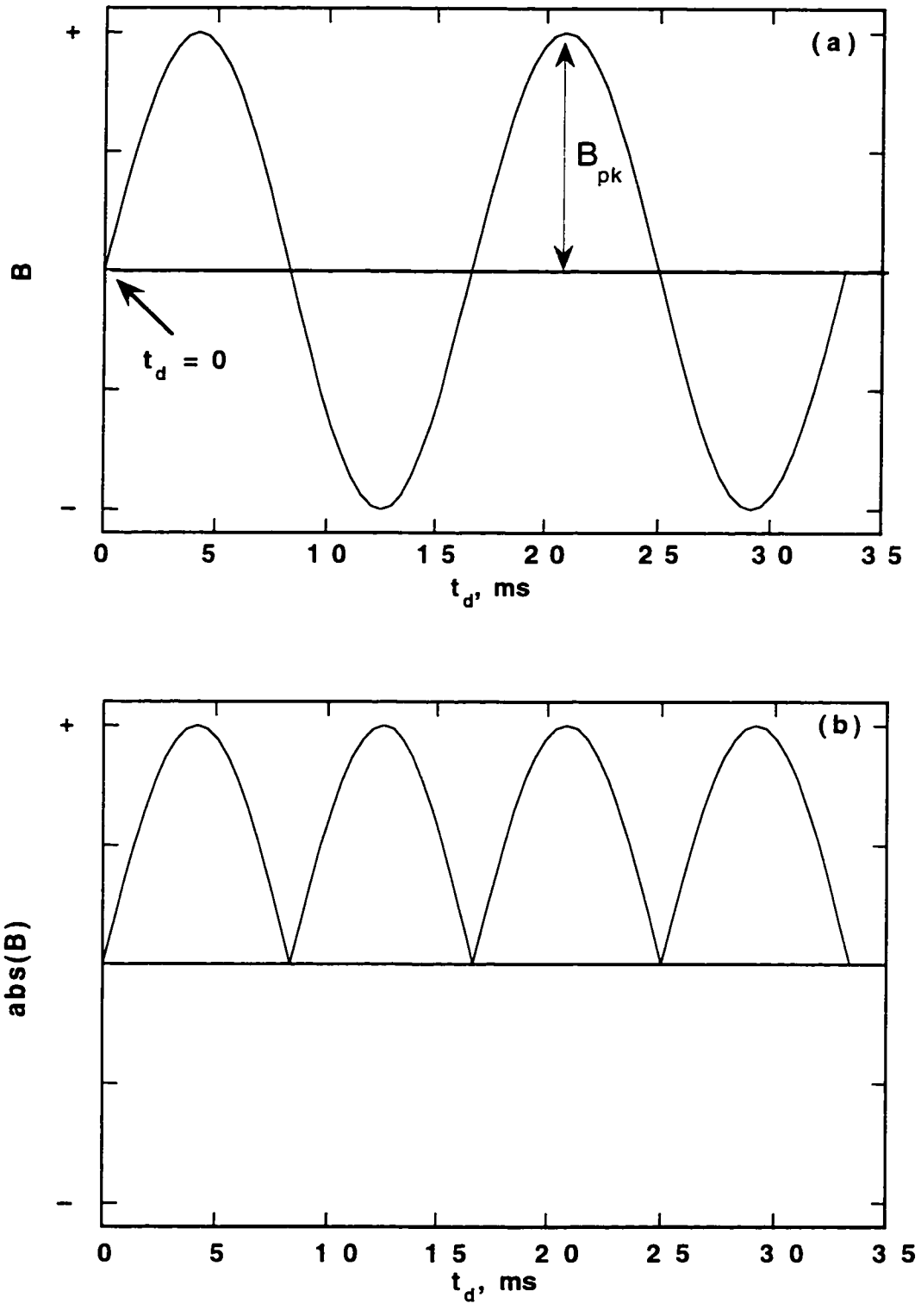

Figure 3.7. Time dependence of a 60 Hz oscillating field (a) and of its absolute value (b).

The relationship that predicts the behaviour of radical oscillation (i.e., fraction escape) with respect to delay time (t_d, the delay period between the beginning of the cycle and the time at which the laser is fired) can be obtained by replacing B in Eq. 3.4 with the absolute value of its time dependence,

$$\text{escape}_{AC} = E_o + (E_\infty - E_o)\left(1 - \exp\left(-\beta B_{pk}\, \text{abs}\left(\sin(21.6\, t_d)\right)\right)\right) \qquad \text{Eq. 3.8}$$

where a conversion between time in milliseconds and angle in degrees for 60 Hz results in the value of 21.6 in the above equation. The product 21.6 t_d is in units of degrees and is related to the phase shift from the beginning of the sine wave. Eq. 3.8 thus allows for the quantitaive prediction of radical behaviour under AC fields, with the knowledge of the radical behaviour under DC fields and the time-dependence of the MF.

As stated earlier, our experimental results do show that oscillating fields of frequency ω lead to fluctuating radical concentrations of frequency 2ω (see Figure 3.8). It can also be concluded that during the short lifetime of radical encounters (random or geminate), a 60 Hz field has the same instantaneous effect on the radical yields as does a static field of equal strength. Figure 3.8 shows the experimental points corresponding to the fraction escape of radicals in 0.15 M SDS generated when the laser is fired during a 60-Hz 100 and 200 gauss cycle,

respectively. The experimental points of fraction escape for the SDS-1,4-cyclohexadiene microemulsions and for 0.15 M SDS with the added salt ([NaCl]= 0.34 M) during a 60-Hz 350 gauss cycle are illustrated in Figure 3.9 and Figure 3.10, respectively. The curves, which fit the experimental data rather well, are predicted from the corresonding DC field alone plots shown in Figure 3.2 and Figure 3.3 for SDS micelles, microemulsions, and SDS micelles with 0.34 M salt, respectively.

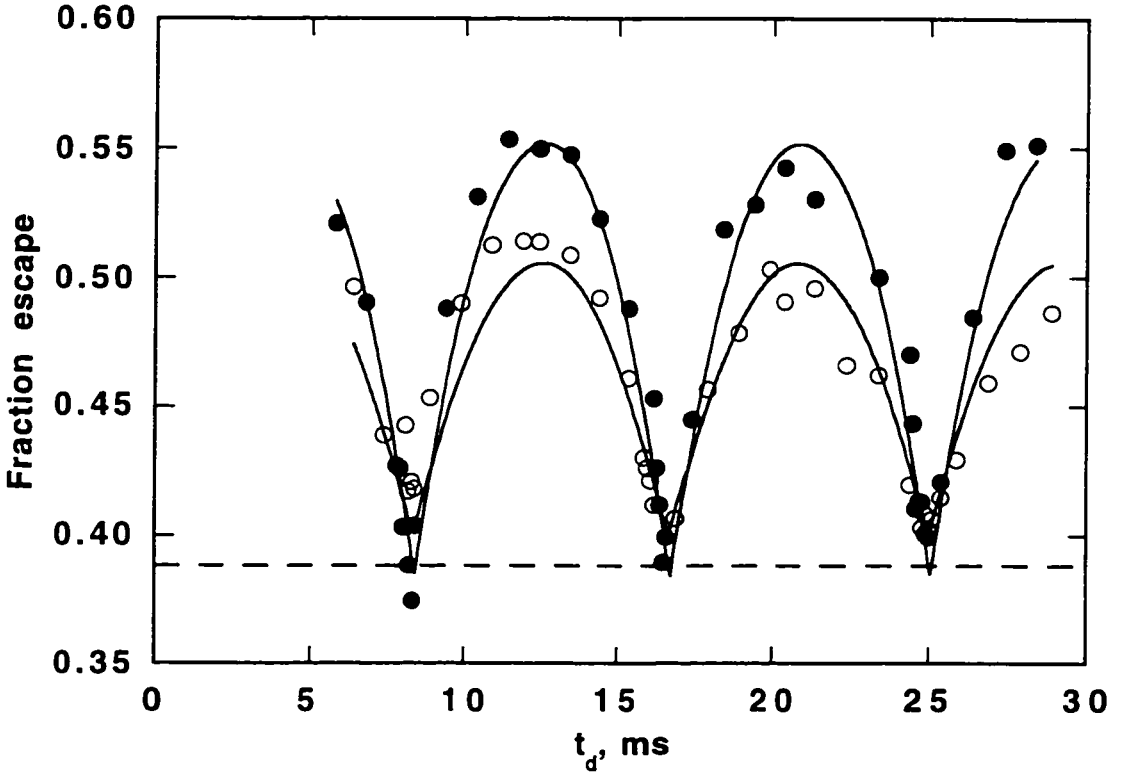

Figure 3.8. Experimental field dependence of the fraction escape (benzophenone ketyl-cyclohexadienyl radical pairs in SDS micelles) as a function of time for a 60 Hz oscillating field with B_{pk} = 100 gauss (o) and 200 gauss (•). Curves are calculated using Eq. 3.8. Dashed line indicates fraction escape in the absence of a field.

Overall, our results show that the effect of an AC MF on the yield of radicals can be predicted quantitatively from knowledge of DC MFE

alone on the same system. This also implies that the time dependence and oscillating nature of AC fields do not change the behaviour and yield of escape radicals any differently than DC fields. It is to be noted that the curves in Figure 3.8 - Figure 3.10 are not a fit of experimental data, but are predicted for radical behaviour based on corresponding data under DC fields alone.

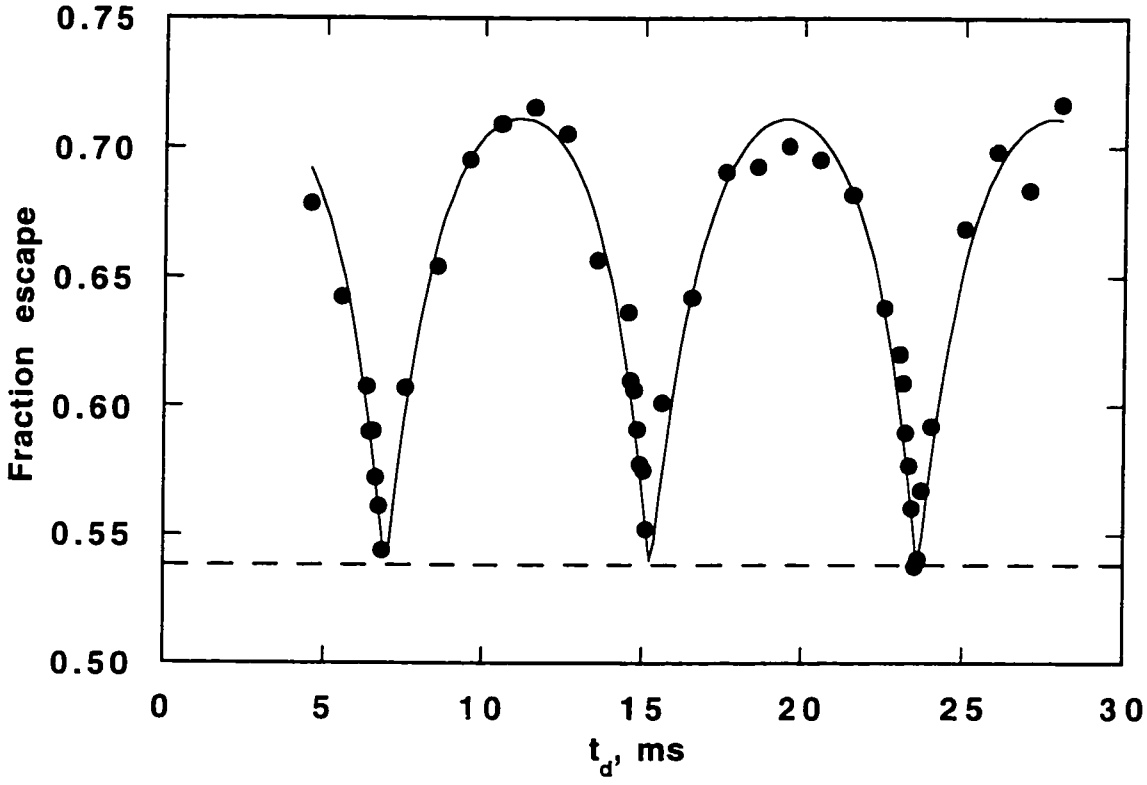

Figure 3.9. Experimental field dependence of the fraction escape (benzophenone ketyl-cyclohexadienyl radical pairs in SDS-1,4-cyclohexadiene microemulsions) as a function of time for a 60 Hz oscillating field with B_{pk} = 350 gauss (•). Curves are calculated using Eq. 3.8. Dashed line indicates fraction escape in the absence of a field.

Note also that as the MF strength increases, the fraction escape fluctuates more sharply when crossing the base line, which is set at the fraction escape in the absence of a field (see Figure 3.8). To better

demonstrate this saturation effect, three calculated curves, based on DC data, of the fraction escape at fields of 70, 150, and 600 gauss are shown in Figure 3.11. It should be emphasized that the spiking effects occur at fields higher than those encountered environmentally, yet their occurrence is important and can be expected.

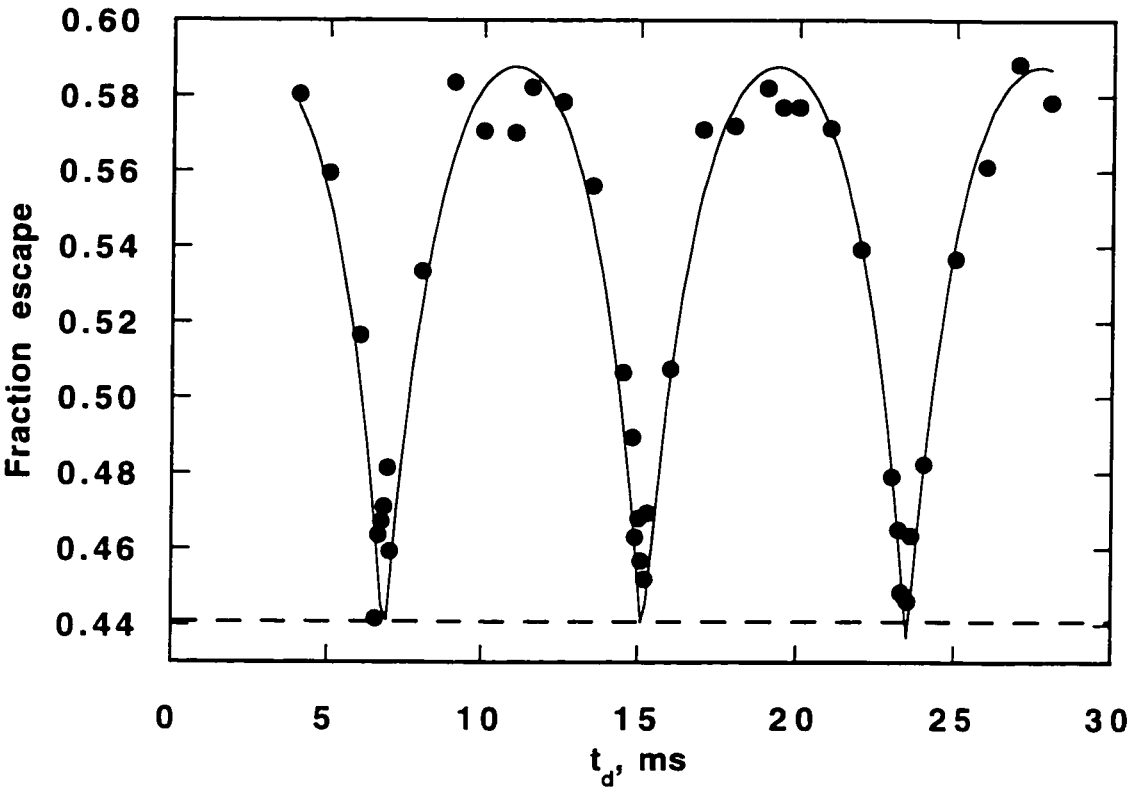

Figure 3.10. Experimental field dependence of the fraction escape (benzophenone ketyl-cyclohexadienyl radical pairs in 0.15 M SDS + 0.34 M NaCl) as a function of time for a 60 Hz oscillating field with B_{pk} = 350 gauss (•). Curves are calculated using Eq. 3.8. Dashed line indicates fraction escape in the absence of a field.

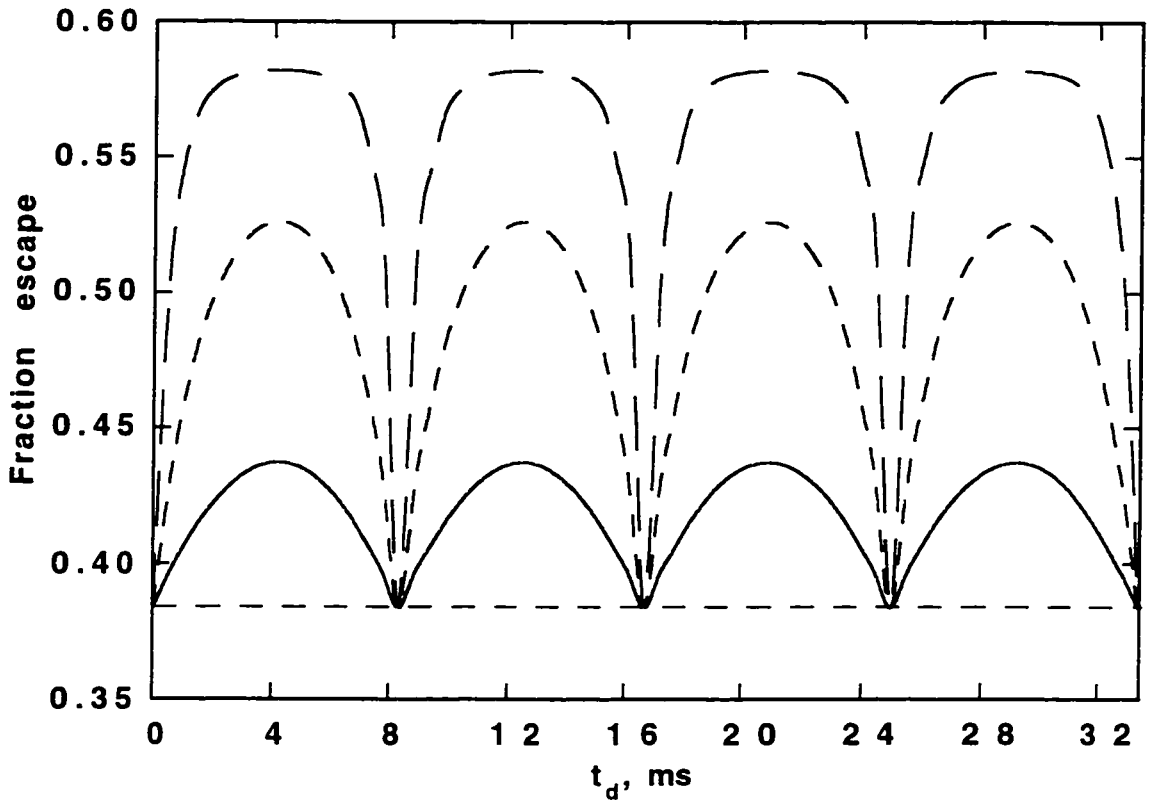

Figure 3.11. Calculated field dependence of the fraction escape as a function of a time varying 60 Hz oscillating field with B^{AC}_{pk} = 70 gauss (—), 150 gauss (--), and 600 gauss (– –). Curves are calculated using Eq. 3.8. Dashed horizontal line indicates fraction escape in the absence of a field.

3.4.1. Concluding remarks relating to AC fields

Our experimental data have thus verified our proposal that oscillating MFs have the same instantaneous effect on radical behaviour as do DC fields on systems that are sensitive to MFEs. These are usually heterogeneous systems such as micelles, vesicles, and lipid bilayers. Micelles have often been used as model systems to mimic biological media. We have attempted to go even further and use proteins as a host for radical reactions influenced by MFEs. It is believed that this is

one step closer to accurately modelling *in vivo* conditions. These results will be presented in the next chapter.

It should be noted that this exact probe, benzophenone, is not found naturally in biological systems. However, similar MFEs are felt by radicals generated by biologically important molecules, such as α-tocopherol, in micellar systems.[38] In conclusion, both static and oscillating MFs have extensive effects on radical behaviour, such as a decrease in the rate of radical decay, an increased radical concentration, and an enhanced radical separation. These are typical chemical effects. However, there is presently not enough knowledge and experimental evidence available in order to extend these effects to biological systems, even though it is anticipated that they are present in biology. For example, oscillating radical concentration may influence signal transduction processes, other cellular RP recombination events,[34,39] and radical-mediated metabolic processes.[35]

A discussion of overlapping AC/DC fields would especially be interesting, since the DC field from the Earth is (at least) always superimposed on 60 Hz oscillating fields of anything that carries and runs on electricity.

3.5. Effects due to combined AC/DC fields

In the following experiments, a DC field is combined with an AC field to illustrate the total effect of their overlap on RP behaviour in micelles. The dominant factor in determining the effect of their overlap is their relative field strengths. Qualitatively, the key factor is whether the AC component can be large enough to reverse the direction of the field with respect to the DC component. As a result, the strength of the DC field (B^{DC}) should be compared with the peak value of the AC field (B^{AC}_{pk}), not its rms value.

Similar to previous arguments, the S-T levels are assumed to be degenerate or that their splitting is smaller than the applied fields. Moreover, the RP recombination occurs on much faster time scales than the time it takes for the completion of a 60 Hz cycle. As with the case of a pure AC field, when the S-T levels are nondegenerate, the complexity of fitting the time dependence of radical concentration, which initiates from the pattern in Figure 3.6 together with an additional DC component in the mathematical formula, increases as well. We address each of the three possible situations which can originate from the relative individual strengths of the AC and DC fields. Note that the AC and DC fields are collinear in our studies.

3.5.1. The DC field exceeds the AC field ($B^{DC} > B^{AC}_{pk}$)

In this case, the direction of the field does not change, since the strength of the DC field is bigger than that of the AC field. Thus the modulation frequency of the radical concentration is the same as that of field oscillation. In other words, the field and its absolute value are always the same. We also find that the time-averaged field strength is equal to the magnitude of the DC field alone, i.e.,

$$B_{average} = B^{DC} \qquad \text{Eq. 3.9}$$

For our system in SDS micelles, it is found that the time-averaged effect on the radical concentration does not depend on the AC component for B < 300 gauss (i.e., before a plateau in the field effect is reached, see Figure 3.2a).

Figure 3.12 shows the experimental data for the field dependence of the fraction escape when $B^{AC}_{pk} = 0.72\ B^{DC}$. The curve fit in Figure 3.12 is done using an equation similar in format to that of Eq. 3.4. Equation 3.10 expresses the time dependence of the field while Eq. 3.11 predicts the escape fraction of the radical.

$$B_t = B^{DC} + B^{AC}_{pk} \sin\sigma \qquad \text{Eq. 3.10}$$

$$\text{escape}_{(AC+DC)} = E_o + (E_\infty - E_o)\left(1 - \exp\left(-\beta\left(B^{DC} + B^{AC}_{pk}\sin(21.6\,t_d)\right)\right)\right) \qquad \text{Eq. 3.11}$$

The fraction escape in Figure 3.12 exhibits a sinusoidal shape since the magnitude of the applied field corresponds to the region of high slope in Figure 3.2a, i.e., B < 300 gauss. The minimum required field for larger aggregates may be lower than 300 gauss.

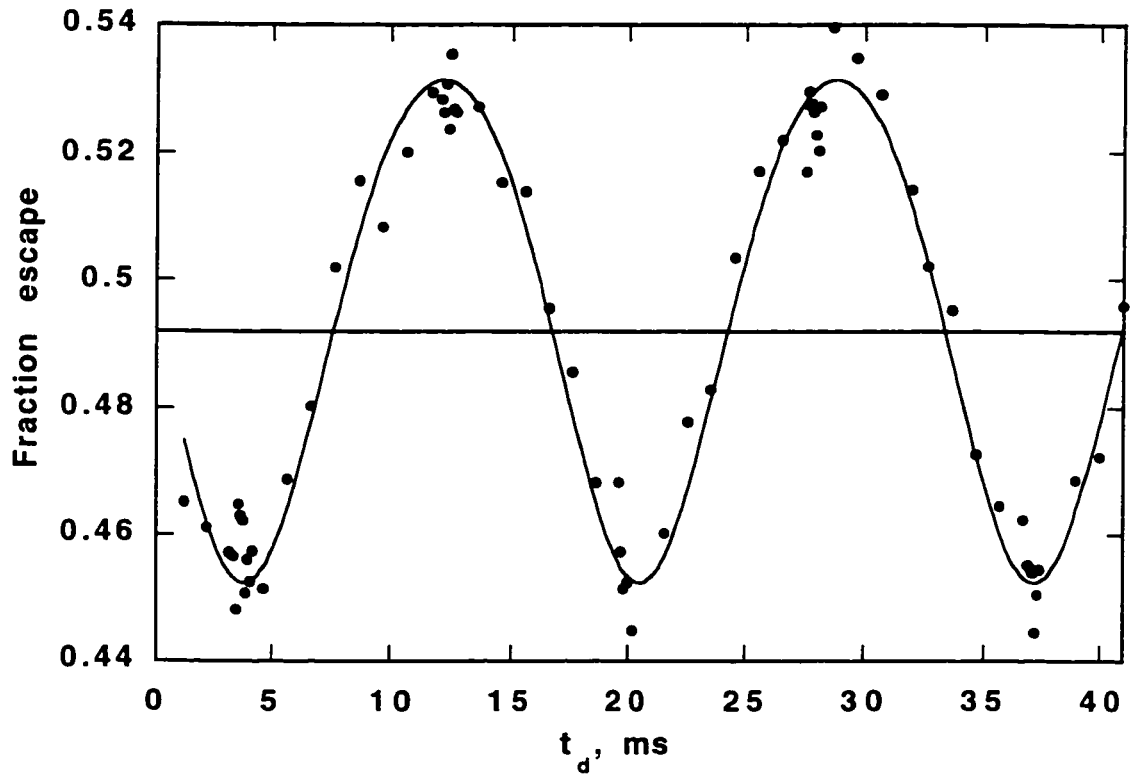

Figure 3.12. Field dependence on the fraction escape for B^{AC}_{pk} = 100 gauss and B^{DC} = 140 gauss. The curve is calculated using Eq. 3.11. The horizontal line indicates the fraction escape in the presence of the DC field alone.

Now consider the situation when the magnitude of $B^{DC} + B^{AC}_{pk}$ falls in a region in Figure 3.2 just before a plateau has been fully achieved. With this case, (see Figure 3.13) the radical behaviour differs from that observed under a DC MF in that it does not follow a perfect sinusoidal shape. Moreover, the fraction of the radical oscillation below the horizontal line, the DC component, is larger than that above it. Here the field dependence of the radical oscillation is shown as a calculated curve. The horizontal line refers to the fraction of radical escape in the presence of a 600 gauss DC field alone and B^{AC}_{pk} = 400 gauss. It is predicted that the same type of behaviour is observed when the field dependence corresponds to a system with a nondegenerate S-T level (see Figure 3.6).

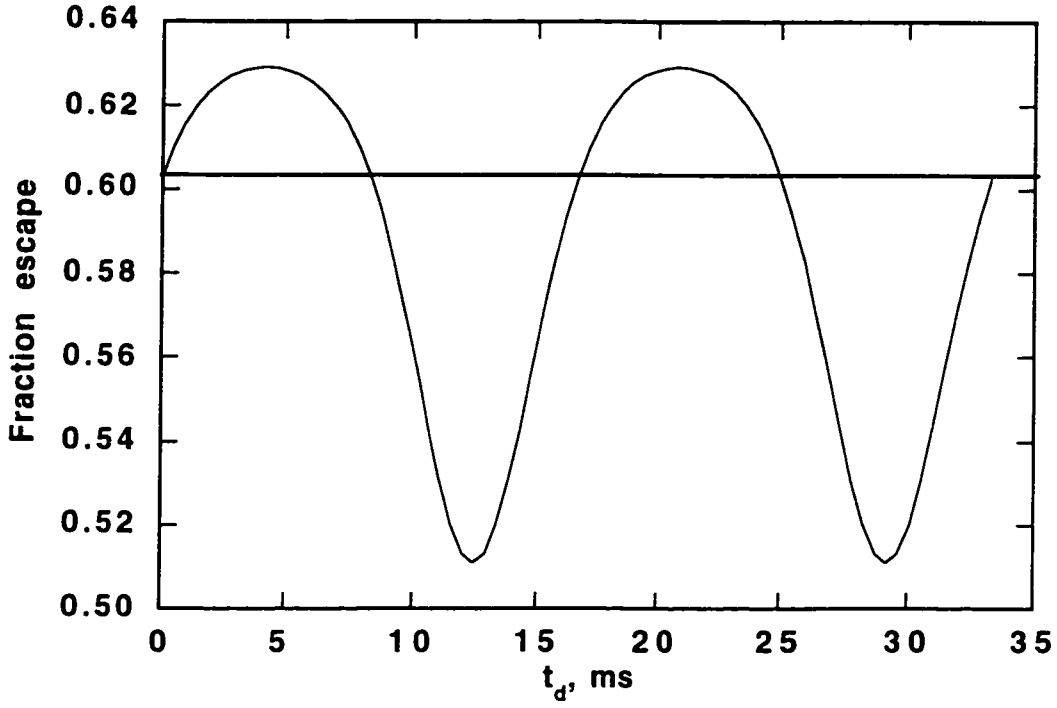

Figure 3.13. Calculated field dependence on the fraction escape for B^{AC}_{pk} = 400 gauss and B^{DC} = 600 gauss. The curve is calculated using Eq. 3.11. The horizontal line indicates the fraction escape in the presence of the DC field alone.

The results for the averaged radical concentration with respect to DC field alone are given in Table 3.1. The calculations use a series of different combinations of DC and AC field strengths. From the results it can be concluded that when $B^{DC} + B^{AC}_{pk} << B_{1/2}$, the AC field component does not affect the average radical concentration. The AC component leads to a slight increase in the average radical concentration when its strength is stronger than that of B^{DC}, provided the DC component is below the $B_{1/2}$. In addition, when the DC component is in the high field region (i.e., above the $B_{1/2}$), a slight

decrease in the average radical concentration is observed when the AC component is ≥ B^{DC} (see Table 3.1).

Table 3.1. Effect of combined AC/DC fields on the fraction escape for the benzophenone/cyclohexadiene system in SDS micelles.

		fraction escape		
B^{DC} (gauss)	B^{AC}_{pk} (gauss)	(DC) only	(AC/DC) average	(AC/DC)[a] max
0	0	0.4	n.a.	n.a.
100	20	0.464	0.464	0.475
100	100	0.464	0.460	0.511
100	200	0.464	0.479	0.545
100	1000	0.464	0.586	0.632
230 [b]	100	0.523	0.520	0.554
230 [b]	500	0.523	0.539	0.615
1000	100	0.629	0.629	0.632
1000	1000	0.629	0.582	0.640
1000	2000	0.629	0.609	0.640

[a] Fraction escape at the maximum
[b] Field corresponding to $B_{1/2}$

3.5.2. The AC field exceeds the DC field ($B^{AC}_{pk} > B^{DC}$)

To illustrate the difference between this case and the preceding one, the overlap of a 300 gauss AC field and a 150 gauss DC field is first calculated. The time-dependence curve and its absolute value are plotted in Figure 3.14. The magnitude of the DC field is also shown as a dashed line. The change in the direction of the fields occurs on different time scales, depending on the relative strengths of the fields. The format of the equation used for fitting these curves, Eq. 3.12, is similar to that of Eq. 3.11. It differs only in that the absolute value of Eq. 3.10 is used to calculate the fraction escape.

$$\text{escape}_{(AC+DC)} = E_o + (E_\infty - E_o)\left(1 - \exp\left(-\beta\, \text{abs}\left(B^{DC} + B^{AC}_{pk}\left(\sin(21.6\, t_d)\right)\right)\right)\right) \qquad \text{Eq. 3.12}$$

Experimental results for the two sets of overlapping fields and their effect on the oscillating behaviour of the radical concentration are shown in Figure 3.15a and Figure 3.15b. It can be seen that the predicted curves based on Eq. 3.12 match the experimental data very well. The field strengths chosen are such that the average radical concentration oscillates at 120 Hz. However, as mentioned previously, the length of time for the major field direction is different from that for the minor one. Note also that the difference between the major and minor fluctuations is more evident when the strength of the DC field is closer to that of the AC field.

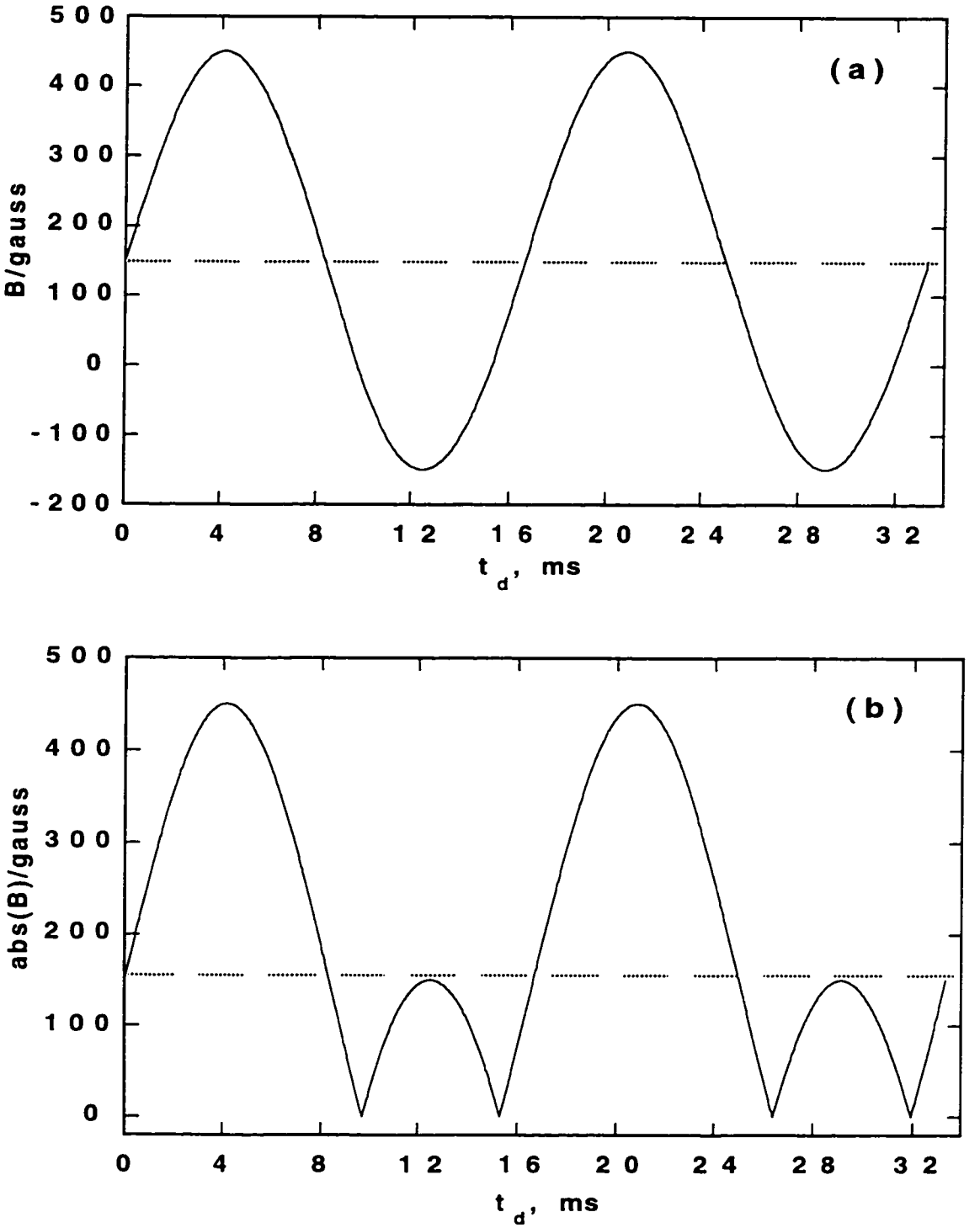

Figure 3.14. Calculated time dependence of the field strength for B^{AC}_{pk} = 300 gauss and B^{DC} = 150 gauss. The dashed lines show DC field strength. (a) actual field; (b) absolute field.

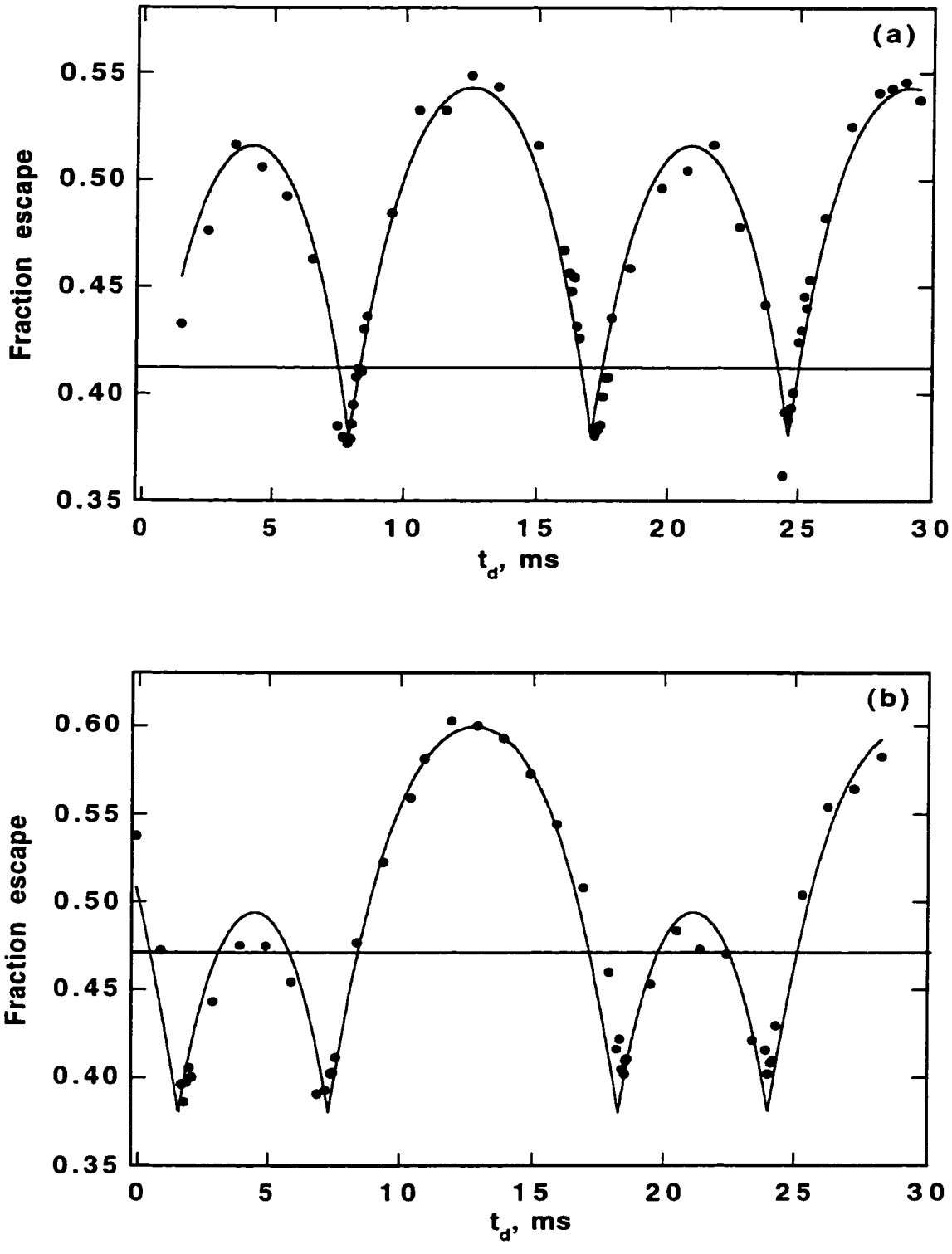

Figure 3.15. Field dependence of the fraction escape for B^{AC}_{pk} = 340 gauss and B^{DC} = 55 gauss (a) and B^{AC}_{pk} = 340 gauss and B^{DC} = 155 gauss (b). The curves are calculated using Eq. 3.12. The horizontal lines indicate the fraction escape in the presence of the DC field alone.

It can be concluded that the average radical concentration has increased with the application of an AC field on top of a DC field. However, when the combination of AC and DC fields is such that their sum reaches the plateau region in Figure 3.2, the average radical concentration decreases as compared to a DC alone field effect (see Table 3.1). It should be mentioned that it is highly unlikely to have this condition occur under environmental MFs.

3.5.3. Equal AC and DC fields ($B^{DC} = B^{AC}_{pk}$)

In this case, it is found that while the time-averaged radical concentration at low fields is the same as that for a pure DC field, the averaged radical concentration is lower at the high field region (see Table 3.1). The field frequency is found to be the same as that of its absolute value, leading to 60 Hz oscillations in the radical concentration. Figure 3.16a shows a calculated curve of the field dependence of the fraction escape at $B^{DC} = B^{AC}_{pk} = 190$ gauss. The theoretical curve is based on an equation similar to Eq. 3.12. The one exception being that the minimum field, B_t^{min}, is set equal to zero.

Figure 3.16b shows our experimental data for an AC field of 190 gauss and a DC field of 175 gauss. The goal was to have equal magnitudes of AC and DC fields. However, in our setup, it was difficult to get smaller than an 8% difference in field strengths. Interestingly, this small

difference is large enough to change the behaviour of the oscillations in the radical concentrations compared to the predicted curve of Figure 3.16a. However, the predicted curve of Figure 3.16b fits the experimental data very well. It is worth mentioning that this predicted curve takes into account the overall difference between the experimental AC and DC fields. Here, as with Figure 3.15a and Figure 3.15b, the radical concentration oscillates with minor and major fluctuations with times of 4.2, 20.8, and 37.5 ms. Two calculated curves, with $B^{DC} = B^{AC}_{pk} = 300$ gauss and $B^{DC} = B^{AC}_{pk} = 600$ gauss fields, are shown in Figure 3.17a and Figure 3.17b, respectively. These two fields are chosen so as to show the behaviour of the fraction escape at fields greater than B_x, and somewhat closer to a region of Figure 3.2a where the field dependence of fraction escape is beginning to plateau. As was seen in Figure 3.13, the oscillating component below the horizontal line of the DC field alone is the major contributor to the radical oscillation. Once again, the shape of the sine wave is different from the usual 60 Hz cycle.

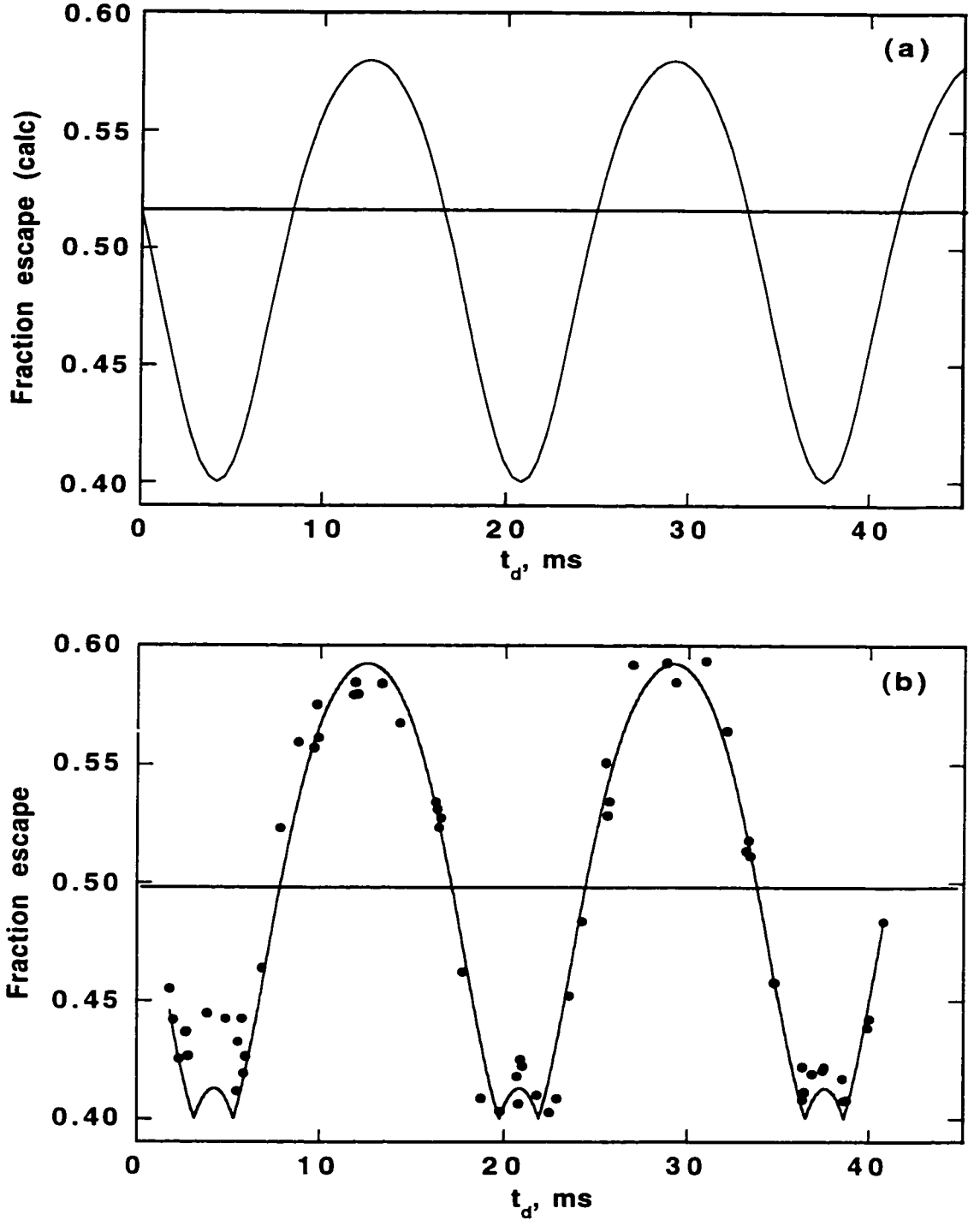

Figure 3.16. The calculated field dependence of the fraction escape for $B^{AC}_{pk} = B^{DC} =$ 190 gauss (a). The observed and predicted field dependences of the fraction escape for $B^{AC}_{pk} = 190$ gauss and $B^{DC} = 175$ gauss (b). The curves are calculated using Eq. 3.12. The horizontal lines indicate the fraction escape in the presence of the DC field alone.

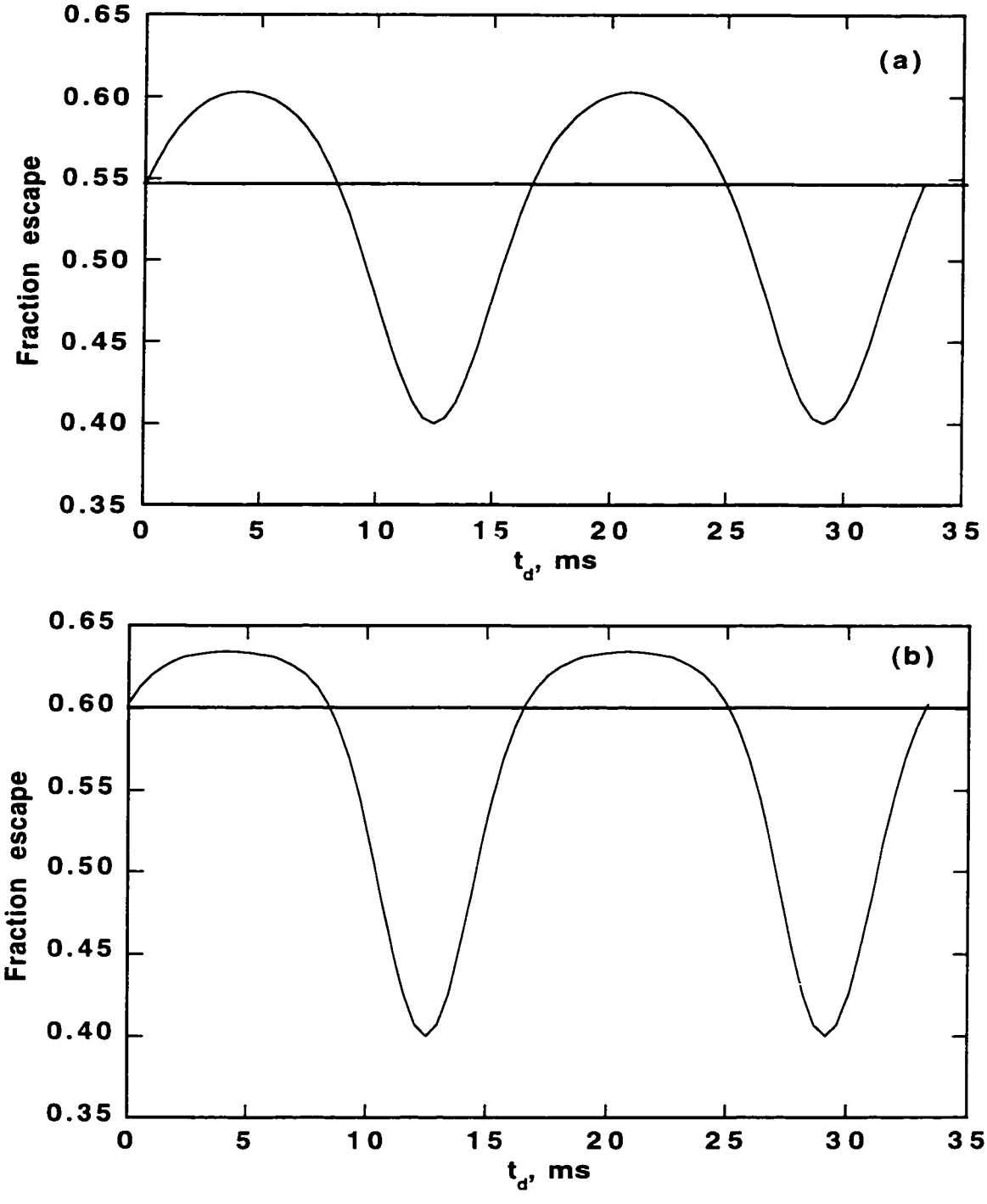

Figure 3.17. The calculated field dependence of the fraction escape for B^{AC}_{pk} = 300 gauss and B^{DC} = 300 gauss (a) and B^{AC}_{pk} = 600 gauss and B^{DC} = 600 gauss (b). The curves are calculated using Eq. 3.11. The horizontal line indicates the fraction escape in the presence of the DC field alone.

3.6. Predictions for nondegenerate S-T levels

The behaviour of radical decay at low fields differs from the case of degenerate S-T levels in that the spin evolution accelerates at fields near B_x (see Figure 3.6) Since environmental MFs fall in the category of low fields, characterizing such field effects is especially important in biological systems.

In the preceding sections, we studied the behaviour of radical reactions in micellar systems under both AC fields alone and combined AC/DC fields. We found that our experimental data matches the corresponding theoretical curves obtained from the appropriate equation. As mentioned before, our test system does not apply to studies of radical pairs with nondegenerate S-T level. There are, however, systems such as biradicals where the radical centers are linked by a long flexible chain that do apply.[27-29,40,41] However, it is anticipated that our analysis of field effects on fraction escape based on Figure 3.5 and Figure 3.6 will provide a qualitative way of predicting the effects in such systems. An empirical formula (Eq. 3.13), based on the approximate shape of field dependence of the fraction escape in Figure 3.6, is used to analyze the field effects. The calculated field dependence of fraction escape using this empirical equation is shown in Figure 3.18.

$$\text{escape} = 0.22 + \underbrace{0.11e^{-6.9B_{norm}}}_{B \approx B_x} + \underbrace{0.44\left(1 - e^{-0.69B_{norm}}\right)}_{B > B_x} \qquad \text{Eq. 3.13}$$

The labels below the exponential terms indicate which part of the equation dominates the curve fit of Figure 3.18. The first term is formatted to fit the fraction escape at low fields or at fields close to the crossing point at B_x, where the rate of ISC is accelerated. The second term, however, fits the increase in the fraction escape with increasing field strengths or with filed strengths > B_x.

In the case of triplet RPs, on a first approximation we assume that all the triplet sublevels are equally populated. Thus one third of radicals undergo separation at zero field, since the T_0 sublevel is not sensitive to a MF. This leads to two thirds of the RPs separating as the strength of external MF increases, since the T_+ and T_- sublevels become decoupled from the S level. The factors of 0.11 and 0.44 in Eq. 3.13 come from one third of 33% and two thirds of 66.7% separation, respectively. Also, the value of 0.22 in Eq. 3.13 is a result of two thirds of 33% separating in the absence of a MF. From Eq. 3.5, a value of $\beta = 0.69$ is determined for $B_{1/2} = 1$. The magnitude of the field is given by the product $B_{norm} \bullet B_{1/2}$. It is also assumed that the field strengths for a nondegenerate S-T levels are ten times lower than that for degenerate. This leads to a value of $\beta = 6.9$ for the first exponential term in Eq. 3.13. This term corresponds to

the region near the crossing point of the S and T_- levels (see Figure 3.5 and Figure 3.6). In our example, the fields for B_x and for the minimum fraction escape are found to occur at 0.384 $B_{1/2}$ and at 0.148 $B_{1/2}$, respectively.

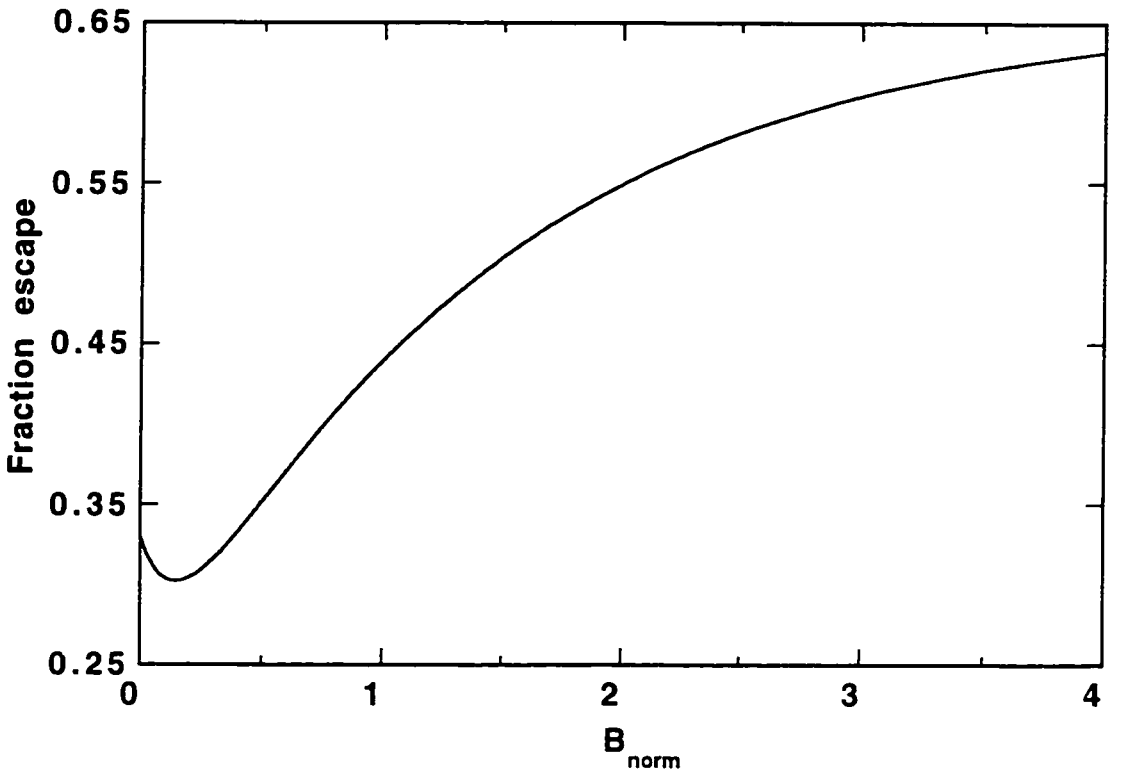

Figure 3.18. Calculated empirical escape for a system with non-degenerate S-T levels, based on Eq. 3.13.

3.6.1. The case of a pure AC field for nondegenerate S-T levels

To exhibit the behaviour of the fraction escape at low fields for the case of nondegenerate S-T levels, three values of AC field strengths are chosen: B^{AC}_{pk} =0.25 $B_{1/2}$, B^{AC}_{pk} = 0.5 $B_{1/2}$, and B^{AC}_{pk} = 2$B_{1/2}$. The following equation, in which the term expressing the fields is replaced

by its time dependence, as in Eq. 3.8, is used to fit the calculated field dependences.

$$\text{escape} = 0.22 + 0.11e^{-6.9 f B_{1/2}\left|\sin\left(21.6 t_d\right)\right|} + 0.44\left(1 - e^{0.69 f B_{1/2}\left|\sin\left(21.6 t_d\right)\right|}\right) \qquad \text{Eq.3.14}$$

Here, 21.6 t_d corresponds to the phase shift from the beginning of the sine wave. Also, a coefficient **f** is introduced to give the ratio of the maximum oscillation to $B_{1/2}$, i.e.,

$$\mathbf{f} = \frac{B_{pk}^{AC}}{B_{1/2}} \qquad \text{Eq. 3.15}$$

The plots for **f** values of 0.25, 0.50, and 2.0 are shown in Figure 3.19. For comparison, a typical 60 Hz sine wave curve is shown at the top of these three figures. When **f** = 0.25, it is found that the fraction of radical escape is decreased. In other words, a decrease of 6.7% in the average radical concentration is calculated due to a decrease in escape, as compared to that seen at zero field, from 0.330 to 0.308. When **f** = 0.50, the average radical escape becomes 0.327. This is only a 0.9% decrease in radical concentration. For the last example, a minimum of 0.302 and a maximum of 0.550 are observed in fraction escape. This leads to an average fraction escape of 0.463, i.e., a 40% increase. The shape of radical fluctuation exhibits a slightly perturbed 120 Hz oscillation as was seen in Figure 3.8. However, at **f** values smaller than

$B_{1/2}$, two overlapping 120 Hz fluctuations, which are out of phase with the sine wave oscillation, are observed. These calculated field dependences of radical behaviour for situations such as those in Figure 3.6 and Figure 3.18 offers an understanding of the role of *windows* in MF dependence.[30]

3.6.2. The case of overlapping AC/DC fields for nondegenerate S-T levels

Clearly, there are many different combinations of overlapping AC/DC fields that can be considered here. However, we have analyzed only cases where $B^{DC} < B^{AC}_{pk}$. This is because when $B^{DC} >> B^{AC}_{pk}$, the radical oscillation is expected to be only slightly different from the corresponding case for degenerate S-T levels. As with the previous case, the basic form of Eq. 3.13, which led to the field dependence curve in Figure 3.18, is used. The effect of three DC field strengths, $B^{DC} = 0$, 0.1 $B_{1/2}$, and 0.25 $B_{1/2}$ with an AC field of $B^{AC}_{pk} = 0.25\ B_{1/2}$ are considered. The time dependent Eq. 3.14, with the added DC component given as **d**, is derived to predict these field effects on radical behaviour,

$$\text{escape} = 0.22 + 0.11e^{-(6.9B_{1/2}\left|\mathbf{d} + 0.25\sin\left(21.6t_d\right)\right|)} + 0.44\left(1 - e^{-\left(0.69B_{1/2}\left|\mathbf{d} + 0.25\sin\left(21.6t_d\right)\right|\right)}\right) \qquad \textbf{Eq.3.16}$$

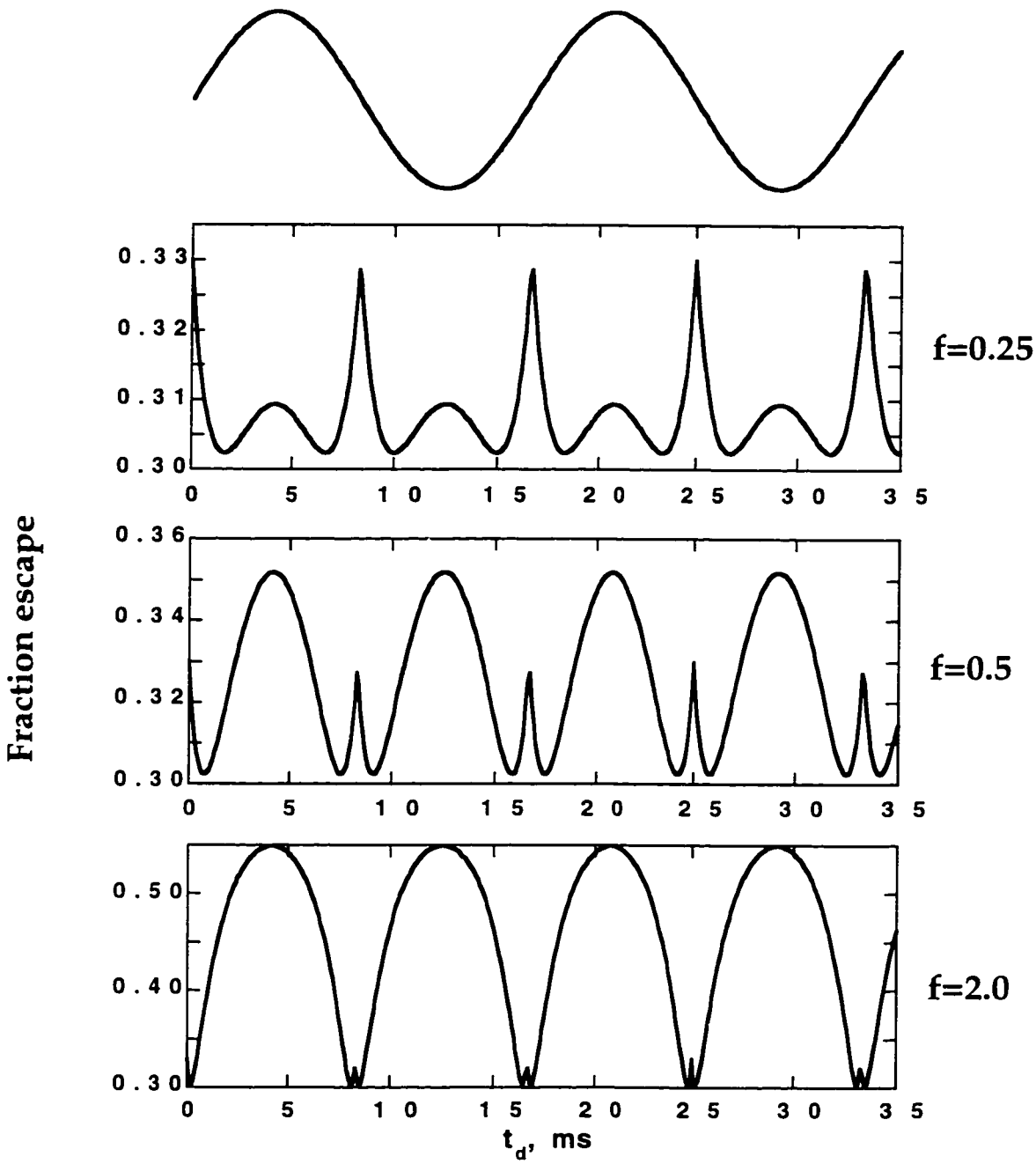

Figure 3.19. Calculated dependence of the fraction escape for a system with non-degenerate S-T levels following the dependence of Eq. 3.14 for f values of 0.25, 0.5 and 2.0. The curve at the top illustrates the sine dependence of the AC magnetic field.

It should be noted that the definitions for all the other parameters used in Eqs. 3.13, 3.14, and 3.15 apply here as well. Figure 3.20 shows the curves created using the above equation at fields mentioned earlier. Note that for each DC field, the value of the AC field, **f**, is fixed at 0.25. Also, for the value of **d** = 0, basically the same plot is obtained as that at the top of Figure 3.19. When the DC component is increased to a value of 0.1, the radical oscillation is already quite different from the previous case. In the last situation though, d = 0.25, the radical oscillation features similarities with the cases shown in Figure 3.14b and Figure 3.15b. From the analysis of nondegenerate S-T levels, it becomes evident that minor differences in the magnitudes of the AC/DC components can have major influences in the time dependence of the radical concentrations.

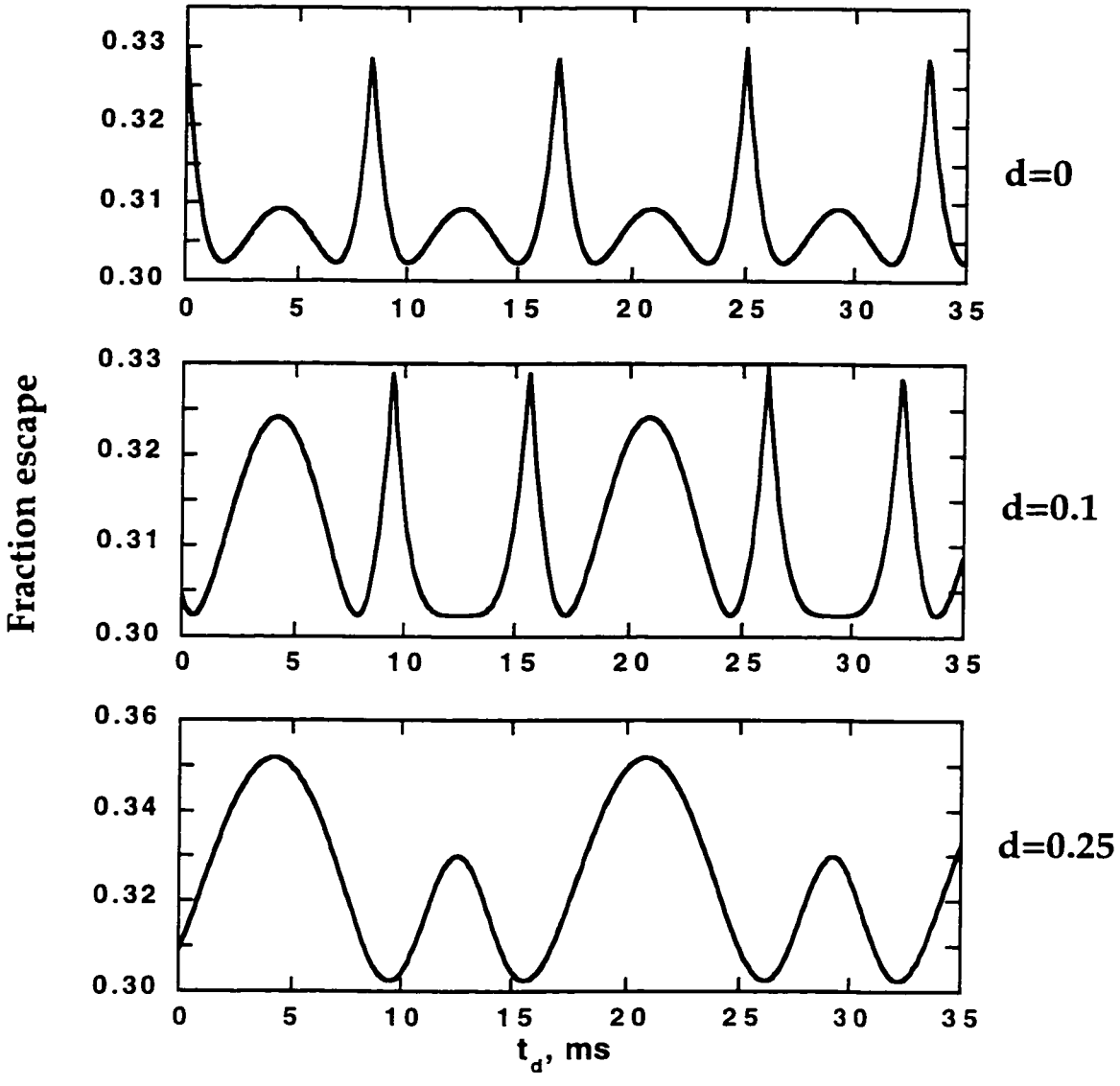

Figure 3.20. Calculated dependence of the fraction escape for a system with non-degenerate S-T levels. The plots are calculated according to Eq. 3.16, for f = 0.25 and d values of 0, 0.1 and 0.25.

3.7. Conclusion

In general, it is well known that MFs influence the behaviour of free radicals in heterogeneous media. These studies have illustrated that an applied MF increases the lifetime and concentration of RPs generated mostly in a triplet state. The consequence of these effects is that radicals, now having a longer lifetime and a lower probability to recombine with their geminate partner, will be more likely to react with another molecule. This results in an increased level of radical-molecule reactions that may be implicated in some biological effects. However, we do not intend to claim that these are the only effects influencing biological systems. Yet, the role of radical involvement in biological processes cannot be denied. It is thus hoped that this chemical study of RP reactions in organized systems in the presence of AC/DC MFs gives us a better understanding of the role of the RP mechanism and field effects in biological systems.

In this work, we have investigated the behaviour of RPs in the presence of 60 Hz oscillating MFs superimposed over static MFs. Our results show that an AC MFE on radical behaviour is identical to that exerted by a DC field of the same instantaneous strength provided that the frequency is small in comparison with the RP dynamics. Most importantly, a knowledge of radical behaviour under the DC fields alone allows one to quantitatively predict the radical behaviour under

an AC field alone or combined AC/DC fields. These results also show that triplet RP reactions in micellar solutions behave the same way under isolated 60 Hz oscillating fields as they do under isolated static fields at any given point in time. Combined AC/DC fields are found to lead to increased radical concentrations and oscillating free radical concentrations. The interesting observation is that the frequency of the radical concentration rarely follows the same pattern as the applied AC MF. In fact, an AC field alone leads to radical oscillations at 120 Hz, twice the frequency of the external AC field used in these experiments. The oscillation patterns get even more complex when S-T levels of the RPs are nondegenerate.

We further discovered that by making small changes in the absolute and relative values of the oscillating and static field components, the field effects on escaping radicals can change dramatically. Our calculations show that when the AC field is weaker than the DC field, no overall change in RP behaviour and its average concentration is observed. With this case, it is found that the radical concentration oscillates with the same frequency as that of the MF. Moreover, when the intensity of the AC field is comparable to that of an overlapping DC field, the average radical concentration is decreased.

Our results also suggest that AC fields weaker than the Earth's DC field of 0.5 gauss will have a negligible impact on the behaviour of RPs in

organized systems. Although our results indicate that the effects of low MF strengths, i.e., environmental fields, on radical behaviour is rather small, it has been suggested that these small field effects can dramatically affect the rates of enzymatic reactions up to a factor of 100 in biological systems.[42] In this study, a model is proposed based on Michaelis-Menten reaction scheme to include an enzyme-substrate complex as an intermediate existing in a spin-correlated RP state.[42]

3.8. References

(1) Bittl, R.; Schulten, K.; Turro, N. J. *J. Chem. Phys.* **1990**, *93*, 8260.

(2) Scaiano, J. C.; Abuin, E. B.; Stewart, L. C. *J. Am. Chem. Soc.* **1982**, *104*, 5673.

(3) Scaiano, J. C. *Trans. Roy. Soc. Canada* **1983**, *21*, 133.

(4) Evans, C. H.; Scaiano, J. C.; Ingold, K. U. *J. Am. Chem. Soc.* **1992**, *114*, 140.

(5) Gould, I. R.; Zimmt, M. B.; Turro, N. J.; Baretz, B. H.; Lehr, G. F. *J. Am. Chem. Soc.* **1985**, *107*, 4607.

(6) Taraban, M. B.; Leshina, T. V.; Salikov, K. M.; Sagdeer, R. Z.; Molin, Y. N.; Margoiskaya, O. I.; Vyazankin, N. S. *J. Oranomet. Chem.* **1983**, *256*, 31.

(7) McLauchlan, K. *Physics World* **1992**, *(January)*, 41.

(8) Milhan, S. *Health Perspect.* **1985**, *62*, 297.

(9) Lin, R. S.; Dischinger, P. C.; Conde, J.; Farrell, K. P. *J. Occup. Med.* **1985**, *27*, 413.

(10) Kivisakk, E.; Moberg, L. "SSi Policy: Health Risks from Electromagnetic Fields," Swedish Radiation Protection Institute, 1993.

(11) Feychting, M.; Ahlbom, A. "MFs and Cancer in People Residing Near Swedish High Voltage Power Lines," Institute of Environmental Medicine, The Royal Caroline Institute, Stockholm, Sweden, 1992.

(12) Turro, N. J.; Kraeutler, B. *Acc. Chem. Res.* **1980**, *13*, 369.

(13) Steiner, U. E.; Ulrich, T. *Chem. Rev.* **1989**, *89*, 51.

(14) Hileman, B. *C & E News* **1993**, *November 8, 1993*, 15.

(15) Encinas, M. V.; Scaiano, J. C. *J. Am. Chem. Soc.* **1981**, *103*, 6393.

(16) Zor, T.; Halifa, I.; Kleihaus, S.; Chorev, M.; Selinger, Z. *Biochem. J.* **1995**, *306*, 253.

(17) Ying, W.; Stepp-Lorenzino, L.; Cai, K.; Aloise, P.; Coleman, P. S. *J. Biol. Chem.* **1994**, *269*, 470.

(18) Breslow, R. *Acc. Chem. Res.* **1995**, *28*, 146.

(19) Williams, N.; Ackerman, S. H.; Coleman, P. S. *Methods Enzymol.* **1986**, *126*, 667.

(20) Artuso, T.; Bernadou, J.; Meunier, B.; Piette, J.; Paillous, N. *Photochem. Photobiol.* **1991**, *54*, 205.

(21) Scaiano, J. C.; Cozens, F. L.; McLean, J. *Photochem. Photobiol.* **1994**, *59*, 585.

(22) Scaiano, J. C.; Lougnot, D. J. *Chem. Phys. Lett.* **1984**, *105*, 535.

(23) Wakasa, M.; Sakaguchi, Y.; Hayashi, H. *Chem. Lett.* **1994**, 49.

(24) Turro, N. J.; Yekta, A. *J. Am. Chem. Soc.* **1978**, *100*, 5951.

(25) Weller, A.; Nolting, F.; Staerk, H. *Chem. Phys. Lett.* **1983**, *96*, 24.

(26) Tanimoto, Y.; Okada, N.; Itoh, M.; Iwai, K.; Sugioka, K.; Takemura, F.; Nakagaki, R.; Nagakura, S. *Chem. Phys. Lett.* **1987**, *136*, 42.

(27) Doubleday, C., Jr.; Turro, N. J.; Wang, J.-F. *Acc. Chem. Res.* **1989**, *22*, 199.

(28) Wang, J.; Doubleday, C., Jr.; Turro, N. J. *J. Phys. Chem.* **1989**, *93*, 4780.

(29) Weller, A.; Staerk, H.; Treichel, R. *Faraday Discuss. Chem. Soc.* **1984**, *78*, 271.

(30) Frey, A. H., Editor *On the Nature of Electromagnetic Field Interactions with Biological Systems*; R.G. Landes Co.: Austin, 1994.

(31) Razi Naqvi, K.; Staerk, H.; Gillbro, T. *Chem. Phys. Lett.* **1977**, *49*, 160.

(32) Staerk, H.; Razi Naqvi, K. *Chem. Phys. Lett.* **1977**, *50*, 386.

(33) Turro, N. J.; Kraeutler, B. *J. Am. Chem. Soc.* **1978**, *100*, 7432.

(34) Grissom, C. B. *Chem. Rev.* **1995**, *95*, 3.

(35) Harkins, T. T.; Grissom, C. B. *Science* **1994**, *263*, 958.

(36) Werner, H. J.; Staerk, H.; Weller, A. *J. Chem. Phys.* **1978**, *68*, 2419.

(37) Nath, D. N.; Chowdhury, M. *Chem. Phys. Lett.* **1984**, *109*, 13.

(38) Evans, C.; Ingold, K. U.; Scaiano, J. C. *J. Phys. Chem.* **1988**, *92*, 1257.

(39) Scaiano, J. C.; Cozens, F. L.; Mohtat, N. *Photochem. Photobiol.* **1995**, *62*, 818.

(40) Nolting, F.; Staerk, H.; Weller, A. *Chem. Phys. Lett.* **1982**, *88*, 523.

(41) Bittl, R.; Schulten, K. *Chem. Phys. Lett.* **1988**, *146*, 58.

(42) Walleczek, J.; Eichwald, C. *Biophysical Journal* **1996**, *71*, 623.

4. Static Magnetic Field Effects on the Behaviour of Free Radicals in Proteins

4.1. Introduction

In the previous Chapter, the behaviour of a triplet RP confined within the heterogeneous medium of micelles was described under the influence of static, oscilllating, and combined static and oscillating MFs. These results showed that the effect of a 60 Hz field can be quantitatively predicted from data obtained under static fields. Thus, during the short lifetime of radical-radical encounters, ~10^{-6} s, the RP senses a static field at each instant in the 60 Hz cycle.

In this work, we have looked at the influence of MFs on the dynamical behaviour of free radicals under conditions which better mimic those of biological systems. An important question thus becomes whether or not proteins provide a similar environment (like micelles) for the

development of MFEs. If so, the RP mechanism of MFEs on radical behaviour in heterogeneous media can be applied to biological systems.

It has been debated in the literature that free radicals are involved in many biological processes and they are thought to be a major initiator of some types of cancer.[1] A MF is known to slow down the rate of recombination of radicals.[2-4] This consequently leads to an increase in the concentration of free radicals which can react with other molecules. If the rates of recombination of radicals are slowed down in the presence of a MF, they have a greater chance to diffuse away and react with proteins and/or with other biomolecules in tissue.[1]

Recently, there have been other studies reporting that a MF can perturb the rates of singlet to triplet conversion of a triplet RP in biological systems. Grissom *et al.* have shown that the enzyme-induced homolysis of the C-Co bond of methylcob(III)alamin (by ethanolamine ammonia lyase) is sensitive to an applied MF and that their results can be explained by the RP mechanism.[5,6] In another study, Chignell and Sik report that the phototoxic ketoprofen-induced photohomolysis of human erthrocytes is also MF dependent.[7]

The expanding use of benzophenones (BPs) as biochemical probes in recent years has been attributed to a number of reasons. More importantly is that BPs are known to be more stable than other

potential photoprobes, such as diazo esters and aryl azides. In addition, BPs can be activated at long wavelengths (i.e., $\lambda_{ex} \geq 300$ nm), where the light-induced damage to the protein is minimal.[8,9] They have also been used in the design of anti-flammatory drugs such as ketoprofen.[7,10,11] Therefore, the study of their photochemistry in biological systems can be useful in the context of their pharmacological applications.

4.2. Experimental

4.2.1. Materials

Bovine serum albumin (BSA, fatty-acid free), human serum albumin (HSA, fatty-acid and globulin free), lysine-tyrosine-lysine (Lys-Tyr-Lys, acetate salt), poly-L-leucine (MW 8,800), poly-L-tyrosine (MW 35,700), poly-L-valine, and poly-L-lysine (hydrobromide, MW 8,200) from Sigma were used as received. 1,2,3,4,5-pentafluorobenzophenone (PFBP), decafluorobenzophenone (DFBP), 4-benzoylbenzoic acid, and N-methyl acetamide were used as received from Aldrich. Benzophenone (BP) from Aldrich was recrystallized twice from ethanol prior to use.

4.2.2. sample preparation

A 0.1 M buffer solution (prepared from potassium dihydrogen ortho-phosphate, pH=7) was prepared with Millipore filtered water. Special 7 X 7 mm^2 quartz cells were used to hold the protein sample in a separate compartment from the buffer solution. With these cells, it is possible to deaerate the aqueous buffer solution prior to mixing it with the protein sample. After the buffer solution is degassed with oxygen-free nitrogen for 30 min., the protein sample (6 mg/ml) is gently mixed in the buffer solution until dissolved. This cautionary step was taken to prevent subjecting the protein solution to the degassing procedure, which might lead to denaturation of the protein.

Benzophenone (1.1 mM), PFBP (1.1 mM), and DFBP (1.5 mM) were incorporated into the protein solution by injecting a small volume of an alcoholic stock solution (methanol) of the ketones into the cell containing the protein solution. The concentration of the ketones gave an absorption of 0.15 - 0.25 at the laser wavelength. The protein concentration (~6 mg/ml) was chosen so that it did not contribute to the absorption of light at the laser wavelength. However, for the DFBP system the protein concentration was higher than the above concentration (~50 mg/ml, *vide infra*) .

Solutions of 4-benzoylbenzoic acid (~1.5 mM) were prepared in a 80:20 v/v mixture of water:acetonitrile. For the quenching experiments of 4-

benzoylbenzoic acid, concentrated aqueous solutions (pH ≈ 6) of Lys-Tyr-Lys and poly-L-lysine were injected into the sample cell. An excimer laser (308 nm, ≤ 60 mJ/pulse) was used to excite the samples and generate the transients. A static MF was obtained with the Hewlett-Packard 6282A power supply on a homemade magnet surrounding the sample holder area (see section 2.1.2).

4.3. Results

As mentioned earlier, BP and its derivatives have been widely used as photoprobes for covalent modification of proteins and other biomolecules.[12] They are known to undergo hydrogen abstraction upon photochemical excitation.[13] Being hydrophobic, these probes can be incorporated into the hydrophobic interior of globular proteins. In the studies previously presented, a hydrogen donor, 1,4-cyclohexadiene, was added to the micelles containing BP to facilitate the generation of the RP. However with the proteins, no additional hydrogen donor was used, as the protein acts as one itself (see Eq. 4.1).

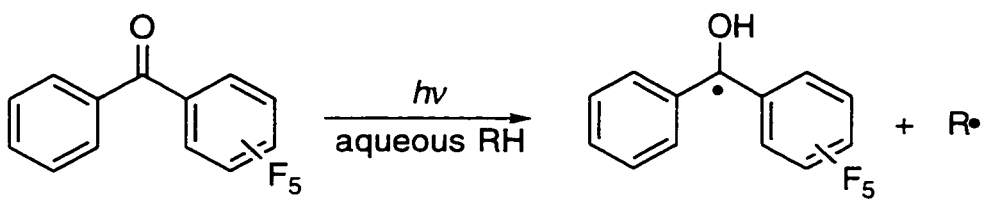

R = BSA
HSA

Eq. 4.1

This ensures that the nature of the hydrogen donor (the protein) is kept fixed in the experiments. In order to accelerate the RP generation, substituted benzophenones with an enhanced reactivity towards hydrogen abstraction reaction were also used as probes. Scaiano and co-workers had previously shown that the hydrogen abstraction reaction of triplet fluorinated BPs occurs at faster rates than triplet BP.[14] For example, the triplet states of BP, PFBP, and DFBP react with 1,4-cyclohexadiene with rate constants of 2.90 X 10^8, 2.53 X 10^9, and 3.04 X 10^9 $M^{-1}s^{-1}$, respectively.[14] In fact, the best choice as the probe for these experiments would be DFBP. However, perfluorinated compounds exhibit solubility problems. In our experiments, the amount of the serum proteins had to be increased to 50 mg/ml in order to solubilize a concentration of DFBP (≥1.5 mM), large enough to produce acceptable transient signals. Therefore, BP and PFBP, which showed no sloubility problems at protein concentrations of 6 mg/ml, were primarily used in these experiments.

The photolysis of 1.1 mM BP in BSA solution at 308 nm laser wavelength leads to the transient absorption spectrum shown in Figure 4.1. The peaks in the 320-340 nm and the 520-550 nm regions can be assigned to the BP ketyl radicals. However, the latter region also includes absorption due to the triplet state of benzophenone. To monitor the behaviour of the ketyl radical in the absence and presence

of an MF, the transients were recorded at 330 nm (see Figure 4.2). Similar MFEs were also observed when the transient radicals were monitored at 540 nm. However in this region, there still exists some overlap with the absorption band due to the triplet BP. From Figure 4.2, it can be seen that the radicals appear before the triplet has completely decayed. The decay of triplet BP, monitored at 620 nm, is shown in Figure 4.2. In fact, at wavelengths > 600 nm, the transient absorption can be assigned to the triplet state of BP only as the ketyl radical has no absorption at 620 nm.[15]

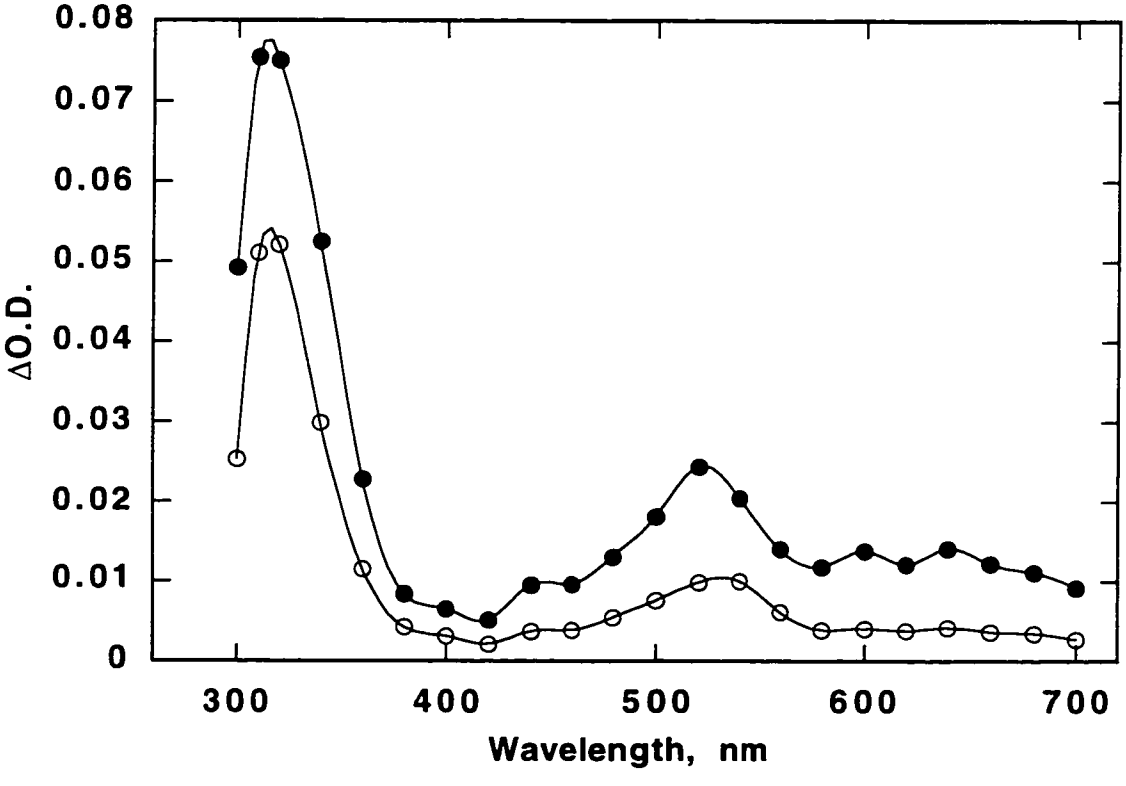

Figure 4.1. The transient absorption spectrum of 1.1 mM benzophenone in 6.5 mg/ml BSA at 280 ns (•) and 2.08 μs (o) after 308-nm excitation.

The appearance of the ketyl radical in Figure 4.2 before the decay of the triplet BP is indicative of the existence of two different triplet populations. The first population, that gives rise to the instantaneous generation of ketyl radicals, is located in the protein environment. The lifetime of this population can be assumed to be too short to be detected on the time scales of our experiment. The lifetime of the second triplet population (shown in Figure 4.2) is however relatively long (~1.8 μs), suggesting that it is not associated with the protein. Therefore, their contribution to the formation of ketyl radical is negligible.

It is worth mentioning that the binding constant of ketoprofen, a molecule similar in structure to BP, to HSA has been determined by the method of circular dichroism.[16] In this study, the association constant for ketoprofen is reported to be 3.8 X 10^6 M^{-1}. However, the binding affinity decreases 100-fold to 5 X 10^4 M^{-1} as the protein concentration increases.[16] As a first approximation, it can be assumed that with the mM concentrations of BPs used in our study, most of the probe is associated with the protein. However, there exists a delicate balance between the concentration of the protein and that of the probe, as the binding constants are found to depend on both concentrations.

Figure 4.2 shows the difference between the decay traces of the ketyl radical monitored at 330 nm in the absence and presence of an external MF. The observed difference is a result of the changes in the dynamics

of the RP formation brought upon by the MF. It should be noted that a MF strength of ~1400 gauss does not affect the decay of the triplet state.[15]

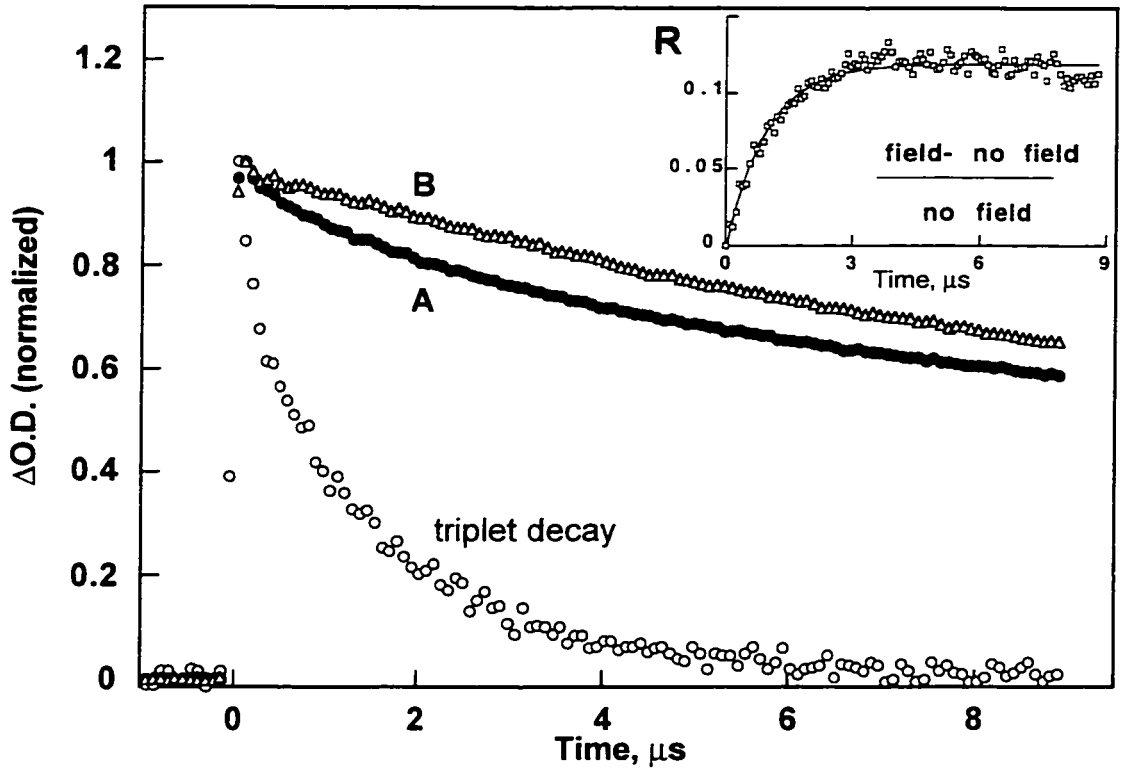

Figure 4.2. Transient decay traces of ketyl radicals monitored at 330 nm generated upon photolysis of 1.1 mM BP in 6.5 mg/ml BSA in the absence (A) and presence (B) of a 1370 gauss external magnetic field. The *triplet decay* trace has been monitored at 620 nm, where the ketyl radical absorption is negligible. The insert shows the ratio (R) of the difference between the decay of the radical in the presence and absence of the magnetic field over that in the absence of a field with respect to time (see Eq. 4.2).

The insert in Figure 4.2 shows a plot of the difference between the normalized decay traces as a function of time according to the following equation,

$$R = \frac{\Delta O.D._{magn} - \Delta O.D._{no\ magn}}{\Delta O.D._{no\ magn}} \qquad \text{Eq. 4.2}$$

where ΔO.D. (with the appropriate subscripts) refers to the unnormalized intensity of each decay trace recorded at 330 nm in the presence and absence of a MF at a given time after laser excitation. This plot is useful in that it clearly shows the time evolution of the MFE on the decay of the ketyl radical. For BP in BSA, the field effect is found to saturate after ~3 μs. It is also found that a mono-exponential growth curve fits the data points (R) quite well and gives a RP lifetime of 0.94 μs. It is worth mentioning that identical experiments on the control system of BP in 0.1 M phosphate buffer exhibits no MFEs.

Lower MFEs observed in proteins than micelles indicate that the field sensitive process (i.e., ISC between S and T levels) is not the dominant process. Thus, separation of the radicals with a rate constant of ca. 10^6 s^{-1} is the main process. The residual absorption seen in the decay traces in Figure 4.2 and Figure 4.3 could partly be a result of LATs (ring coupling products). These transients however are not affected by a MF. Since similar MFEs are observed with the ketyl traces monitored at 540-550 nm region (where there is no absorption due to the LATs), the contributions from the absorption of LATs at 330 nm are considered to be small. Figure 4.3 shows the decay traces of the triplet state and ketyl radical of PFBP in HSA. Comparing the time scales of these decay traces with those seen in Figure 4.2, it is apparent that the photoreduction of this fluorinated ketone occurs faster than for BP itself. A field effect of ~12% is observed with PFBP in HSA (see the insert in Figure 4.3).

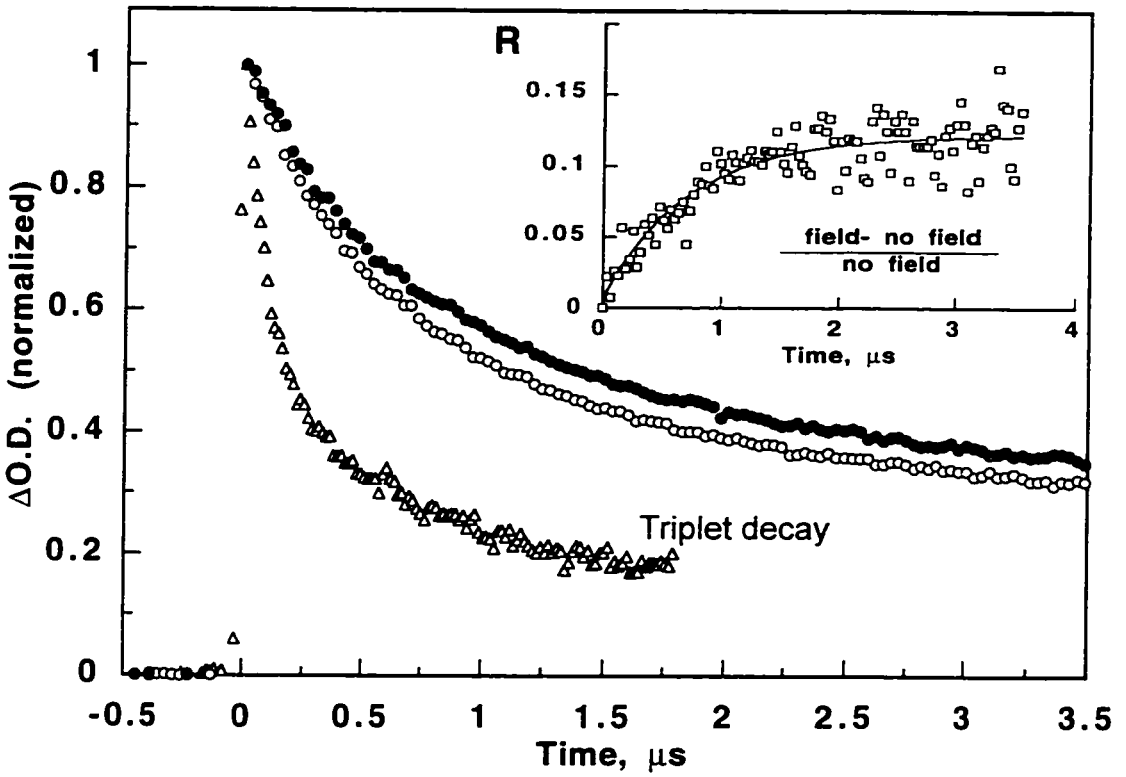

Figure 4.3. Transient decay traces of ketyl radicals monitored at 330 nm generated upon photolysis of 1.1 mM PFBP in 6.5 mg/ml HSA in the absence (o) and presence (•) of a 1370 gauss external magnetic field. The *triplet decay* trace has been monitored at 620 nm, where the ketyl radical absorption is negligible. The insert shows the ratio (R) of the difference between the decay of the radical in the presence and absence of the magnetic field over that in the absence of a magnetic field with respect to time (see Eq. 4.2).

Note that the field effect with this system mainly occurs during the first microsecond and starts to plateau after 2 μs. The growth fit of the time evolution of the field effect gives a RP lifetime of 0.72 μs. Again, the ketyl radical is monitored at 330 nm, as the transient absorption is weaker in the 520-550 nm region.

As mentioned earlier, in order to incorporate sufficient concentrations of DFBP (i.e., ≥ 1.5 mM) into the protein, the experiments had to be

carried out at higher concentrations of the protein (50 mg/ml). Although the transient absorption spectrum with this concentration of protein shows absorption bands at wavelengths such as 360, 440, and 600-700 nm regions, the overlap between the two spectra (i.e., the protein with and without DFBP) is minimal in the 520-580 nm region (see Figure 4.4). Figure 4.4 illustrates the difference between the transient absorption spectra of DFBP in BSA and the blank BSA. Therefore, the transient absorptions observed in the region of 520-580 nm can be safely assigned to the triplet and the ketyl radical of DFBP. Consequently, the behaviour of the ketyl radical in the absence and presence of an MF was monitored at 560 nm. The strong transient absorption band at 360 nm may incorporate contributions due to the peptide radicals, as similar transient absorption spectra have been observed with cyclic dipeptides.[17]

Figure 4.5 shows an average of three traces of the ketyl radical taken in the absence and presence of the MF, so as to minimize the noise associated with weak signals. Shown in the Figure is also the decay of the triplet state with a lifetime of ~200 ns, which is faster than those seen for BP and PFBP triplets. The insert is a plot of Eq. 4.2 as a fuction of time. The MFE observed with this system is bigger (~25%) than those observed with BP and PFBP. Note that the signal-to-noise ratio is also poor in this case, specifically at longer times where the decay of the radical is almost complete.

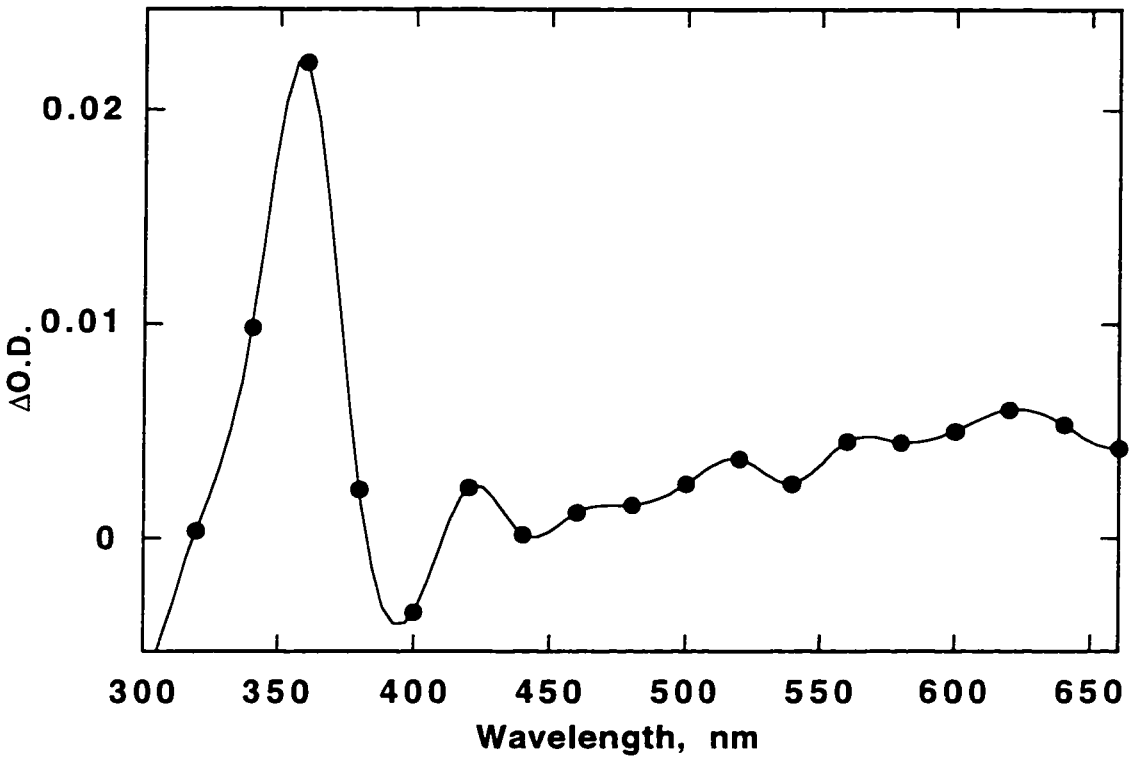

Figure 4.4. The difference between the transient absorption spectra of 1.5 mM decafluorobenzophenone in 50 mg/ml BSA and that of 50 mg/ml BSA at 136 ns (•) after 308-nm excitation.

The poor quality of the traces may be due to lower solubility of DFBP in the aqueous solution compared with BP and PFBP. Moreover, it should be emphasized that the signals are weak in this region (i.e., 520-580 nm), thus their subtraction and division from each other (R) leads to the amplification of the noise seen in the insert plot. The fit of the data points of this plot leads to a RP lifetime of 0.48 μs. It is during this period that the competition between the geminate recombination of the radicals and the escape from the microreactor cage occurs (see Scheme 3.1). Those radicals that succeed in separating from their partner can participate in random reactions with another radical.

Reactions of this type, however, take place on longer time scales than geminate reactions.[18] Also, as the nature of the triplet probe to generate the RP (by hydrogen abstraction) changes, the time scales for the separation of the radicals changes as well. In our experiments, the separation becomes a faster process when the benzophenone probe is fluorinated.

The observable triplet decay in Figure 4.2, Figure 4.3, and Figure 4.5 is attributed to a population that is not associated with the protein and thus is in a less reactive environment. Yet, the triplet lifetime of DFBP is the shortest while that of BP is the longest in this medium, which suggests that the triplets are still being quenched by reactive sites. It is to be noted that the lifetime of triplet BP in 0.1 M buffer (pH=7) is 6.5 μs.

As with the studies in the micelles, the fraction of radical escape as a function of MF strength (see Figure 3.2 and Figure 3.3) was followed. However, these experiments proved to be difficult for the following reasons. Firstly, the field effects on the radical behaviour in the bovine proteins are 3-4 times smaller than those observed with the micellar systems. Secondly, no additional hydrogen donor was added to the protein systems, which means that the photoreduction of triplet ketones that are not associated with the protein is not an instantaneous process (i.e., on the time scales of the experiment).

As pointed out earlier, it is believed there are two different triplet populations. The first leads to the rapid generation of the ketyl radical. This step is necessary for the determination of the MF-dependence of separating radicals. The second population however leads to the observable triplet decays shown in Figure 4.2, Figure 4.3, and Figure 4.5.

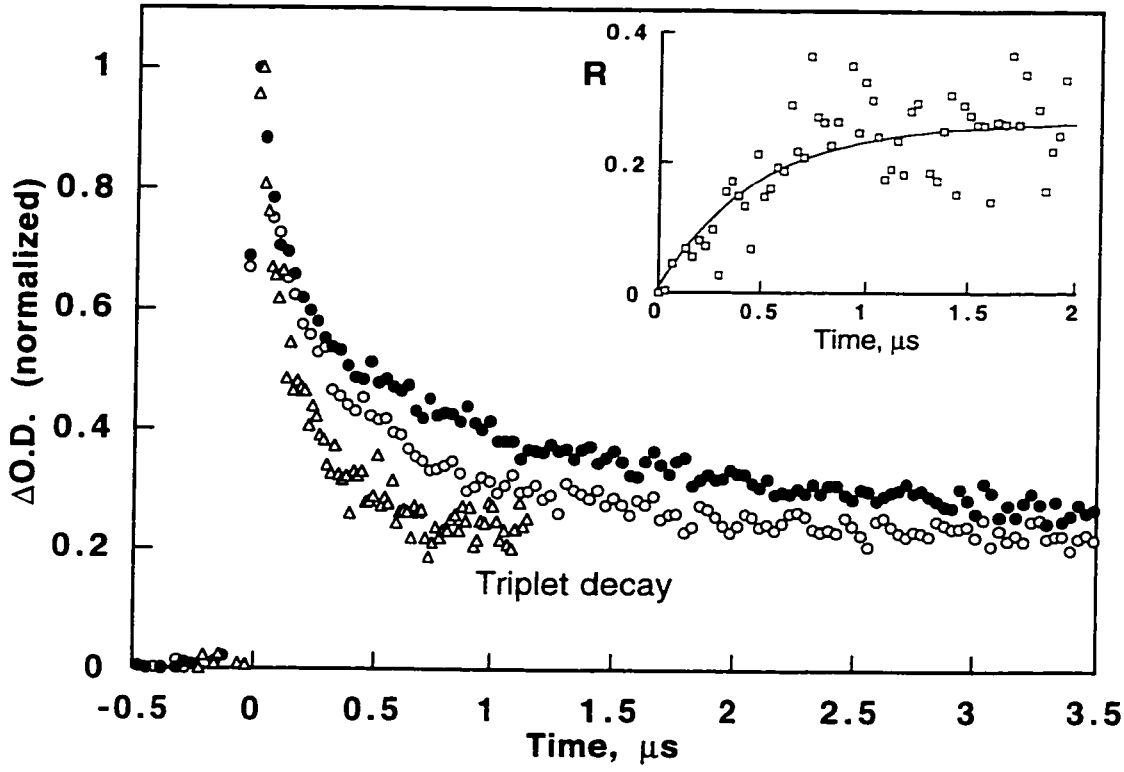

Figure 4.5. The average of three transient decay traces of ketyl radicals monitored at 560 nm generated upon photolysis of 1.8 mM DFBP in 50 mg/ml BSA in the absence (o) and presence (•) of a 1370 gauss external magnetic field. The *triplet decay* trace is monitored at 600 nm, where the ketyl radical absorption is negligible. The insert shows the ratio (R) of the difference between the decay of the radical in the presence and absence of the magnetic field over that in the absence of a magnetic field with respect to time (see Eq. 4.2).

As a result of the above uncertainties, we claim that a plot of the type shown in Figure 4.6, provides only a semi-quantitative measure of the

behaviour of radical escape with a change in MF strength. Since the magnetic field strength is the only variable in this case, they are adequate to judge the significance of the trends observed. Figure 4.6 illustrates our analysis of the ketyl radical derived from BP in both HSA and BSA. The fraction escapes in Figure 4.6 are determined by the method described in section 3.3.

As seen in Figure 4.2, the signals are less noisy in the BP system compared to those in the PFBP and DFBP (Figure 4.3 and Figure 4.5). Thus, the BP system was chosen for the MF-dependence analysis. The value of the fraction escape was calculated by taking the ratio of the signal intensity at a delay time of 1 μs for HSA and of 4.5 μs for BSA relative to the time of laser excitation. At these delay times, up to 75% of the corresponding traces have decayed. A magnetic field-dependence plot of free radical production (Figure 4.6) also provides us with the values of $B_{1/2}$, the field strength at half saturation. The values of $B_{1/2}$, calculated by an exponential fit of the data points, are 770 and 413 gauss for BSA and HSA, respectively. Despite the general expectation that the values of $B_{1/2}$ are lower in the larger aggregates,[15,19,20] these values are surprisingly bigger than expected. Although the bovine proteins on the whole are larger aggregates than micelles (see sections 1.2 and 1.4), it may be that the probes are largely associated in the smaller microheterogeneous regions of the protein.

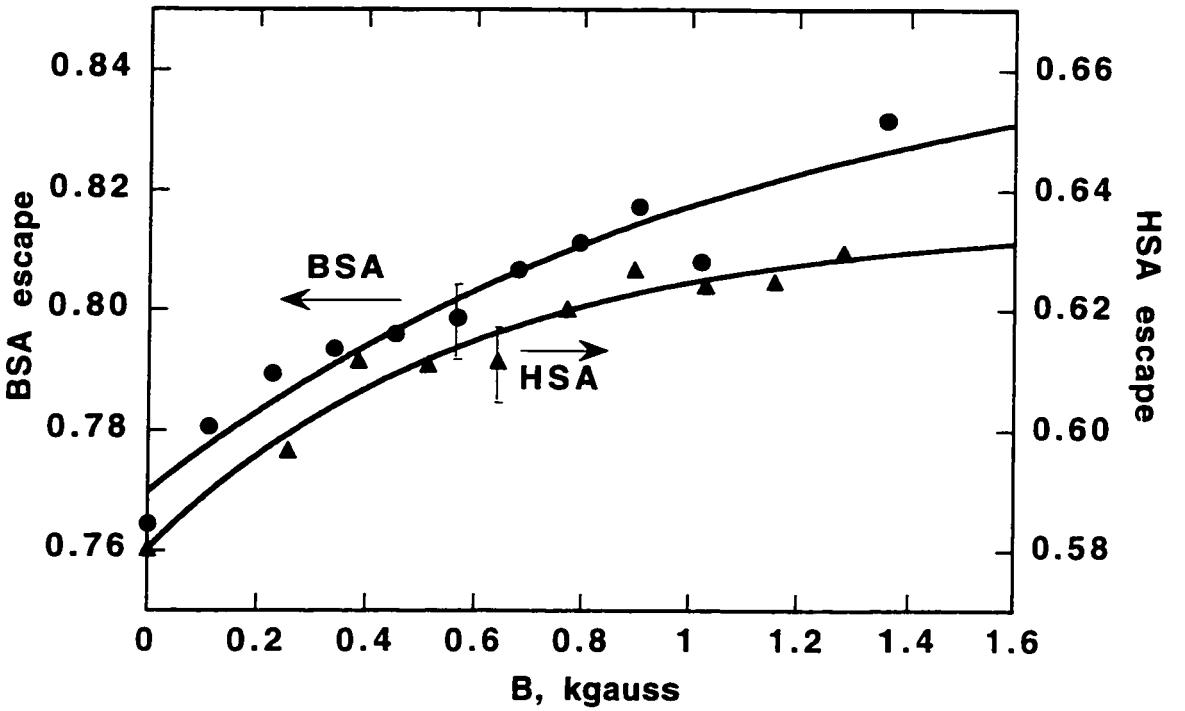

Figure 4.6. Magnetic field dependence of the ratio between the signal after 4.5 μs (•, BSA) or 1 μs (▲, HSA) to that immediately after laser excitation. The value is proportional to the fraction of radical separation. Representative error bars have been included; they reflect the reproducibility within a given set of experiments and not the absolute errors.

When attempting to establish which site of the protein donates the hydrogen by using model compounds, we mainly encountered solubility difficulties. Among the many different commercially available amino acids tried for these experiments, we were able to carry out kinetic studies with only one of them and with a tripeptide. Since BP is sparingly soluble in aqueous solutions, we choose its water soluble derivative, 4-benzoylbenzoic acid, instead. The transient absorption spectrum of this ketone in the absence (Figure 4.7) and presence of a hydrogen donor (0.03 M 1,4-cyclohexadiene, Figure 4.8) in

acetonitrile can be seen below. The characteristic absorption maximum due to the triplet state is around 560 nm for this ketone. In the presence of the hydrogen donor, the absorption peak of the ketyl radical, which is red shifted with respect to the triplet state peak, is seen around 570 nm (see Figure 4.8).

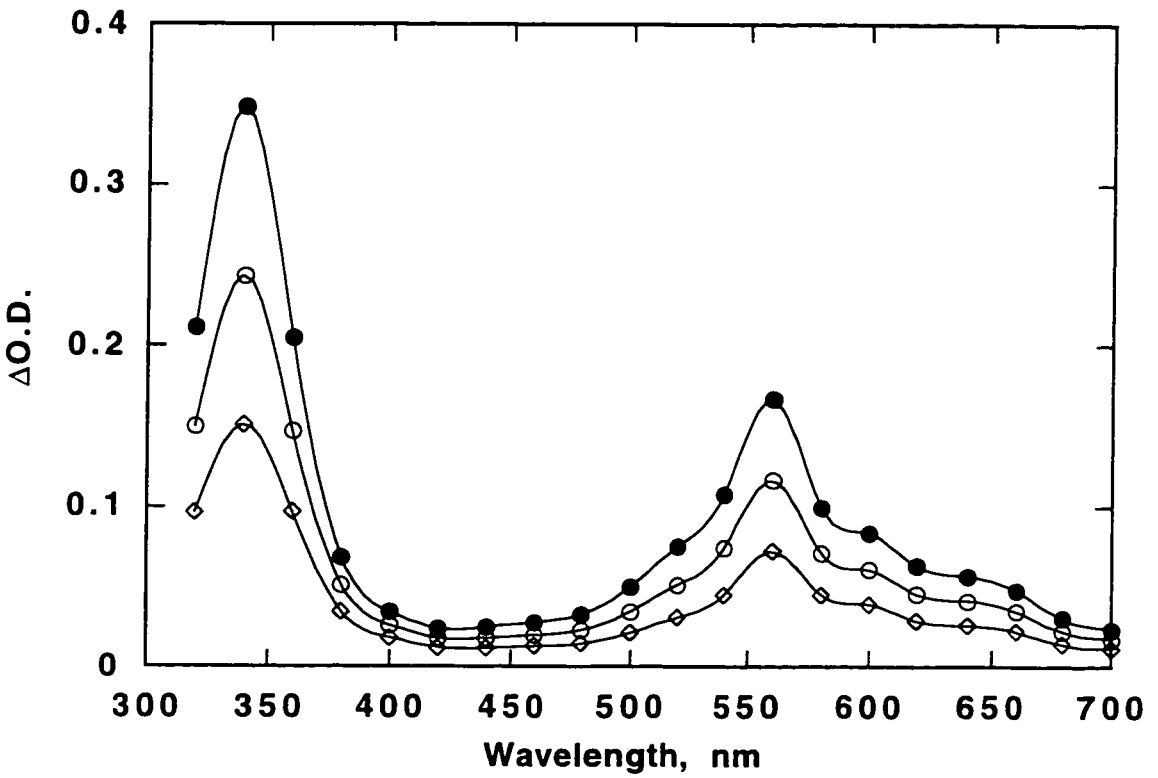

Figure 4.7. The transient absorption spectrum of 1.6 mM of 4-benzoylbenzoic acid in acetonitrile at 280 ns (•), 960 ns (o), and 2.16 μs (◊) after 308-nm excitation.

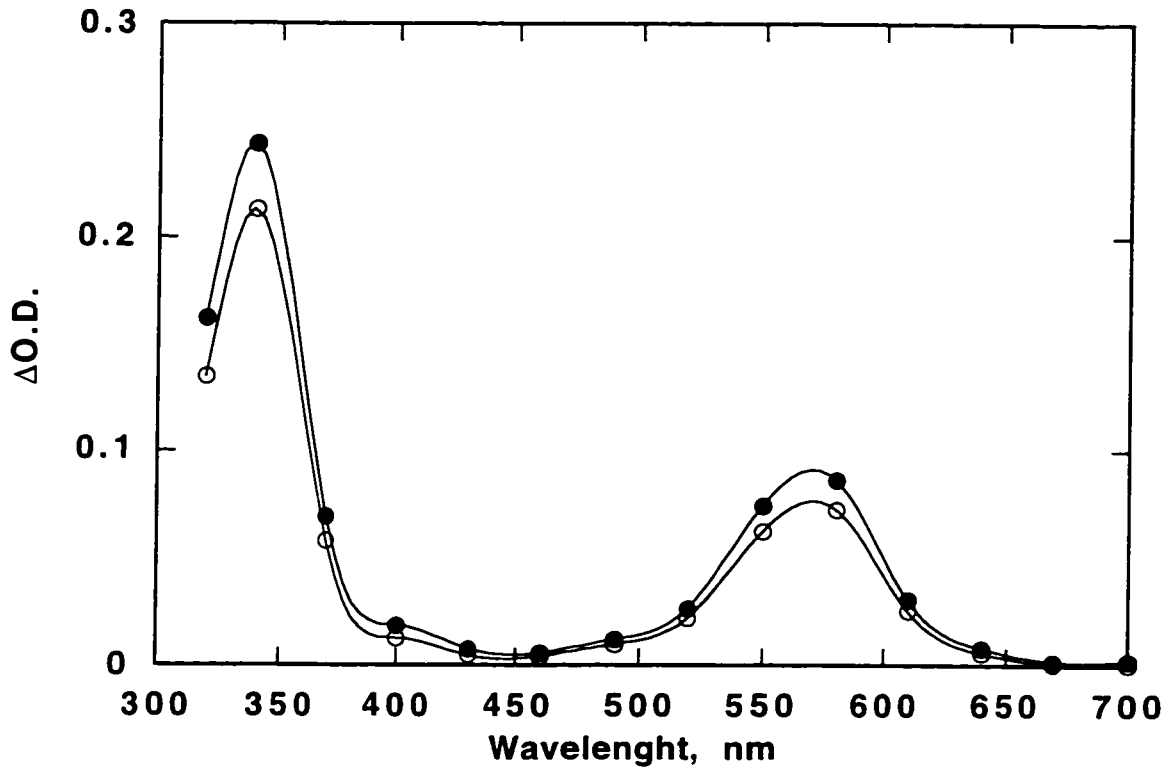

Figure 4.8. The transient absorption spectrum of 1.6 mM of 4-benzoylbenzoic acid in acetonitrile in the presence of 0.03 M 1,4-cyclohexadiene at 48 ns (•) and 1.52 μs (o) after 308-nm excitation.

The triplet state quenching of the 4-benzoylbenzoic acid by Lys-Tyr-Lys and poly-L-lysine occurs with rate constants of 3.2 X 10^9 $M^{-1}s^{-1}$ and 1.2 X 10^{10} $M^{-1}s^{-1}$, respectively. The quenching rate constants are obtained from a plot of the first-order observed triplet decay as a function of the quencher concentration, i.e.,

$$k_{obs.} = \tau_0^{-1} + k_q[quencher] \qquad \text{Eq. 4.3}$$

where τ_0^{-1} is the triplet lifetime in the absence of quencher. Figure 4.9 and Figure 4.11 show quenching plots for the above quenchers, i.e., the

tripeptide and the amino acid, respectively. The insert plot in Figure 4.9 and Figure 4.11 illustrate representative triplet decay traces in the absence and presence of the corresponding quenchers.

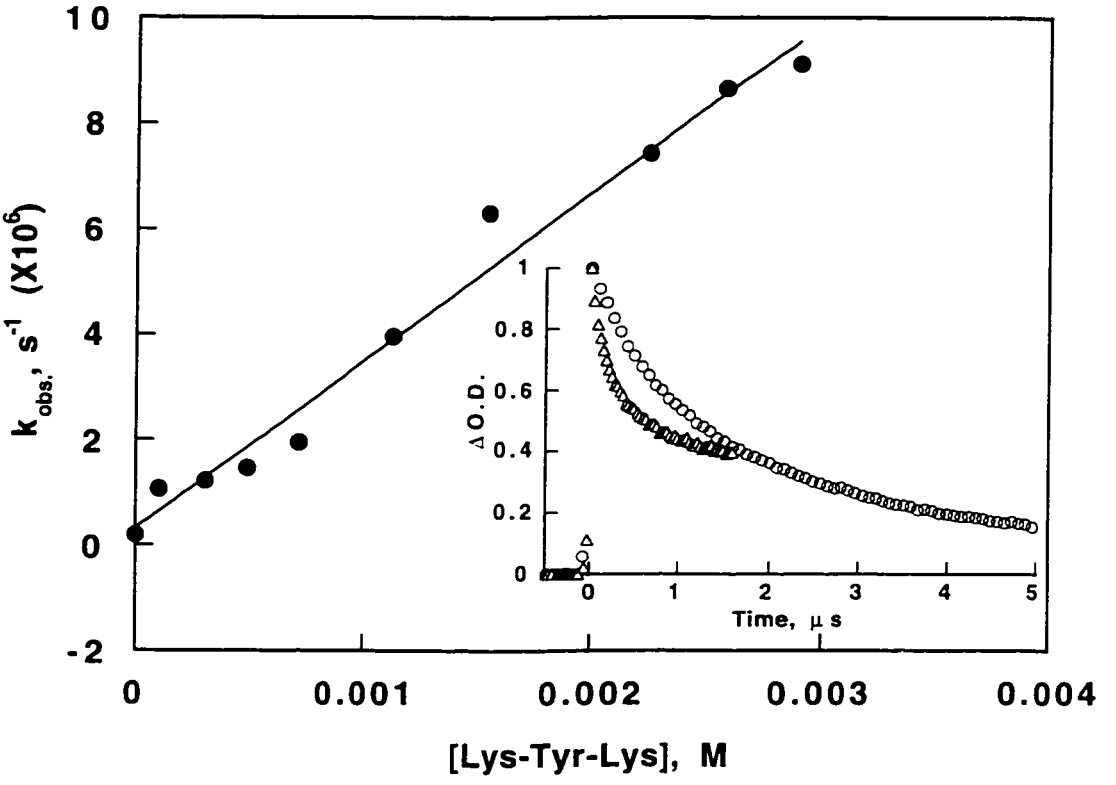

Figure 4.9. The quenching plot of 1.5 mM 4-benzoylbenzoic acid in 80:20 water:acetonitrile with Lys-Tyr-Lys (•); the fit is according to Eq. 4.3. The insert shows two representative triplet decay traces in the absence (o) and presence of 1.3 mM (Δ) of the quencher monitored at 540 nm.

Figure 4.10 is the transient absorption spectrum of 4-benzoylbenzoic acid in 80:20 water:acetonitrile in the presence of 2.6 mM of Lys-Tyr-Lys. The growth of the ketyl radical monitored at 340 nm is shown in the insert plot in Figure 4.10. Note that the radical growth occurs with similar kinetics as the triplet state of the ketone disappears, as expected.

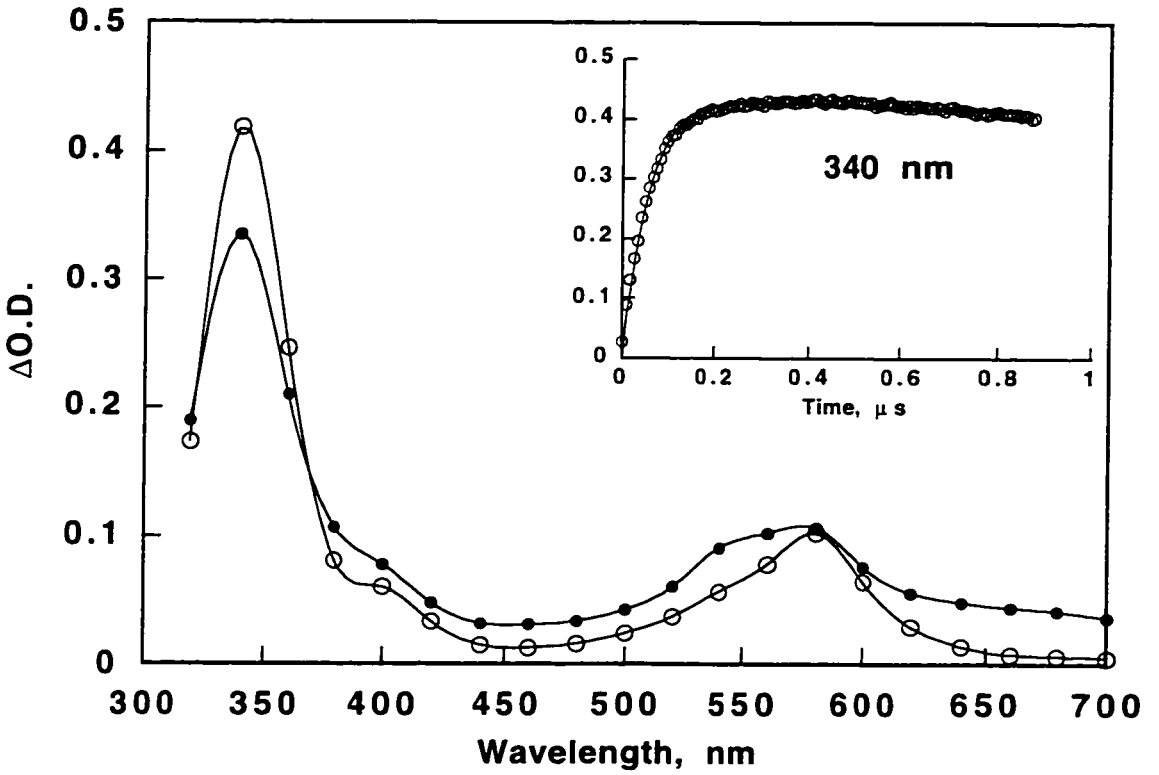

Figure 4.10. The transient absorption spectrum of 1.5 mM of 4-benzoylbenzoic acid in 80:20 water:acetonitrile in the presence of 2.6 mM of Lys-Tyr-Lys at 96 ns (•) and 712 ns (o) after 308-nm excitation. The insert is the growth of the ketyl radical (o) monitored at 340 nm.

The 308 nm laser photolysis of 1.3 mM 4-benzoylbenzoic acid in 80:20 water:acetonitrile in the presence of 0.42 mM poly-L-lysine leads to the transient absorption spectrum shown in Figure 4.12.

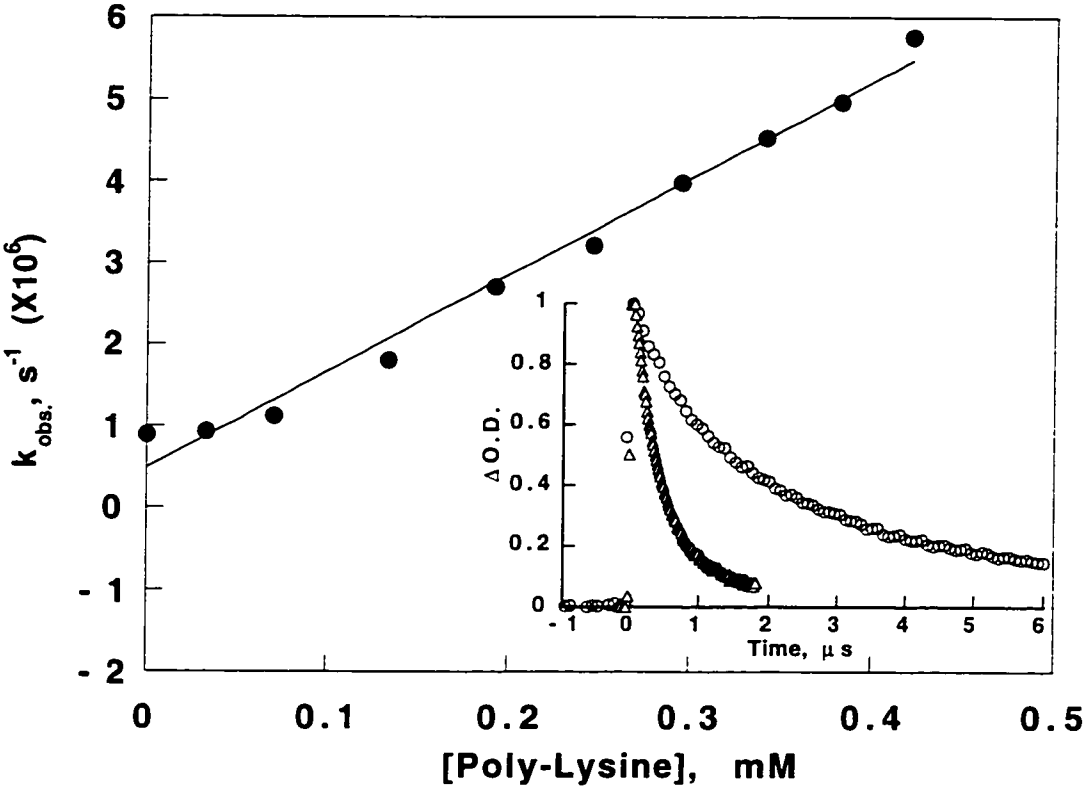

Figure 4.11. The quenching plot of 1.3 mM 4-benzoylbenzoic acid in 80:20 water:acetonitrile with the amino acid poly-L-Lysine (•); the fit is according to Eq. 4.3. The insert shows two representative triplet decay traces monitored at 550 nm in the absence (o) and presence of 0.19 mM (Δ) of the amino acid.

As with the proteins, the growth of the ketyl radical is not observed on the experimental time scales and that it appears before the triplet state has completely disappeared. It may be that the ketone is associated with the poly amino acid and the RP formation is too fast to be observed on the time scale of the experiment. However with this system no MFEs are observed. This indicates that the poly amino acid does not provide sufficient confinement for the RP to be affected by a MF. It is also noted that this poly amino acid contains 46 lysine units which explains the relatively high quenching rate constant obtained here.

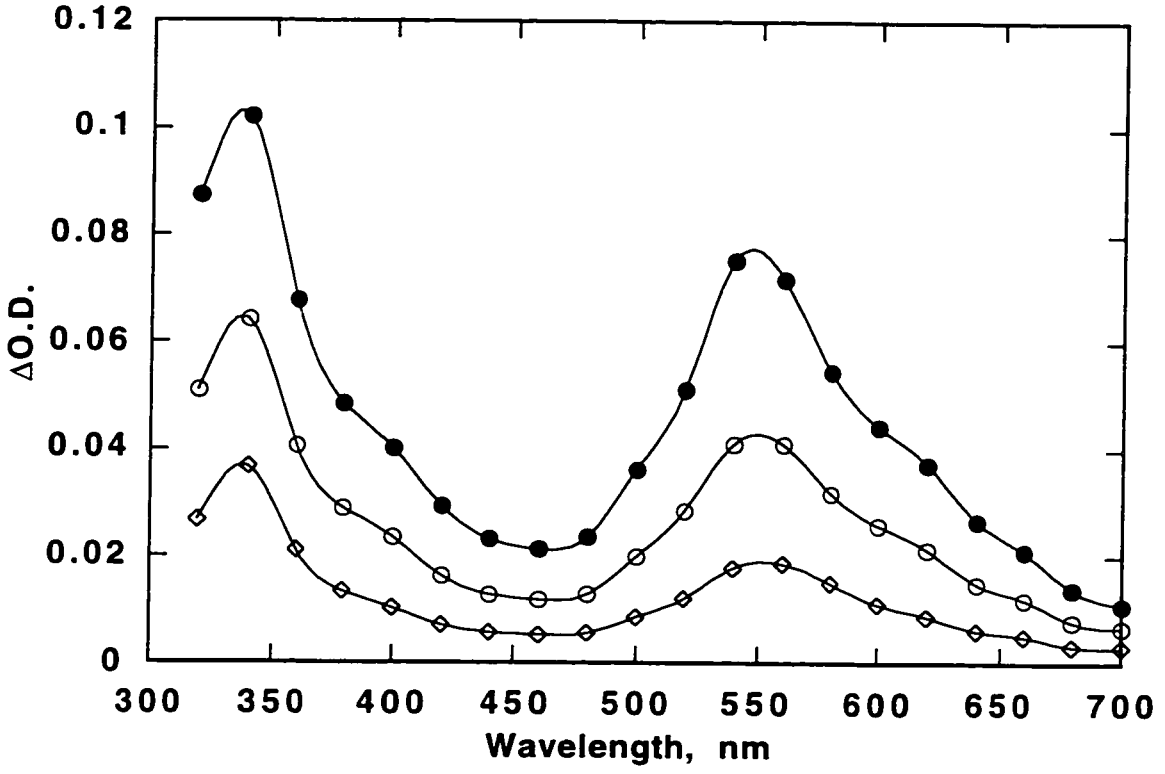

Figure 4.12. The transient absorption spectrum of 1.3 mM of 4-benzoylbenzoic acid in the presence of 0.42 mM poly-L-Lysine at 56 ns (•), 192 ns (o), and 416 ns (◊) after 308-nm excitation.

We also used N-methyl acetamide as a model compound to examine the reactivity of the peptide links in the protein structure. The quenching rate constant of triplet BP with N-methyl acetamide was found to be 4.4 x 10^5 $M^{-1}s^{-1}$ in acetonitrile. The above rate constant is lower than those found with some of the other amino acids and/or phenols (as in tyrosines).[21] The reactivity of the protein lysozyme toward triplet BP has also been studied.[22] The quenching rate constant for the triplet BP with native lysozyme is reported to be 4 X10^9 $M^{-1}s^{-1}$

and significant amounts of ketyl radical have been observed with this system as well.[22]

It must also be remembered that these proteins (i.e., BSA and HSA) have an extensive number of amide links associated with them. Thus, a low quenching rate constant may be compensated by a high number of reactive amide links available to the probe. However, knowing these rate constants, nothing definite can be said about the specific site of the photoreduction reaction of the triplet ketones in this study. It may be that a number of different groups and molecules collectively contribute to the RP generation.

4.4. Discussion

When geminate RPs are generated from a hydrophobic precursor in organized structures with hydrophobic interior, they stay geminate for a longer period of time than in homogeneous solutions as their exit is slow. As discussed in Chapters 1 and 3, the extended duration of RP encounters provides an opportunity for the two processes of spin evolution and RP separation to compete. Application of an external MF leads to an increase in the fraction of radicals that escape the cage. The increased level of radical separation can be explained by the Zeeman splitting of the triplet sublevels as the MF strength increases. The Zeeman effect thus leads to the decoupling of the T sublevels from

the S state, which are otherwise nearly degenerate in the absence of a MF (see Figure 3.4). However, the exchange interactions, which lead to a small separation of the T_0 and S levels (see Figure 3.5), become particularly important at low fields,[23-25] such as with environmental fields (< 5 gauss). Magnetic effects produced by a laboratory magnet are considered to be strong enough to allow one to treat the experimental data based on degenerate S-T energy levels on a first approximation (see Figure 3.4 and the discussions presented in Chapter 3).

Our protein-mediated radical is found to be affected by an external MF, although the effects seen in BSA and HSA are found to be moderate compared to those in micelles. It should also be noted that in biological systems, the RPs are usually generated from random radical-radical encounters as opposed to geminate processes (see section 1.9).[18] Even though proteins are found to host radical reactions that are influenced by MFs, our results suggest that the radical confinement provided by the protein environment is not as efficient as with the micelles. Also, the escape process for hydrophobic radicals is found to occur on the microsecond time scale, which possibly indicates that no specific site of interaction exists for these radicals in the protein.

The quenching experiments indicate that the tyrosine and lysine residues are relatively good quenchers of triplet benzophenone-like ketones. The amide links in a peptide bond can also act as a possible

hydrogen donor site in a photoreduction reaction in the protein. A conclusive reaction site can not be decided based upon these results alone. The results do show that there are many reaction sites in the complex molecules of proteins which collectively lead to the generation of RPs upon photoreduction of a benzophenone probe.

Radicals are also involved in "protein-radical enzymes" containing a free radical on amino acid residues such as tyrosine and tryptophan.[26] An increase in the cellular free radical concentration (due to a MFE) may lead to an increase in the potential damage of the target protein or other important cellular components such as DNA. This may contribute, in turn, to an existing level of background damage in, for example, protein-bound hydroperoxides and protein-bound catechols.[27] These protein-derived radicals may cause further damage by reacting with other neighboring sites, which can be amplified even more when a protein-bound transition metal ion is present.[28] The sources of free radicals are not limited to photochemical reactions, since they can also be formed in a cellular metabolic process or randomly in processes involving radiomimetic chemicals or physical agents.[29]

Another surprising observation was the higher $B_{1/2}$ values (particularly in BSA) than those usually seen in micelles, where radicals can separate up to 30 Å within the micelle's boundary.[20,30] It has been shown in the literature that the smaller the aggregate, the larger the

value of $B_{1/2}$.[30-32] Thus, the higher $B_{1/2}$ values imply that the separation distance between the radicals achieved in the microenvironment of the protein is smaller than in micelles.

With the proteins and the poly amino acid used in this study, it was interesting to note that no radical growth was detected, even though the decay of the triplet takes place on the time scale of the experiment (see Figure 4.2, Figure 4.3, and Figure 4.5). This observation also indicates that the triplet population, that leads to the formation of the radicals in $\leq$ 50 ns, is probably bound to the protein. The observed decay of the triplet state is thus due to a second population that exists in a less reactive environment.

In the context of environmental fields, it can be concluded that MFEs on the reaction rates will be small. However, it has been suggested that the primary small changes on the rates of free-radical mediated reactions in biological systems may result in significant secondary changes.[33] The rate changes due to a MF involving reactions related to cellular signal transduction have been studied in some detail.[33,34] Fluctuations in the cellular redox state involving free radicals have been suggested to lead to modulation of cellular Ca^{2+} fluxes.[34] Other results indicate evidence that reactive oxygen intermediates, such as the superoxide radical, $O_2^{\bullet -}$, the hydroxyl radical, $OH^{\bullet}$,[35] and the nitric

oxide radical, $NO^{\bullet}$,[36] may function as potential cell signaling messengers.

Other secondary effects of MFs in biochemical reactions *in vivo* also involve radical reactions. For example, a change in the amounts of free radicals in a cell may amplify damages such as lipid peroxidation.[33] Although more experimental work is necessary in the area of MFEs on biochemical reactions in biological systems, there are theoretical predictions that low MF strengths of less than 10 gauss can significantly affect the rates of spin-dependent reactions.[37] One interesting example is the possible effect of the geomagnetic field or fields of less than 1 gauss on spin correlated RPs, generated by electron transfer processes through a biomagnetic sensory mechanism, which enables organisms to detect the Earth's field and its direction.[37]

4.5. References

(1) Scaiano, J. C.; Cozens, F. L.; McLean, J. *Photochem. Photobiol.* **1994**, *59*, 585.

(2) Turro, N. J.; Kraeutler, B. *Acc. Chem. Res.* **1980**, *13*, 369.

(3) Turro, N. J. *Tetrahedron* **1982**, *38*, 809.

(4) Gould, I. R.; Zimmt, M. B.; Turro, N. J.; Baretz, B. H.; Lehr, G. F. *J. Am. Chem. Soc.* **1985**, *107*, 4607.

(5) Chagovetz, A. M.; Grissom, C. B. *J. Am. Chem. Soc.* **1993**, *115*, 12152.

(6) Grissom, C. B. *Chem. Rev.* **1995**, *95*, 3.

(7) Chignell, C. F.; Sik, R. H. *Photochem. Photobiol.* **1995**, *62*, 205.

(8) Dormán, G.; Prestwich, G. D. *Biochemistry* **1994**, *33*, 5661.

(9) Dormán, G.; Prestwich, G. D. *ChemTracts.* **1993**, *6*, 131.

(10) Alomar, A. *Contact Dermatitis* **1985**, *12*, 112.

(11) Boscá, F.; Miranda, M. A.; Carganico, G.; Mauleón, D. *Photochem. Photobiol.* **1994**, *60*, 96.

(12) Prestwich, G. D.; Dormán, G.; Elliott, J. T.; Marecak, D. M.; Chaudhary, A. *Photochem. Photobiol.* **1997**, *65*, 222.

(13) Scaiano, J. C. *J. Photochem.* **1973/74**, *2*, 81.

(14) Boate, D. R.; Johnston, L. J.; Scaiano, J. C. *Can. J. Chem.* **1989**, *67*, 927.

(15) Scaiano, J. C.; Abuin, E. B.; Stewart, L. C. *J. Am. Chem. Soc.* **1982**, *104*, 5673.

(16) Russeva, V.; Rakovska, R.; Stavreva, N.; Mihailova, D.; Berova, N. *Pharmazie* **1994**, *49*, 519.

(17) Hayon, E.; Simic, M. *J. Am. Chem. Soc.* **1971**, *93*, 6781.

(18) Cozens, F. L.; Scaiano, J. C. *J. Am. Chem. Soc.* **1993**, *115*, 5204.

(19) Evans, C.; Ingold, K. U.; Scaiano, J. C. *J. Phys. Chem.* **1988**, *92*, 1257.

(20) Evans, C. H.; Scaiano, J. C.; Ingold, K. U. *J. Am. Chem. Soc.* **1992**, *114*, 140.

(21) Das, P. K.; Encinas, M. V.; Steenken, S.; Scaiano, J. C. *J. Am. Chem. Soc.* **1981**, *103*, 4162.

(22) Encinas, M. V.; Lissi, E. A.; Vasquez, M.; Olea, A. F.; Silva, E. *Photochem. Photobiol.* **1989**, *49*, 557.

(23) Closs, G. L.; Forbes, M. D. E.; Norris, J. R., Jr. *J. Phys. Chem.* **1987**, *91*, 3592.

(24) Forbes, M. D. E. *The Spectrum* **1995**, *8 (summer issue)*, 1.

(25) Tarasov, V. F.; Ghatlia, N. D.; Avdievich, N. I.; Turro, N. J. *Z. Phys. Chem.* **1993**, *182*, 227.

(26) Stubbe, J. A. *Biochemistry* **1988**, *27*, 3893.

(27) Dean, R. T.; Gieseg, S.; Davies, M. J. *Trends in Biochemical Sciences* **1993**, *18*, 437.

(28) Breimer, L. H. *Molecular Carcinogenesis* **1990**, *3*, 188.

(29) von Sonntag, C. In *Physical and Chemical Mechanisnms in Molecular Radiation Biology*; W. A. Glass and M. N. Varma, Eds.; Plenum Press: New York, 1991; pp 287.

(30) Barra, M.; Bohne, C.; Zanocco, A.; Scaiano, J. C. *Langmuir* **1992**, *8*, 2390.

(31) Scaiano, J. C.; Lougnot, D. J. *J. Phys. Chem.* **1984**, *88*, 3379.

(32) Steiner, U. E.; Wu, J. Q. *Chem. Phys.* **1992**, *162*, 53.

(33) Walleczek, J. *Adv. Chem. (ACS)* **1995**, *250*, 395.

(34) Walleczek, J. In *On the Nature of Electromagnetic Field Interactions With Biological Systems*; A. Frey, Ed.; R. G. Landes Co.: Austin, Texas, 1994; pp 167.

(35) Schreck, R.; Baeuerle, P. A. *Trends Cell Biol.* **1991**, *1*, 39.

(36) Lowenstein, C. J.; Snyder, S. H. *Cell* **1992**, *70*, 705.

(37) Schulten, K.; Windemuth, A. In *Biophysical Effects of Steady Magnetic Fields*; G. Maret, J. Kiepenheuer and N. Bocarra, Eds.; Springer: Berlin, 1986; pp 99.

5. Exit of Excited Triplet Xanthone from Micelles

5.1. Introduction

It was pointed out in Chapter 1 that micelles with hydrophobic cores are often used to solubilize hydrophobic organic molecules in aqueous solutions. However, a probe is not rigidly fixed within the micelle. A hydrophobic probe would favor the micelle over the aqueous phase and its residence time in the micelle can be on the microsecond time scale. Studies reporting the exit rates (k_{-}) of various probes from micelles go back two decades.[1] The usual method for monitoring the exit process is to use a quencher that is only soluble in the aqueous phase. It is best to use a quencher with a charge that has the same sign as that of the micelle used, so that coulombic repulsion keeps the quencher from approaching the micelle's surface. With anionic micelles, the water soluble nitrite ion is often used and is known to quench the triplet state effectively.[2] Yet, prior to its exit, a probe moves

intramicellarly, and it is also in equilibrium with the aqueous phase. The rates of entry are as important as those of exit in determining the reactivity of an organic molecule in supramolecular assemblies. The rates of entry for hydrophobic molecules are usually found to fall within an order of magnitude of the diffusion limit.[3]

The distribution of molecules and their dynamics in heterogeneous systems is important in that it can lead to information on reaction mechanisms. Several studies have been done to characterize heterogeneous systems. Most of these have been based on monitoring the fluorescence properties of an incorporated probe.[4-8] The drawbacks of the fluorescence techniques are 1) restrictions on the time scales as singlet states are often short-lived and 2) high concentrations of the quencher are needed for the fluorescence quenching measurements. Meanwhile, triplet states require only low quencher concentrations and the study is not limited to such short time domains. Our study takes advantage of the properties of an appropriate probe that can be monitored by picosecond and nanosecond transient absorption spectroscopy. We are interested in the detailed processes involved in micellar exit. Xanthone in its triplet state has proven to be the probe of choice in many studies involving heterogeneous systems such as cyclodextrin complexes.[2,9-13,14]

It is known that the triplet state of xanthone changes from (n,π^*) to (π,π^*) as the polarity of its medium is increased.[11,12] Thus, in an aqueous environment, the excited state of xanthone finds itself in a (π,π^*) state. In this state, its reactivity towards hydrogen abstraction is reduced compared to when it is in a (n,π^*) state. This reduced reactivity leads to a relatively long-lived transient (several microseconds) in most polar solvents[11] and in micellar solutions[2] as well. Based on dielectric loss experiments, ketones of this type are known to possess large dipole moments in their triplet states.[15] Upon excitation, their dipole moments increase and exhibit solubilities that differ from their corresponding ground states. In fact, the triplet-triplet absorption maximum of xanthone exhibits a noticeable blue shift with increasing solvent polarity, going from a maximum at 650 nm in carbon tetrachloride to 615 nm in 2-propanol.[11] Thus, the shift in the maximum of its transient absorption spectrum with the polarity of its environment can be a direct indication of the mobility of triplet xanthone within the micelle. Also, due to the increase in its dipole moment following excitation, xanthone tends to eventually relocate itself from the less polar medium of the micellar core to the more polar aqueous phase. All the above characteristics make xanthone a suitable probe for inspecting the polarity of organized systems.

5.2. Experimental

5.2.1. Materials

Xanthone (Aldrich) was recrystalized from ethanol. Sodium dodecyl sulfate (SDS) (Fluka, microselect), sodium n-decyl sulfate (SDecS) (Lancaster), sodium n-tetradecyl sulfate (STDS) (Lancaster), and hexadecyltrimethyl ammonium chloride (CTAC) (Kodak) were used as received. Cupric sulphate (BDH chemicals) and sodium nitrite (Fisher Scientific) were also used as received. Water was purified through a Millipore MilliQ system. The solvents from BDH (Omnisolv) were used as received.

5.2.2. Sample preparation

Aqueous solutions 0.1 mM in xanthone were prepared in the following surfactants: 0.1 M SDS, 0.05 M SDecS, 0.01 M STDS, or 0.06 M CTAC. The samples were nitrogen saturated prior to use. Sodium chloride, 0.2 M and 0.3 M, was added to 0.1 M SDS solution, prior to the addition of xanthone. Solutions for recording the transient spectra were made to flow through the 7 X 7 mm^2 Suprasil quartz cell, which held 2 mL. However, static samples were used for the quenching experiments. These samples were shaken after each laser shot to prevent product buildup. The samples were excited by pulses of a Surelite Nd: YAG laser (< 25 mJ per 8 ns pulse) using the third harmonic, 355 nm. The

nanosecond absorption, picosecond absorption, and picosecond emission setups are described in Chapter 2.

5.3. Results

5.3.1. The time-resolved emission studies

The intersystem crossing rate (k_{ISC}) of xanthone, as with other aromatic ketones, has been measured in different solvents. A value of 8 picoseconds (ps) has been reported for the triplet absorption buildup (k_{ISC}^{-1}) of xanthone in benzene,[16] p-dioxane and ethanol.[17] A later study reports a value of 13 ps for the k_{ISC}^{-1} of xanthone in benzene.[18]

In this study time-resolved picosecond emission spectroscopy is first used to determine the singlet state lifetime of xanthone in aqueous solution and various surfactants. The singlet lifetime of xanthone in solvents such as acetonitrile and isopropanol is found to be shorter than our picosecond laser resolution of 35 ps. This is to be expected, as the buildup absorption of xanthone in acetonitrile is found to be within the response time of the pump pulse (i.e., ≤35 ps). Also, from previous studies, the k_{ISC} of xanthone in most organic solvents is reported to be less than 20 ps.[17] Xanthone is however known to fluoresce in aqueous solution with a λ_{max} of ~400 nm, and its singlet lifetime has been estimated to be less than 1 ns.[12] The fluorescence spectrum of

xanthone in water using the streak camera and the setup described in section 2.1.5 is shown in Figure 5.1.

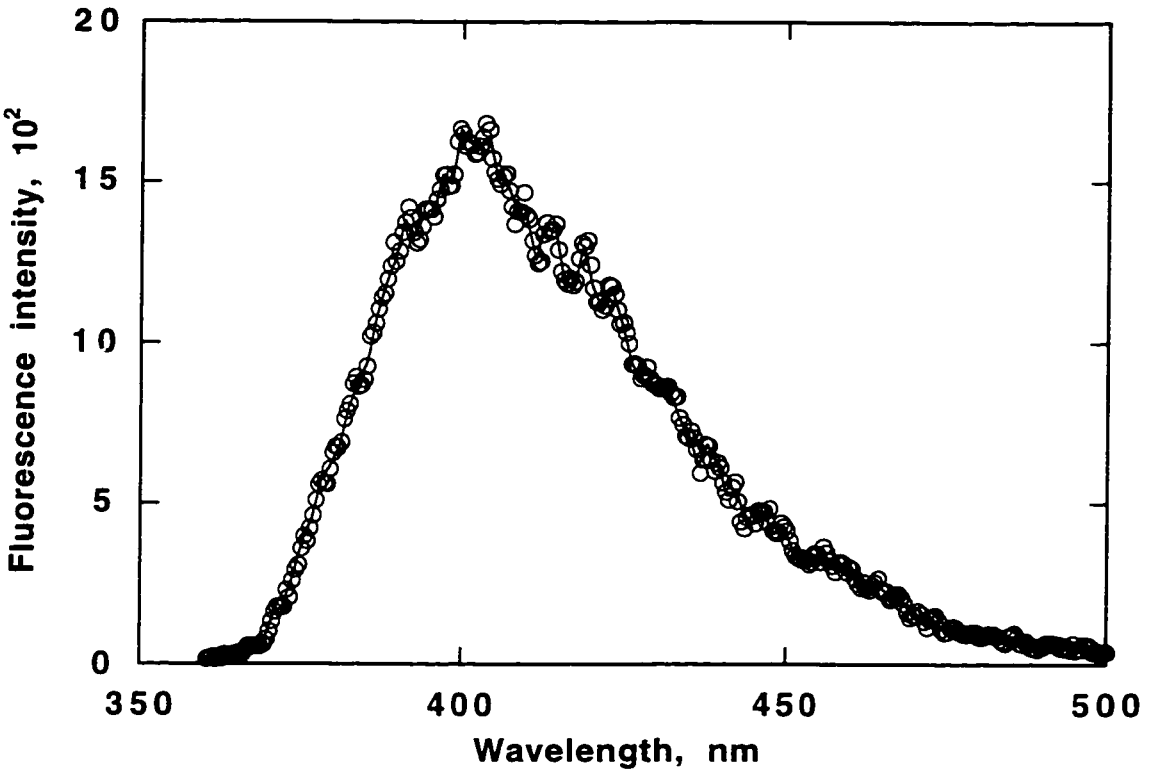

Figure 5.1. The fluorescence spectrum of xanthone in water, λ_{ex} = 355 nm.

We measured a singlet lifetime of 600 ± 20 ps for xanthone in water. A typical fluorescence decay recorded by our system equipped with a streak camera is shown in Figure 5.2. The decay shown is that of singlet xanthone in water and can be fitted by a mono-exponential function. The laser profile shown in this figure is deconvoluted from the fluorescence decay by the Photolumni 2.2.7 software that calculates fluorescence lifetimes. The insert is the semi-logarithmic plot of the

fluorescence decay. It clearly shows that this decay has one component only. The difference between the actual decay curve and the fitted curve is plotted on the right y-scale as the residual dispersion.

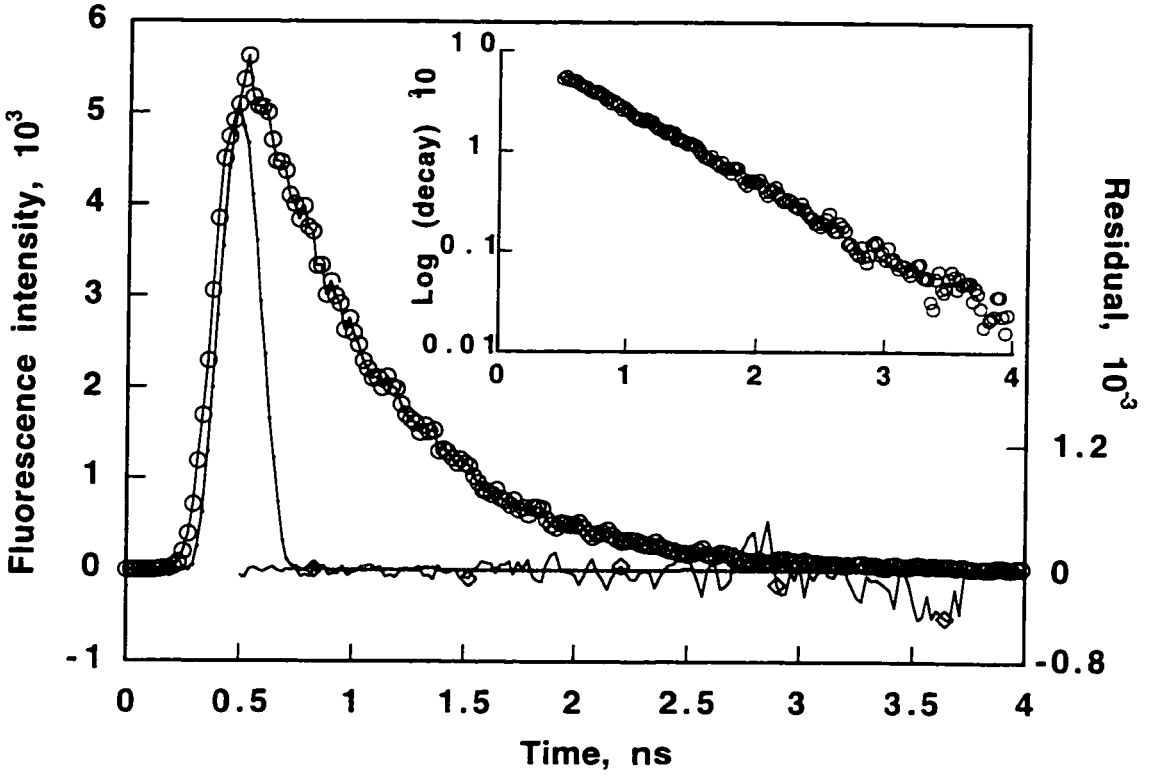

Figure 5.2. The fluorescence decay of 0.1 mM xanthone in water (o, λ_{max} = 400 nm) and the normalized short lived 355 nm laser pulse profile (—). The residual dispersion of the fit (◊) is shown on the right y-scale. The inset is the semi-logarithmic plot of the fluorescence decay.

The singlet lifetimes of xanthone in various micelles are listed in Table 5.1. The fluorescence decay of xanthone in micelles consists of two components (see Figure 5.3), yet the contribution from the second component is a very small fraction of the total decay. The semi-logarithmic plot of the fittted fluorescence decay of xanthone in SDecS micelles exhibits a two component decay.

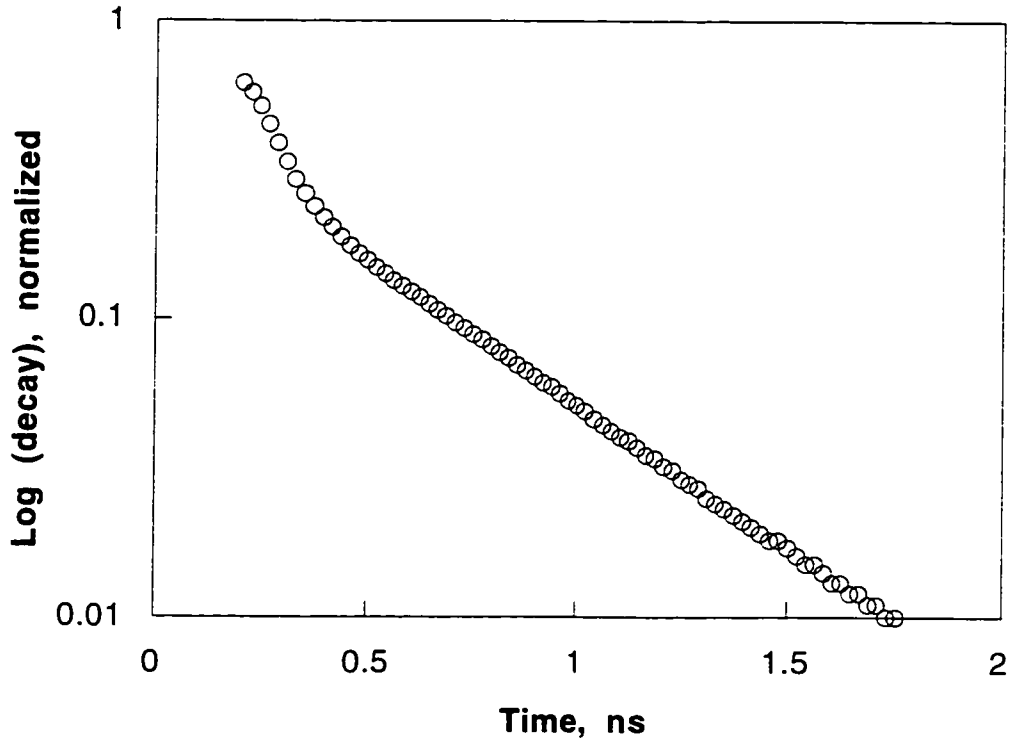

Figure 5.3. The semi-logarithmic plot of the fitted fluorescence decay (normalized) of 0.1 mM xanthone in SDecS micelles (o, λ_{max} = 400 nm).

It is not surprising to have a long-lived component as water molecules are available within the micellar structure. However, the theoretical modelling of anionic micelles indicates that they still have an essentially dry inner core.[19] In fact, the polarity of the micelle's interior is comparable to that of alcohols. Thus, the long-lived component is due to a small fraction of xanthone molecules solubilized in water outside the micelle. The lifetimes due to this component are on average close to that of xanthone in water. The errors involved with the first and the second lifetimes are in the range of ± 2 ps and ± 15 ps, respectively. Yet, the error associated with the lifetime (i.e., 36 ps) that

is very close to the laser resolution may in fact exceed 2 ps and cannot be estimated accurately.

Table 5.1. The singlet lifetime of ~0.1 mM xanthone in the following environments.

Solvent	Singlet lifetime	Fraction contribution
water	LT= 600 ps	0.99
acetonitrile	<30 ps	
isopropanol	<30 ps	
SDS	LT_1 = 67 ps LT_2 = 236 ps	0.90 0.10
SDecS	LT_1 = 36 ps LT_2 = 450 ps	0.90 0.10
STDS	LT_1 = 92 ps LT_2 = 668 ps	0.90 0.10
CTAC	LT_1 = 90 ps LT_2 = 730 ps	0.90 0.10
SDS + 0.2 M NaCl	LT_1 = 127 ps LT_2 = 454 ps	0.94 0.06
SDS + 0.3 M NaCl	LT_1 = 149 ps LT_2 = 1260 ps	0.96 0.04

5.3.2. Transient absorption studies

Picosecond pump-probe absorption spectroscopy is used to study the pre-exit process. By varying delay times after excitation, the spectral shift associated with the excited state absorption of xanthone in micelles of varying size is monitored as a function of time. The experimental details of this setup can be found in Chapter 2. Transient

absorption spectra of xanthone in micelles of varying size are recorded up to a maximum of 9 ns delay after excitation by the picosecond laser. After this, the spectral changes are monitored using the nanosecond laser excitation up to microsecond times. As shown in Figure 5.4, the maximum absorption band (λ_{max}) is determined by fitting the spectrum to a gaussian function. The choice of a gaussian function is an arbitrary one and other functions may be used instead. The spectral shifts can easily be detected before the spectra are fitted by the gaussian functions. However, this approach was taken to eliminate any subjectivity in the determination of the λ_{max} values. It is also worth noting that the xanthone concentration does not exceed 10^{-4} M, which makes the occupancy levels of xanthone in micelles ≤ 1.

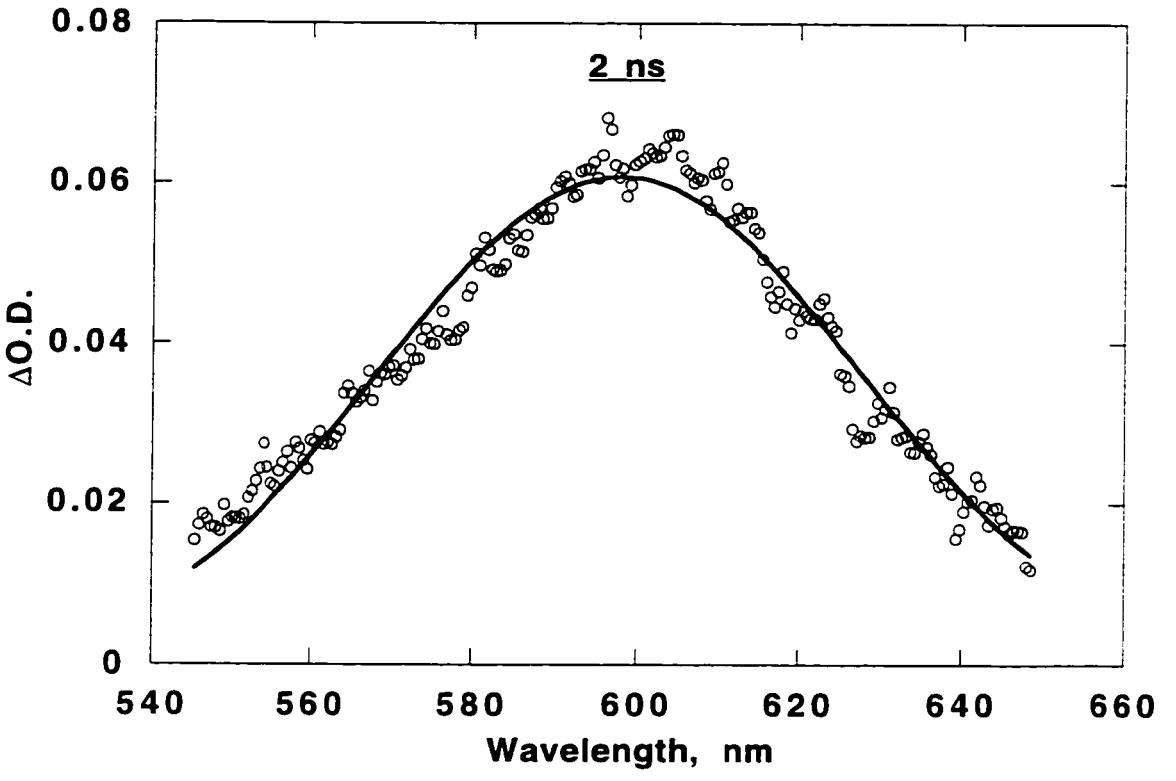

Figure 5.4. The plot of the transient absorption spectrum of 0.1 mM xanthone in 0.1 M SDS micelles taken at 2 ns (o) delay after 355 nm laser excitation.

In the case of micelles, a rapid spectral shift occurs in the first 200 ps. This shift arises from intersystem crossing from the singlet to the triplet state, as the S-S absorption is often red shifted with respect to the T-T absorption. A spectral shift from longer to shorter wavelengths is also observed with benzophenone in ethanol within the first 50 ps following a ps excitation.[18] The red-shifted maximum at early times is attributed to the S_1 absorption. The lifetime of the spectral changes for benzophenone is found to be ~20 ps.[18] This lifetime is in close agreement with a value of 12 ± 2 ps calculated for the buildup of T-T

absorption of benzophenone in benzene at 533 nm following excitation at 355 nm.[17]

Spectral changes of xanthone continue to occur over long delay times of up to 9 ns. This time limit for the picosecond laser is set by the physical dimensions of the delay stage controlling the delay of the probe pulse (see Figure 2.7). The spectral changes in the long delays correspond to a second process that occur in the 1-50 ns range. This process is attributed to the migration time of xanthone from the micellar core towards the surface of the micelle. These times (i.e., $\tau <$ 50 ns) are considered to be too short to correspond to the actual exit into the aqueous phase.[2] The spectral changes associated with the exit process into the aqueous phase are small and occur on the microsecond time scale (*vide infra*).

The shift following the picosecond laser excitation has been plotted as a function of delay time. A representative plot is shown in Figure 5.5 for xanthone in SDS micelles. The time evolution of data in Figure 5.5 is fitted to the double-exponential function shown below. The double-exponential function is given by

$$\lambda^{t}_{max} = (\lambda^{\circ}_{max} - \lambda^{\infty}_{max})(a_1 e^{-k_1 t} + a_2 e^{-k_2 t}) \qquad \text{Eq. 5.1}$$

where λ°_{max} is recorded at the earliest delay (<35 ps) after laser excitation, k_1 and k_2 are rate constants for spectral evolution, and the preexponential parameters (a_1 and a_2) indicate the fraction of picosecond spectral evolution that is associated with k_1 and k_2, respectively. The double-exponential fit of the data according to Eq. 5.1 yields $k_1 = 1.8 \times 10^{10}$ s^{-1} and $k_2 = 3.1 \times 10^{8}$ s^{-1} for the system presented in Figure 5.5. The infinite level is set to the value of λ_{max} obtained from the spectrum recorded at the shortest delay (i.e., $\lambda^{40\ ns}_{max}$) using the nanosecond LFP system. The spectra on the nanosecond time scales are taken at four delay times after the nanosecond excitation (see Figure 5.9 and Figure 5.10).

The first rate constant (k_1) corresponds to a lifetime of 60 ± 10 ps. This is assigned to k_{ISC}^{-1} for xanthone in SDS micelles. It is to be noted that this value is in close agreement with the singlet lifetime of xanthone in SDS (see Table 5.1). The second rate constant (k_2) results from smaller spectral shifts and consequently carries bigger errors. The lifetime for this process is 3.2 ± 0.7 ns for the above system.

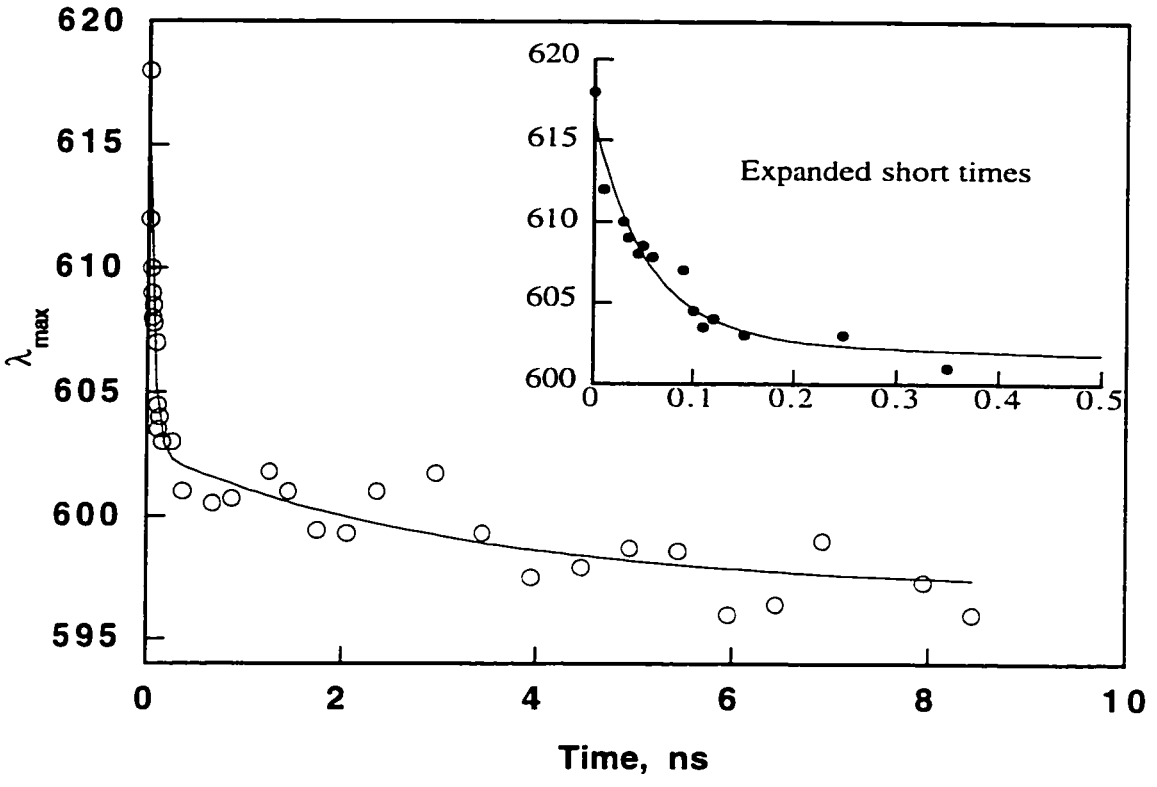

Figure 5.5. The plot of λ_{max} of xanthone transient absorption (o) in 0.1 M SDS as a function of time. The insert shows the decay trace at short times between 0 to 500 ps (•).

The results for other surfactants examined by the above approach are listed in Table 5.2. Since the total time scale is limited to ~9 ns, lifetimes exceeding ~20 ns become highly unreliable. Therefore for these systems, the values of k_2 are indicated as $< 5 \times 10^7$ s^{-1} (see Table 5.2).

Table 5.2. Picosecond data for the evolution of the spectral characteristics of the xanthone in micellar solution following excitation.

System	k_1 (s^{-1}) (k_{ISC})	a_1	k_2 (s^{-1})	a_2
water	1.88×10^9	-	-	-
SDecS	1.55×10^{10}	0.94	104×10^7	0.06
SDS	1.82×10^{10}	0.71	31×10^7	0.29
SDS + 0.2 M NaCl	5.31×10^9	0.67	5.5×10^7	0.33
SDS + 0.3 M NaCl	5.76×10^9	0.86	$<5 \times 10^7$	0.14
CTAC	1.09×10^{10}	0.63	$<5 \times 10^7$	0.37
STDS	1.57×10^{10}	0.88	20×10^7	0.12

Although this method of monitoring the spectral evolution is an indirect and unusual way of obtaining ISC rate constants, the values of k_{ISC}^{-1} we obtained do agree well with the singlet lifetimes presented in Table 5.1. It is also known that the quantum yield for the ISC of xanthone is almost one (e.g., $\Phi_{ISC} = 0.97 \pm 0.05$ at 25 °C in carbon tetrachloride).[11] Moreover, the buildup of T-T absorption following picosecond excitation is also measured for xanthone in the SDS system. The value of k_{ISC}^{-1} found this way is around 80 ps, which compares well with the value of 60 ps found by the above method. The growth of the

T-T absorption of xanthone in SDS and in acetonitrile is shown in Figure 5.6. The absorption buildup of xanthone in acetonitrile has a lifetime similar to the rise time of the pump pulse (i.e., ~35 ps). This value is used for the deconvolution of the triplet buildup of the SDS system.

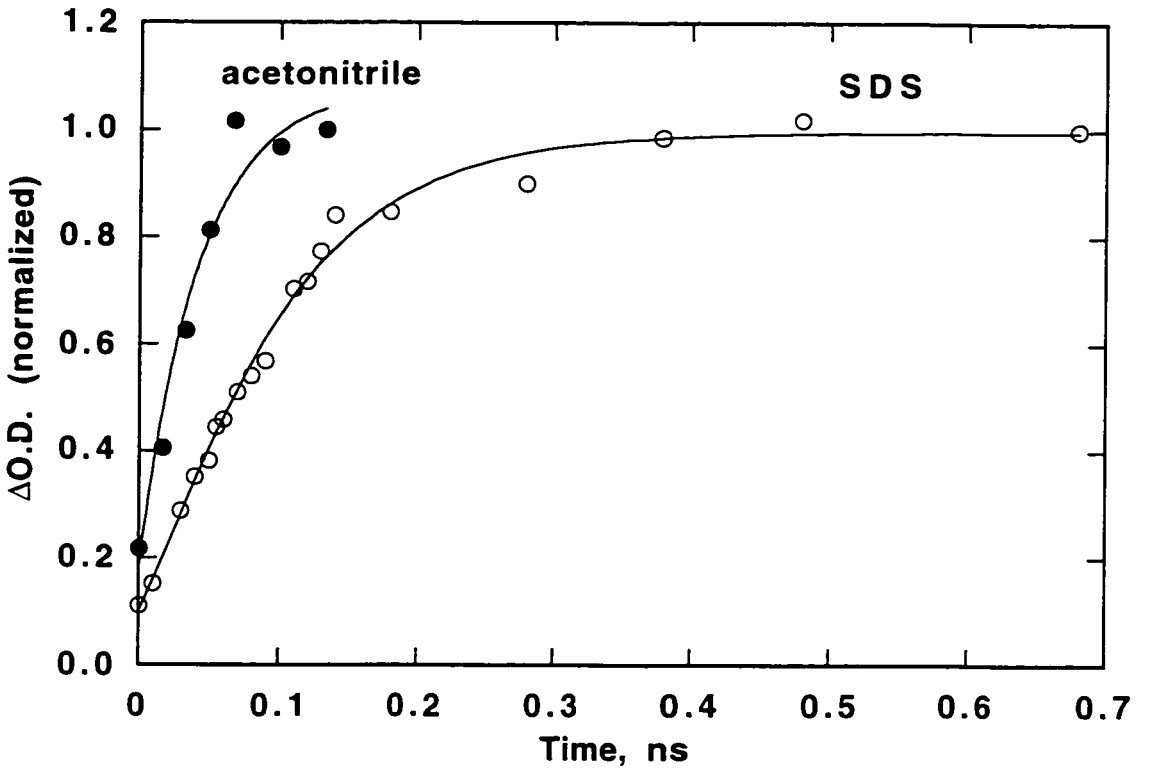

Figure 5.6. The time profiles for the appearance of absorption of xanthone in SDS micelles (o) and in acetonitrile (•) after 355 nm picosecond laser excitation. The signals are normalized for easy comparison of the kinetics.

Picosecond transient absorption spectrum of xanthone in water is also recorded at different delay times. Spectral shifts on picosecond time scales for xanthone in water indicate the occurrence of one process only (see Figure 5.7). This decay is attributed to the intersystem crossing

process. The mono-exponential decay of Figure 5.7 leads to a lifetime of 530 ± 60 ps, which is in excellent agreement with the singlet lifetime of xanthone in water (see Table 5.1).

We note that the rate constants obtained from the first spectral changes (k_1) give reasonable values for the intersystem crossing rates from the $S_1 \rightarrow T_1$ state. It is noted that the λ_{max} value of xanthone in water is smaller than those in the micelles (see Figure 5.7 and Table 5.3). The spectral shifts of xanthone in micelles are more pronounced in the picosecond times (see Figure 5.8) than in the nano- to micro-second times (see Figure 5.9 and Figure 5.10). The effect of added salt to SDS micelles, leading to larger micelles,[20] is also examined (see Table 5.2). The effect of 0.2 or 0.3 M salt is found to be almost the same as the intact SDS micelles.

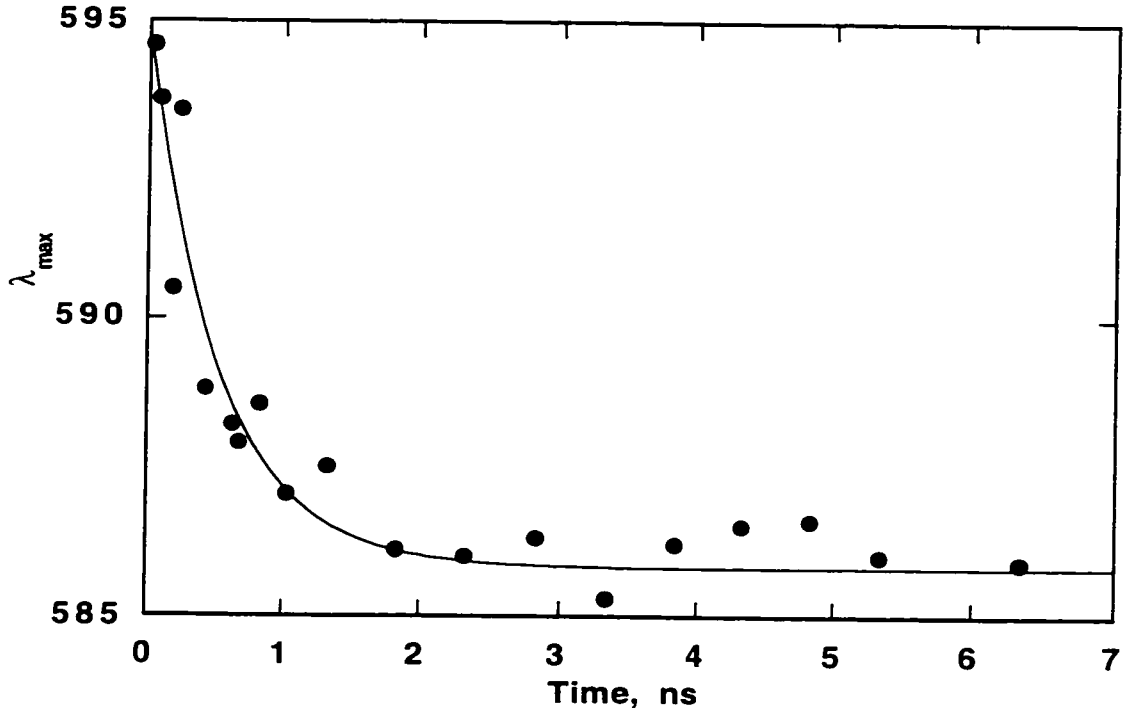

Figure 5.7. The plot of λ_{max} of xanthone transient absorption (•) in water as a function of time following 355 nm picosecond laser excitation.

Nanosecond laser excitation (355 nm) is used to monitor the exit of xanthone into the aqueous phase, as this process is known to occur with rates of ~10^6 s^{-1} for ketones of similar size.[2] The spectral shifts with time are rather small in the case of anionic micelles, when the nanosecond resolution is used to record the spectra. Figure 5.9 illustrates the nanosecond transient absorption spectra of xanthone in SDS micelles. The blue shift here is too small (within the experimental error) to give any meaningul information on the exit rates. However, as the triplet xanthone decays in time, there is a clear shift towards shorter wavelengths in the case of the positively charged CTAC micelles (see Figure 5.10).

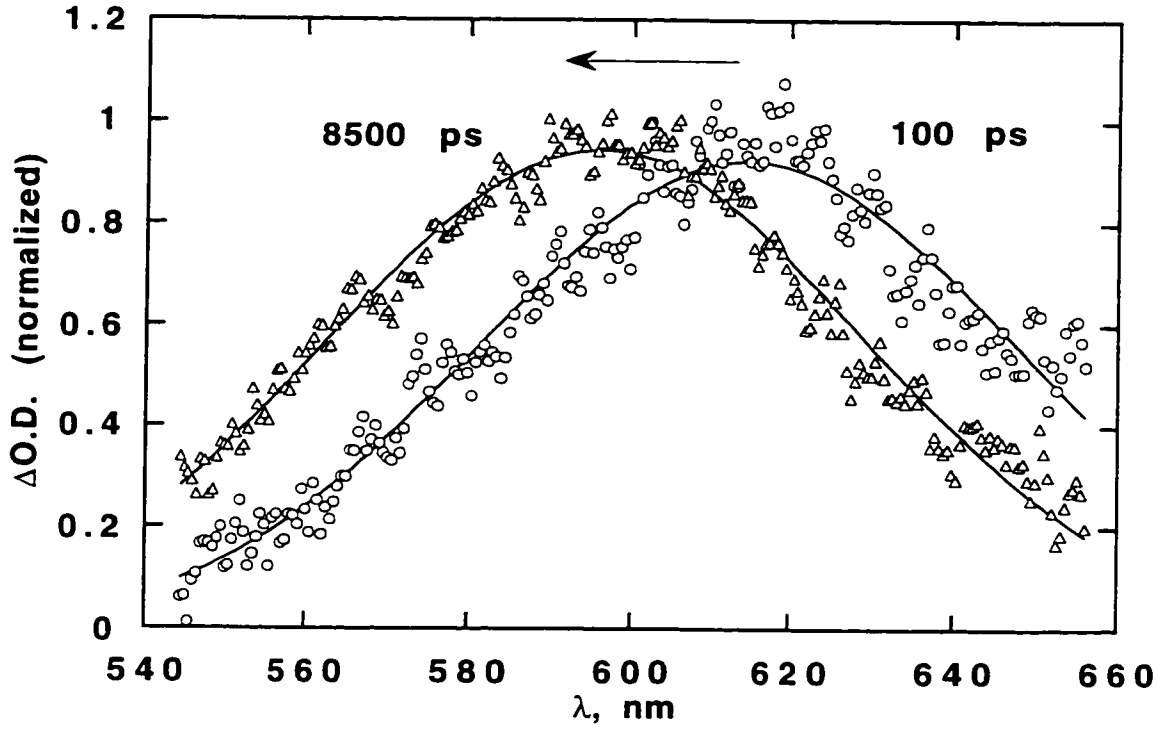

Figure 5.8. The transient absorption spectra of xanthone in 0.1 M SDS taken at 100 ps (o, λ_{max} = 615 nm) and at 8,500 ps (Δ, λ_{max} = 596 nm) delay after excitation.

To avoid bias, the nanosecond spectra are also fitted by a gaussian function. The time-evolved maxima in Figure 5.9 and Figure 5.10 are joined by a straight line to highlight the shift. Even though the shift is in the right direction (i.e., a more aqueous environment), it is not large enough to provide information on the exit rates (see Table 5.3). This is partly due to the gap between the resolutions provided by our picosecond and nanosecond systems.

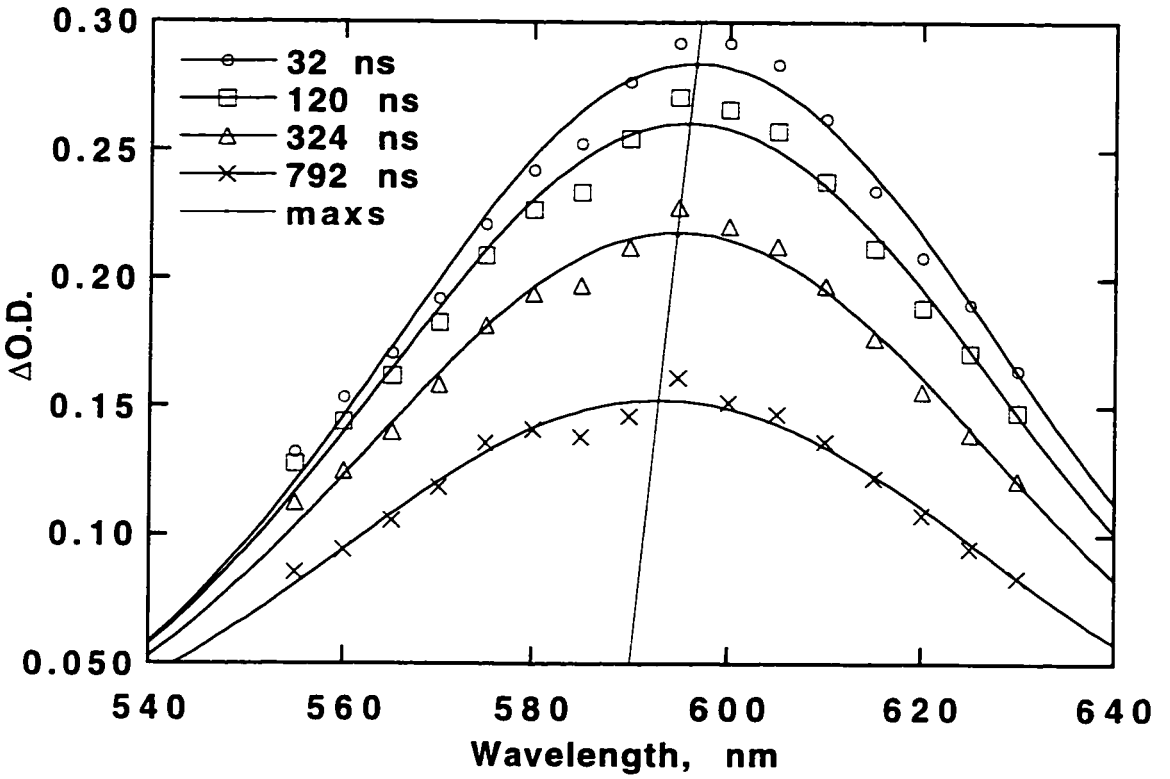

Figure 5.9. The nanosecond transient absorption spectra of xanthone in 0.1 M SDS taken at delays of 32 ns (o), 120 ns (□), 324 ns (Δ), and 792 ns (x) after laser excitation, respectively.

Table 5.3 lists the λ_{max} values from the spectra recorded at the shortest delays ($\lambda^{40\ ns}_{max}$) and those extrapolated to long times (λ^{∞}_{max}). It is also noted that these values (i.e., $\lambda^{40\ ns}_{max}$) are different for various surfactants. Surprisingly, at first glance, they also differ from the λ_{max} value of xanthone in water (584 nm). Therefore, this observation indicates that the environment sensed by the probe does not exactly correspond to an aqueous medium. Moreover, it implies that there exists an exit/entry equilibrium with significant fractions of xanthone triplets in both phases. This equilibrium in turn leads to averaged values of λ^{∞}_{max}, arising from contributions from both the micellar and

aqueous phases. Using the values of λ^{∞}_{max}, the fraction of xanthone in the aqueous phase at long times is also calculated (see the last column in Table 5.3).

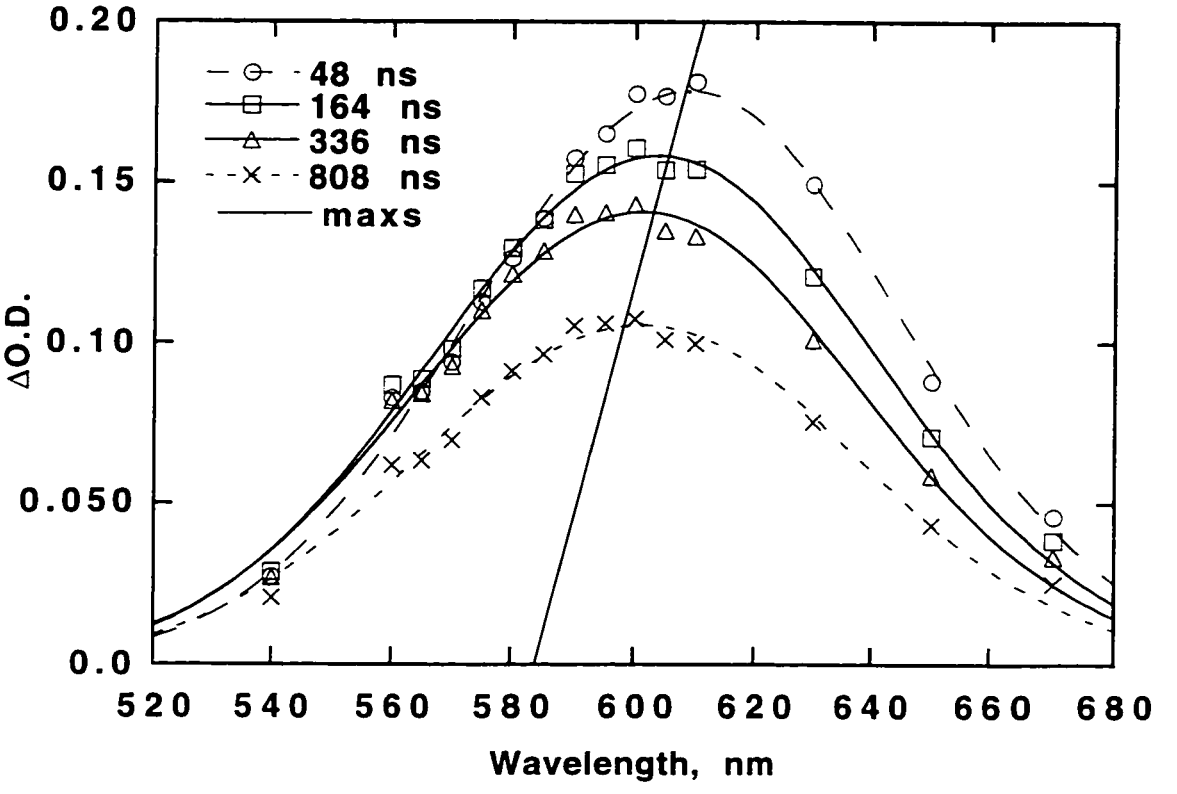

Figure 5.10. The nanosecond transient spectra of xanthone in 0.05 M CTAC taken at delays of 48 ns (o), 164 ns (□), 336 ns (Δ), and 808 ns (x) after the laser excitation, respectively.

Table 5.3. The mole fraction of xanthone in water and evolution of the position of λ_{max} on the picosecond and nanosecond time scales.

System	λ^{0}_{max}	$\lambda^{300\ ps}_{max}$	$\lambda^{8\ ns}_{max}$	$\lambda^{40\ ns}_{max}$	λ^{∞}_{max}	X_{H2O}
	(nm)					
SDecS	609	601.6	596	596	595	0.56
SDS	618	602	597	597	595	0.68
SDS + 0.2 M NaCl	614	605.5	602	599	598	0.53
SDS + 0.3 M NaCl	615	602.4	599	597	596	0.61
CTAC	623	618	615	609	597	0.67
STDS	621	604	597	597	595	0.70
water	596	586	584	584	584	1

It is noted that the triplet decay traces in anionic micelles recorded at wavelengths 570, ~600, and 630 nm exhibit first-order kinetics except in CTAC micelles. Figure 5.11 shows the transient traces of xanthone in CTAC micelles monitored at these three wavelengths. The decay at 630 nm consists of two components with lifetimes of 80 and 1000 ns, respectively. The trace recorded at 570 nm exhibits a growth followed by a slow decay. This trace can be fitted to a growth followed by a decay function. The lifetime of the growth of the transient (~80 ns) is very similar to that of the first decay at 630 nm. The lifetime of the slower component is ~1700 ns. However, this lifetime contains a large error as

the slow decay is far from complete. In conclusion, it can be said that the kinetics of this transient parallel that observed at 630 nm.

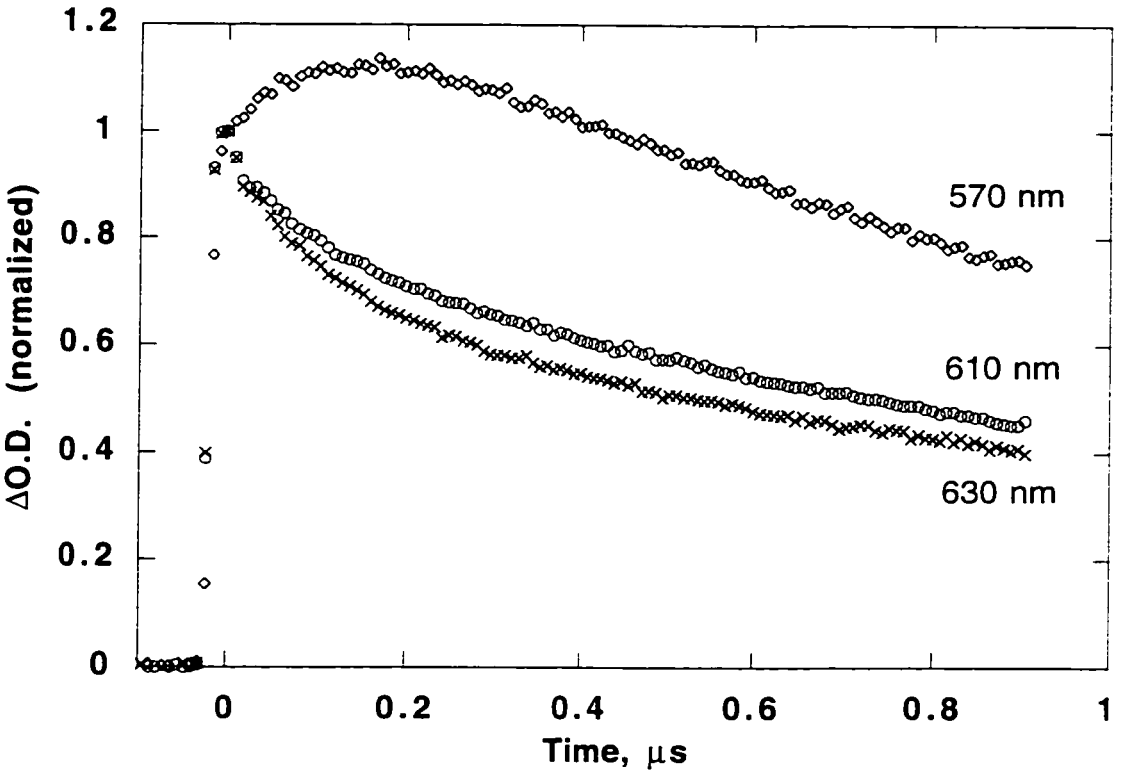

Figure 5.11. The transient traces of 0.1 mM xanthone in 0.06 M CTAC micelles.

This behaviour indicates the presence of two triplet transients. The first one, with a shorter lifetime, is interconverting to a second triplet transient with a longer lifetime. The presence of two distinct transients is also evident from the clear shift seen in the spectra of Figure 5.10. The maximum in the spectrum recorded at the first delay (48 ns) corresponds to a relatively less polar environment (610 nm) than that at the latest delay (597 nm). Thus, the relocation of xanthone into the aqueous phase is a slower process in larger cationic CTAC micelles than

in anionic micelles. As a result, this process can be monitored with nanosecond-time resolution. Similar behaviour is observed when polyelectrolyte-surfactants are used as aggregates.[13]

As stated earlier, by using an appropriate quencher, those probes that have exited into the aqueous phase can be quenched selectively. Water soluble negatively and positively charged triplet quenchers are used with the anionic and cationic surfactants, respectively. Using this method we have determined the rate constants of the probe's exit from micelles. The following equations summarize the processes studied in this work.

$$X_m \xrightarrow{h\nu} X^*_m \qquad \text{Eq. 5.2}$$

$$^1X^*_m \xrightarrow{ISC} {}^3X^*_m \qquad \text{Eq. 5.3}$$

$$^3X^*_m \xrightarrow{k_0} X_m \qquad \text{Eq. 5.4}$$

$$^3X^*_m \xrightarrow{k_-} {}^3X^*_{aq} + M \qquad \text{Eq. 5.5}$$

$$^3X^*_{aq} + M \xrightarrow{k_+} {}^3X^*_m \qquad \text{Eq. 5.6}$$

$$^3X^*_{aq} + Q \xrightarrow{k_q} X_{aq} + M \qquad \text{Eq. 5.7}$$

X is xanthone, M is the micelle's concentration, Q is the quencher, and the subscripts 'm' and 'aq' refer to the micellar and aqueous phases, respectively. The micellar concentration is calculated using the CMC

and the aggregation number for each particular system.[21,22] The rates of entry and quenching are k_+ and k_q, respectively. With the above mechanism, the rate of experimentally observed decay is given by

$$k_{expt} = k_0 + \frac{k_- k_q [Q]}{k_q [Q] + k_+ [M]} \qquad \text{Eq. 5.8}$$

where k_{expt} is the rate constant for the observed triplet decay (i.e., the total concentration of the triplet state). It is worth noting that the ISC rate is very fast compared to the other decay processes. This equation assumes that xanthone is largely solubilized in the micellar phase at the time of excitation. Also, it is assumed that the triplet decay in the water phase is due only to quenching by Q. Note that Q is insoluble in the micellar phase. The hydrophobic interior of the micelle, the ionic nature of the micellar surface, and the choice of an appropriately charged Q ensure that the above assumptions are justified and hold well for our experiments.

According to Eq. 5.8, at high quencher concentrations, k_{expt} is given by $k_0 + k_-$, and all the triplet probes exiting the micelle are quenched irreversibly. This in turn leads to a plateau in the values of k_{expt}. A representative plot of k_{expt} as a function of quencher concentration is shown in the insert of Figure 5.12. Although it is possible to obtain the exit rates from plots of this type, the plateau is not clearly defined at

higher quencher concentrations, since the lifetimes are shorter and carry bigger errors. The exit rates (k_-) are best obtained by modifying Eq. 5.8 to give the following equation. Figure 5.12 is a representative plot according to Eq. 5.9 for xanthone in SDS micelles.

$$\frac{1}{k_{expt} - k_0} = \frac{1}{k_-} + \frac{k_+ [M]}{k_- k_q [Q]} \qquad \text{Eq. 5.9}$$

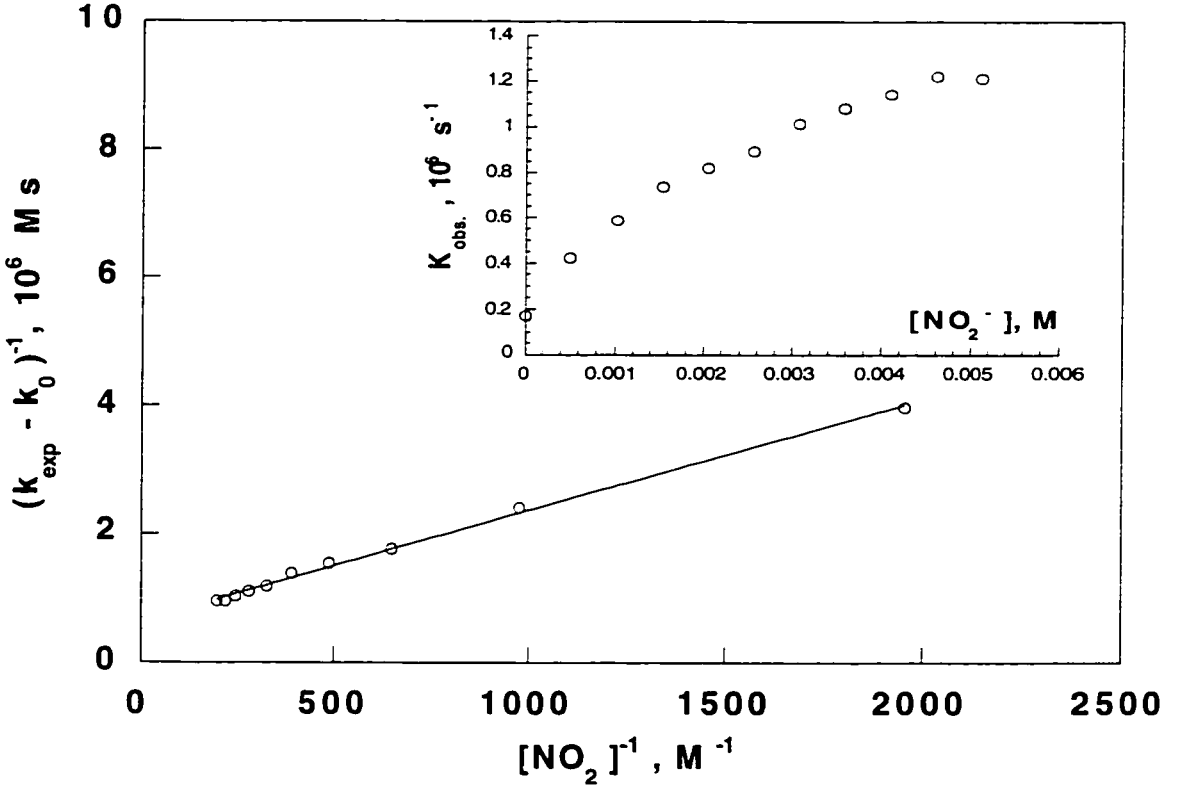

Figure 5.12. Quenching plot based on Eq. 5.9 for xanthone monitored at 600 nm (o) in 0.1 M SDS using nitrite ion (as $NaNO_2$) as quencher. The insert shows a quenching plot of the same system (o) based on Eq. 5.8.

From these plots, the rates of exit (k_-) and the ratios of k_+/k_q are obtained (see Table 5.4). The quenching plots for other systems

examined in our study also yield linear plots by the above approach. The value of k_q, which corresponds to the quenching of triplet xanthone by the nitrite ion, in aqueous solution has previously been determined as 6.5 x 10^9 $M^{-1}s^{-1}$.[2] As anticipated, exit rate constants are lower than the k_2 values obtained in the picosecond experiments. However, they are in the expected range of ~10^6 s^{-1} observed in similar studies of other aromatic ketones.[2] For example, the exit rates of propiophenone and benzophenone in SDS micelles are 3.0 X 10^6 s^{-1} and 2.0 X 10^6 s^{-1} , respectively.[2] It is noted that the error associated with the exit rate constants is ≤ 12%.

Table 5.4. Exit and entry data based on quenching studies of xanthone in the following systems on the nanosecond/microsecond time scale.

System	quencher	k_- (s^{-1})	k_+/k_q	k_+ (M^{-1} s^{-1})
SDecS	$Na(NO_2)$	2.70 x 10^6	3.69	2.40 x 10^{10}
SDS	$Na(NO_2)$	1.71 x 10^6	2.42	1.57 x 10^{10}
		2.7 x 10^6 (lit.[2])	2.62	
SDS+ 0.2 M NaCl	$Na(NO_2)$	2.66 x 10^6	~2.77	~1.80 x 10^{10}
SDS+ 0.3 M NaCl	$Na(NO_2)$	2.12 x 10^6	2.29	1.49 x 10^{10}
CTAC	$Cu(SO_4)$	0.58 x 10^6	9.97	0.86 x 10^9
STDS	$Na(NO_2)$	1.07 x 10^6	1.11	7.19 x 10^9

5.4. Discussion

It is known that the variation in solvent polarity changes the energetic ordering of the excited states of xanthone. In our study, it is found that the ISC rate from S→T is slowed down dramatically in water compared to organic solvents. Extremely polar solvents with hydrogen bonds have the ability to stabilize relatively polar molecules. This is evidenced by the longer lifetimes of triplet xanthone in polar media mentioned earlier. It is also known that the excited state of a low lying π,π^* ketone is usually more polar than its ground state. In particular, the dipole moment of excited xanthone is much higher than that of its ground state. In addition, Turro *et al.* also report a slight decrease in the values of k_{ISC} for benzophenone and its derivatives with increasing solvent polarity.[23] In particular, the solvent effect on the values of k_{ISC}^{-1} is moderately high with the case of acetophenone changing from 25 ps in isooctane to 39 ps in acetonitrile.[23] As with xanthone, it is known that acetophenone has closely spaced (n,π^*) and (π,π^*) states.[24] As solvent polarity increases, it undergoes an inversion of states to (π,π^*). Consequently, the ΔE_{S-T} will increase with the concurrent lowering of the T_1 (π,π^*) state and raising of the S_1 state. The ISC rate thus decreases, since the coupling between the triplet and the singlet states is reduced. Hence, it is not surprising that singlet xanthone is much longer lived (600 ps) in water than in acetonitrile.

The micelles used in our study contain a hydrophobic interior. However, it is not unlikely for water to penetrate the micellar surface.[25] Following picosecond excitation of xanthone in micelles, two distinct processes are observed. The first process, occurring between 60-180 ps, is assigned to the ISC of xanthone in various micelles. The values of the ISC rate (k_1) are found by temporal spectral evolution after a picosecond excitation. The singlet absorption maximum is red-shifted compared to that of the triplet and is monitored with respect to time (see Figure 5.5). Our reults show that these rates agree well with the singlet lifetimes of xanthone in the corresponding systems. The buildup absorption of $T_1 \rightarrow T_n$ is also measured for the SDS system with a lifetime of 80 ps. Thus, our analysis of the ISC rates based on spectral evolution is acceptable within the experimental errors. It is also observed that the ISC rate constant is moderately slowed down to approximately 180 ps with the addition of 0.2-0.3 M salt. This may indicate that the micellar growth is accompanied by an increase in polarity due to the penetration of water.

The second rate constant is attributed to the intramicellar mobility of the probe in micelles of various size (see Table 5.2). This process occurs in the 1-50 ns range. Excited xanthone has a low lying π,π^* character in relatively polar to polar media. The T-T absorption band shifts to lower wavelengths as the polarity of its environment increases. Excited xanthone relocates since it exhibits different solubilities than its ground

state. This is due to the fact that it possesses larger dipole moment than its ground state. Therefore, the spectral blue shift indicates a relocation of the probe towards a more polar environment.

The current design of our picosecond system allows for a maximum delay of 9 ns. This limitation makes the values of $k_2 < 5 \times 10^7$ s^{-1} unreliable. Thus, the migration lifetimes of 18, 28, and 55 ns found for the systems of SDS + 0.2 M NaCl, CTAC, and SDS + 0.3 M NaCl, respectively, have large uncertainties. However, they follow the right trend. As the micelle's dimensions increase,[21] the migration times increase. The values of k_2 lead to migration lifetimes of approximately 1, 3, and 5 ns for the SDecS, SDS, and STDS systems, respectively. These values compare well with the increase in the size of the micelles based on their corresponding aggregation numbers of 41, 65, and 80, respectively.[22]

The spectral shift on the nanosecond time scales are quite small with the exception of large CTAC micelles. This observation suggests that the polarity near the micellar surface is noticeably different from that in the aqueous phase. Thus, CTAC micelles exhibit an environment that is more nonpolar than anionic micelles. Further evidence for the nonpolar nature of CTAC micelles is the values of λ_{max} that are red shifted at different delay times compared to those of other systems (see

Table 5.3).

The exit of xanthone triplets into the aqueous phase is the last stage of the dynamics of a probe following excitation in compartmentalized systems. This process basically occurs on the microsecond time range (see Table 5.4). Both the values of the exit/entry rates (see Table 5.4) and the position of maximum transient absorption bands (see Table 5.3) indicate the existence of an equilibrium between the aqueous and micellar phases. However, this equilibrium is achieved slower in larger CTAC and STDS micelles than in SDS and/or SDecS micelles. This behaviour is consistent with the slower exit/entry rates observed with these larger micelles (see Table 5.4). The position of λ_{max} at long times for all the systems does not coincide with that of xanthone in water. However, it is the longest of all (i.e., 609 nm) in the case of CTAC micelles (see Table 5.3). The values of k_- are calculated according to Eq. 5.9, using an aqueous substrate that quenches the exiting triplets. Similar concepts are used in other studies for the evaluation of exit/entry rates in cyclodextrin systems[14] and in surfactant-polyelectrolyte aggregates.[13]

5.5. References

(1) Almgren, M.; Grieser, F.; Thomas, J. K. *J. Am. Chem. Soc.* **1979**, *101*, 279.

(2) Scaiano, J. C.; Selwyn, J. C. *Can. J. Chem.* **1981**, *59*, 2368.

(3) Selwyn, J. C.; Scaiano, J. C. *Can. J. Chem.* **1981**, *59*, 663.

(4) Gehlen, M. H. *J. Phys. Chem.* **1995**, *99*, 4181.

(5) Gehlen, M. H.; De Schryver, F. C. *J. Phys. Chem.* **1995**, *99*, 14407.

(6) Turro, N. J.; Okubo, T. *J. Am. Chem. Soc.* **1981**, *103*, 7224.

(7) Jay, J.; Johnston, L. J.; Scaiano, J. C. *Chem. Phys. Lett.* **1988**, *148*, 517.

(8) Infelta, P. P.; Gratzel, M.; Thomas, J. K. *J. Phys. Chem.* **1974**, *78*, 190.

(9) Weir, D.; Scaiano, J. C. *Tetrahedron* **1987**, *43*, 1617.

(10) Wilkinson, F.; Willsher, C. J.; Casal, H. L.; Johnston, L. J.; Scaiano, J. C. *Can. J. Chem.* **1986**, *64*, 539.

(11) Scaiano, J. C. *J. Am. Chem. Soc.* **1980**, *102*, 7747.

(12) Barra, M.; Bohne, C.; Scaiano, J. C. *J. Am. Chem. Soc.* **1990**, *112*, 8075.

(13) Abuin, E. B.; Scaiano, J. C. *J. Am. Chem. Soc.* **1984**, *106*, 6274.

(14) Liao, Y.; Frank, J.; Holzwarth, J. F.; Bohne, C. *J. Chem. Soc., Chem. Commun.* **1995**, *4*, 199.

(15) Fessenden, R. W.; Carton, P. M.; Shimamori, H.; Scaiano, J. C. *J. Phys. Chem.* **1982**, *86*, 3803.

(16) Hochstrasser, R. M.; Nelson, A. C. In *Lasers in Physical Chemistry and Biophysics*; J. Joussot-Dubien, Ed.; Elsevier: Amsterdam, 1975; pp 305.

(17) Scott, G. W.; Anderson Jr., R. W.; Hochstrasser, R. M.; Lutz, H. *Bull. Am. Phys. Soc.* **1975**, *20*, 46.

(18) Greene, B. I.; Hochstrasser, R. M.; Weisman, R. B. *J. Chem. Phys.* **1979**, *70*, 1247.

(19) Watanabe, K.; Ferrario, M.; Klein, M. L. *J. Phys. Chem.* **1988**, *92*, 819.

(20) Hayashi, S.; Ikeda, S. *J. Phys. Chem.* **1980**, *84*, 744.

(21) Leigh, W. J.; Johnston, L. J. In *Handbook of Organic Photochemistry*; J. C. Scaiano, Ed.; CRC Press: Boca Raton, Florida, 1989; Vol. II; pp 401.

(22) Aniansson, E. A. G.; Wall, S. N.; Almgren, M.; Hoffmann, H.; Kielmann, I.; Ulbricht, W.; Zana, R.; Lang, J.; Tondre, C. *J. Phys. Chem.* **1976**, *80*, 905.

(23) McGarry, P.; Doubleday, C.; Wu, C.-H.; Staab, H.; Turro, N. *J. Photochem. Photobiol., A:Chem.* **1994**, *77*, 109.

(24) Lutz, H.; Breherdt, E.; Lindquist, L. *J. Phys. Chem.* **1973**, *77*, 1758.

(25) Rodgers, M. A. J.; DaSilva E Wheeler, M. E. *Chem. Phys. Lett.* **1976**, *43*, 587.

6. Claims to Original Research

1) Most environmentally relevant magnetic fields are associated with 60 Hz electrical currents. The radical pair mechanism is proposed as a viable mechanistic route in which a magnetic field can influence the behaviour of radicals in heterogeneous systems such as micelles. This work contributes to the understanding of the effects of oscillating magnetic fields on radical pair dynamics in systems that mimic biological media. This is important since free radicals are involved in many biological processes such as enzymatic catalysis and DNA strand cleavage.

i. Despite the general belief that oscillating magnetic fields are more hazardous than static magnetic fields, it is shown that the effect of a time dependent 60 Hz oscillating magnetic field can be quantitatively predicted from knowledge of the behavior of the triplet radical pair under static field conditions.

ii. It has been demonstrated that the equation derived from the parameters obtained under static field conditions fits the radical escape data obtained when the magnetic field is oscillating in a 60 Hz cycle. This predictability can be expanded over numerous cycles.

iii. It is shown that when the oscillating field is significantly weaker than the static field, the fraction of radical escape oscillates around the static field and the total fraction escape over an entire cycle is no different than it would be under the static field alone.

iv. We present the first evidence that proteins can provide a suitable environment (like micelles) for the observation of magnetic field effects on free radical processes.

v. We present the first indication that the effect of a magnetic field on radical pairs generated in the protein medium causes an increase of up to 20% in the fraction of radicals that survive the geminate decay process and become available for other reactions such as radical-molecule reactions.

2) The triplet-triplet absorption band of xanthone is known to shift with solvent polarity. Xanthone is thus used as a sensor to obtain information on the photophysical properties of microheterogeneous systems. This work contributes to the understanding of those phenomena that precede a probe's exit into the aqueous phase.

i. We present the first measurement of the time taken for intramicellar motion of a triplet probe prior to the exit process. We find it takes 1-50 nanoseconds for the probe to migrate to the surface of a micelle.

ii. It is found that the spectral changes associated with the exit of the probe in the nanosecond to microsecond region are unexpectedly minimal.

iii. We present the first measurement of the intersystem crossing rate of xanthone in water.

iv. The intersystem crossing from the singlet to the triplet state of xanthone in various micelles is found to occur on the 60-180 picosecond time scale.

3) Other studies in which I have participated are not included in this thesis. Parts of this work have been included in two previous theses by Ron Boch and Yvonne Lear and in a publication (see appendix). The photochemistry of covalently conjugated and freely associated α-terthienyl in bovine serum albumin was studied. This work was performed in colaboration with R. Boch and Y. Lear. Boch, a former graduate student in our group, investigated the generation of singlet oxygen by α-terthienyl conjugated to the protein. Lear, a former

graduate student of Dr. T. Durst, synthesized the conjugated α-terthienyl-protein compounds.

The reactivity of the triplet α-terthienyl associated and conjugated with the protein towards two potential electron acceptors was investigated. My contributions included:

i. The first study to show two distinct triplet α-terthienyl populations for the conjugated protein complexes when a water soluble electron acceptor, methyl viologen, is used.

ii. The electron transfer rates using a nonpolar electron acceptor, benzoquinone, are similar for both the conjugated and associated protein complexes. These rates are 100 times slower in proteins than in homogeneous solution.

iii. The first measurement of the intersystem crossing rate of α-terthienyl in the protein by picosecond emission and pump-probe absorption spectroscopy.

Publications resulting from the work presented in this thesis

(1) Scaiano, J. C.; Mohtat, N.; Cozens, F. L.; McLean, J.; Thansandote, A. *Bioelectromagnetics* **1994**, *15*, 549.

(2) Scaiano, J. C.; Cozens, F. L.; Mohtat, N. *Photochem. Photobiol.* **1995**, *62*, 818.

(3) Mohtat, N.; Cozens, F. L.; Hancock-Chen, T.; McLean, J.; Kim, J.; Scaiano, J. C. *Photochem. Photobiol.* **1997**, *Submitted*,

(4) Boch, R.; Mohtat, N.; Lear, Y.; Arnason, J. T.; Durst, T.; Scaiano, J. C. *Photochem. Photobiol.* **1996**, *64*, 92.

(5) Mohtat, N.; Cozens, F. L.; Scaiano, J. C. *manuscript in preparation* **1997**.

(6) Berinstain, A. B.; Mohtat, N.; Scaiano, J. C. *manuscript in preparation* **1997**.

Other publications

(7) Baldoví, M. V.; Mohtat, N.; Scaiano, J. C. *Macromolecules* **1996**, *29*, 5497.

(8) Connolly, T. J.; Baldoví, M. V.; Mohtat, N.; Scaiano, J. C. *Tetrahedron Lett.* **1996**, *37*, 4919.

(9) Scaiano, J. C.; Connolly, T. J.; Mohtat, N.; Pliva, C. N. *Can. J. Chem.* **1997**, *25*, 92.

(10) Mohtat, N.; Scaiano, J. C. *manuscript in preparation* **1997**.

Appendix

IMAGE EVALUATION TEST TARGET (QA-3)

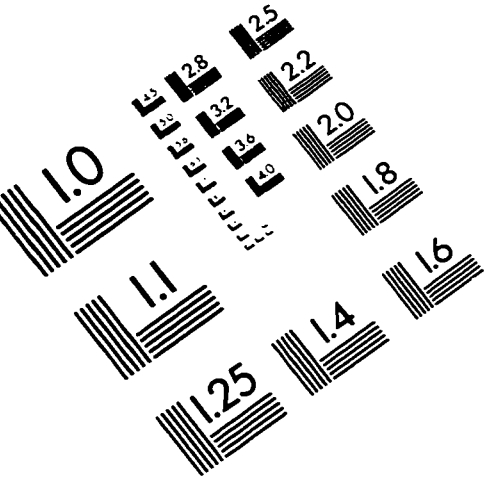

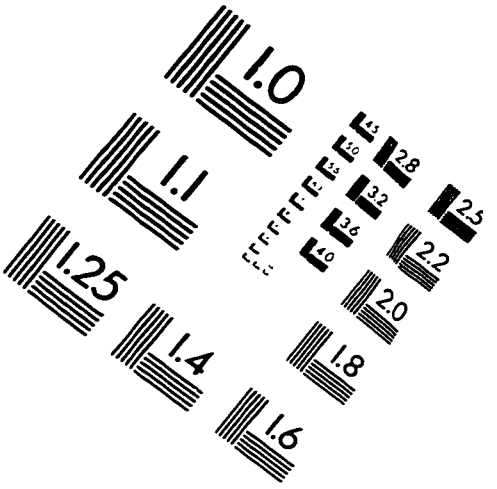

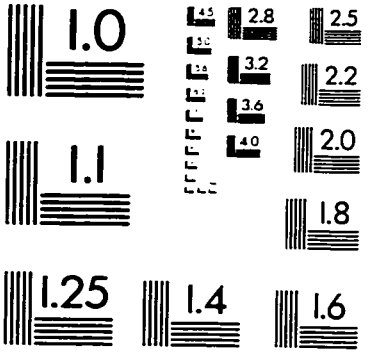

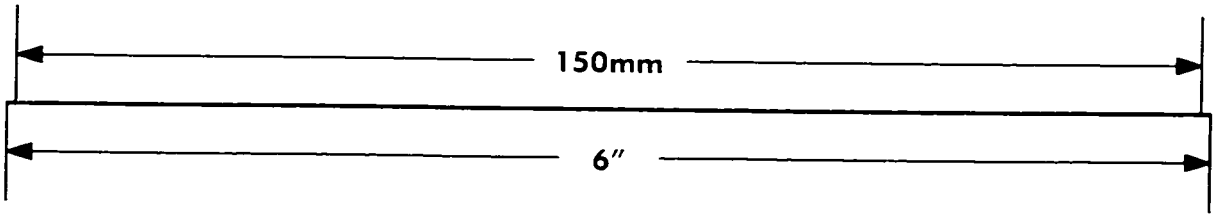

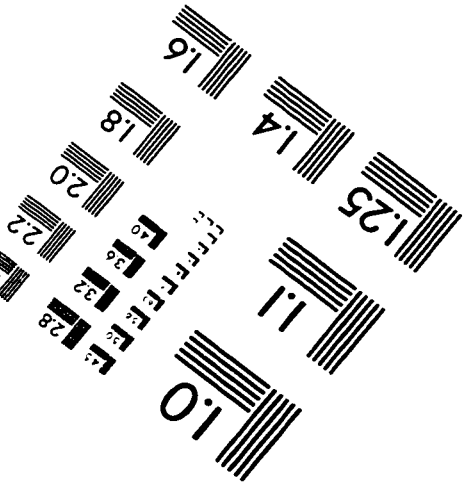

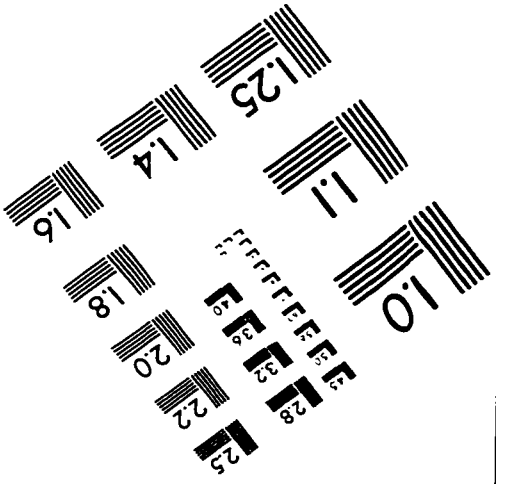

APPLIED IMAGE, Inc
1653 East Main Street
Rochester, NY 14609 USA
Phone: 716/482-0300
Fax: 716/288-5989